DEVELOPMENT OF A NEW DIAGNOSTIC TOOL BY WAVELET TRANSFORM & APPLICATIONS TO STIMULATION AND WATERFLOODING OPERATIONS

A Dissertation

Presented to

the Faculty of the Department of Petroleum Engineering

University of Houston

In Partial Fulfillment

of the Requirements for the Degree

Doctor of Philosophy

in Petroleum Engineering

by

Ebru Unal

August 2019

DEVELOPMENT OF A NEW DIAGNOSTIC TOOL BY WAVELET TRANSFORM & APPLICATIONS TO STIMULATION AND WATERFLOODING OPERATIONS

Ebru Unal

Approved:

Chair of the Committee
Mohamed Y. Soliman,
Professor, Chair
Petroleum Engineering Department

Committee Members:

Birol Dindoruk, Professor,
Petroleum Engineering Department

Kyung Jae Lee, Assistant Professor,
Petroleum Engineering Department

Guan Qin, Associate Professor,
Petroleum Engineering Department

Ahmad Sakhaee-Pour,
Assistant Professor,
Petroleum Engineering Department

Shah Kabir, Lecturer,
Petroleum Engineering Department

Suresh K. Khator, Associate Dean,
Cullen College of Engineering

Mohamed Y. Soliman, Professor, Chair
Chair of Department in
Petroleum Engineering

ACKNOWLEDGEMENTS

The first and the foremost gratitude is definitely towards to my advisor Prof. Dr. Mohamed Soliman for not only his technical advices but also his endless patience, trust and guidance towards my studies and also my personal development as well. From the very first day of my PhD journey, he has been always there in every stage of this degree to support me in any aspect, it would not be possible to get this degree without his support. It was an honor to work within his research group with invaluable colleagues. In addition, I would like to express my gratitude towards my committee members, Dr. Birol Dindoruk, Dr. Quan Qin, Dr. Ahmad Sakhaee-Pour, Dr. Kyung Jae Lee and Mr. Shah Kabir for their support, directions and all the feedback they provided whenever I needed it. Thank you all for being a part of my committee.

I would also like to extend my gratitude towards to University of Houston Hydraulic Fracturing Diagnostic Consortium and its members; Marathon Oil, Southwestern Energy, HESS, Shell International Exploration and Production Inc., and Halliburton for sponsoring and supporting this dissertation.

Many teachers, instructors, professors, mentors, friends, and colleagues in my life have influenced me and have endeavored me towards being who I am and where I am today. Among all of those special people, I would like to express my gratitude specifically to my first and the most valuable mentor Dr. Bora Oz and his colleagues who believed in me and supported me for my graduate studies in the USA. His support initiated to shape my career, and provided many opportunities during my graduate studies, and no doubly it

will open many more doors in life. The support I got long years ago has been appreciated and will be much appreciated by more accomplishments for many years.

Also, I would like to thank to all of my friends from all over the world, just for being a part of my life during my studies and have a positive impact on me. Especially to those who helped me to solve a problem, did a homework with me, prepared a lab experiment together, wrote a report, or a research paper together, attended a conference, being there with me to enjoy a dinner or movie, and even sent me a funny picture from miles away, thank you all.

Last but not the least, I would like to thank to my family for their unconditional love, support and encouragement. Thank you for reminding me who I am and what I can do in life.

DEVELOPMENT OF A NEW DIAGNOSTIC TOOL BY WAVELET TRANSFORM & APPLICATION TO STIMULATION AND WATERFLOODING OPERATIONS

An Abstract

of a

Dissertation

Presented to

the Faculty of the Department of Petroleum Engineering

University of Houston

In Partial Fulfillment

of the Requirements for the Degree

Doctor of Philosophy

in Petroleum Engineering

by

Ebru Unal

August 2019

ABSTRACT

Due to the shift from conventional reservoirs towards unconventional, ultra-low permeability reservoirs in the last decade, multistage hydraulic fracturing in horizontal wells and Diagnostic Fracture Injection Test (DFIT) has become one of the dominant and economically practical stimulation techniques and pressure transient tests, respectively. It is crucial to analyze and interpret both fracturing and DFIT data correctly to obtain essential features of the fracture and reservoir in order to have successful stimulation designs. In addition, it is also crucial to understand interwell connectivity (IWC) for improving the performance of any secondary flooding in conventional reservoirs.

This research presents a new diagnostic tool/methodology developed by wavelet transform and its applications to hydraulic fracturing, diagnostic testing in unconventional reservoirs and waterflooding operations in conventional reservoirs. This new diagnostic tool provides a better understanding of fracture behavior during both injection and fall-off periods mainly in hydraulic fracturing operations and fracture diagnostic injection tests, respectively. Furthermore, the flexibility of this methodology allows for implementation to conventional reservoirs to determine interwell connectivity between injection and production wells and thus leading to better diagnostics beyond the wellbore.

The objective of this research is to develop a new technology that is applicable for both conventional and unconventional reservoirs to decrease uncertainty not only in commonly used conventional fracture diagnostic techniques such as G-function, log-log analysis, square-root-time, cross-correlation to identify fracture and reservoir parameters, but also level of connectivity in conventional reservoirs to ultimately improve the overall

efficiency of hydraulic fracturing designs and enhanced oil recovery where the assessment of connectivity is critical.

Unlike other conventional techniques, this new methodology treats hydraulic fracturing pressure, DFIT fall-off pressure and injection/production rates as non-stationary signals and extracts relevant key information in wavelet/scale domain instead of time domain.

TABLE OF CONTENTS

LIST OF FIGURES

LIST OF TABLES

CHAPTER I

INTRODUCTION

Analog signals are continuous, and they can be represented as a function of a time variable *(t)*, where *f (t)* is the value of signal *f* at time *t*, and it may vary with some other spatial dimension other than time. On the other hand, discrete signals are not continuous, they occur at separate time instants, they have values at isolated points and can be represented as a function of on a subset, *f (n)*. Even though the original signal and its waveform are analog in nature, the signal can be displayed as discrete at regular time instants. In this case, the signal *f (n*) appears continuous due to a large number of samples as shown in Figure 1.1, for example, pressure signal of a hydraulic fracturing treatment is originally continuous in its nature, but we measure and record pressure values by pressure gauges at regular time intervals and overall pressure signal appears continuous in time-domain. However, most of the signals are discontinuous, irregularly shaped, or not smooth in their nature.

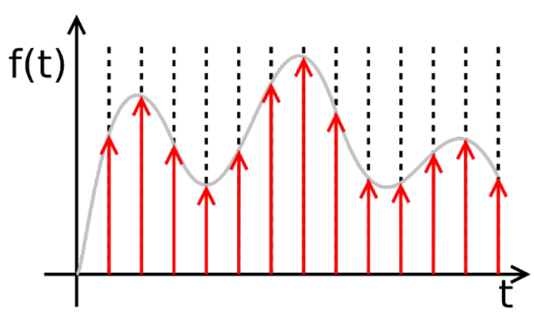

Figure 1.1 An example of a discrete signal.

The time-domain representation may not always reveal the discontinuities within the signal so other dimensions such as frequency-domain or scale-domain representation are required. Frequency-domain decomposes the raw signal into its oscillatory components by sinusoidal signals (*sin (t)* and *cos (t)*) whereas scale-domain representation breaks the signal into a sum of similarly shaped smaller signals (wavelets). Fourier transformation has been used as a mathematical tool for frequency-domain representation of the signals, whereas wavelet transformation is used for scale-domain representation (Allen, Mills 2004), and both representations can be seen in Figure 1.2.

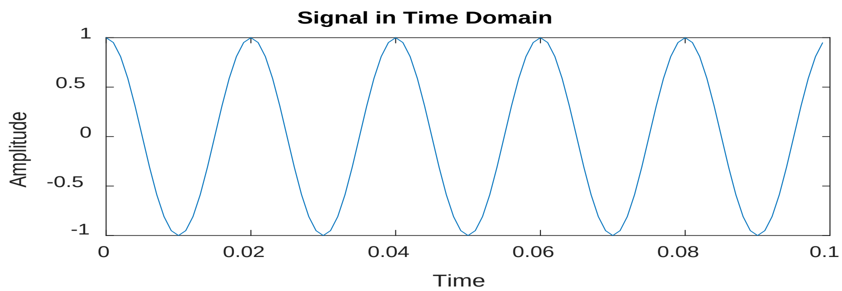

(a)

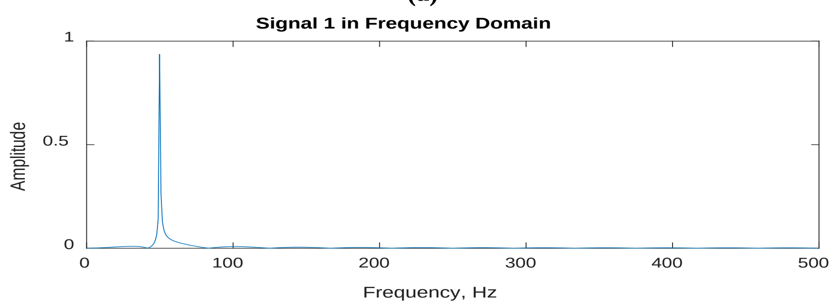

(b)

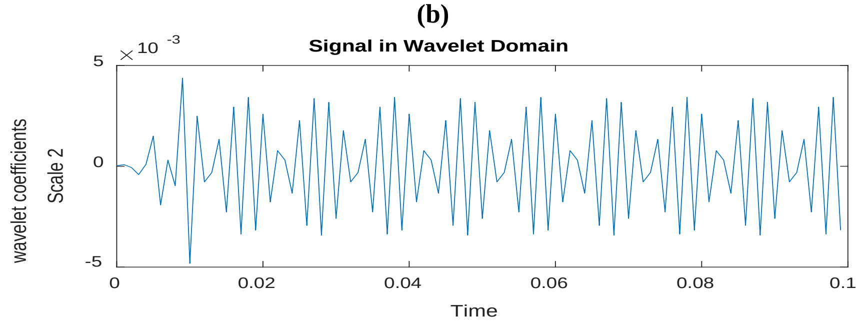

(c)

Figure 1.2 (a) Signal in time domain, (b) Signal in frequency domain, and (c) Signal in wavelet domain.

Many signals such as seismic data, well test data, and hydraulic fracturing treatment data in the petroleum industry are non-stationary. In other words, the seismic waves and pressures are transient, they occur in various scales or frequencies, and they have sharp transitions. Since those non-stationary signals occur in a finite duration, that makes it possible to divide the signal into many components and analyze them individually with various frequencies. Therefore, wavelet transformation is suitable to analyze those non-stationary signals.

1.1 Problem Statements

Due to the increase in drilling and production activities in ultra-low permeability shales reservoirs, demand of horizontal, multi-stage stimulation jobs also increased. Therefore, successful hydraulic fracture treatment, evaluation, and design in cost and time efficient manner is crucial. Surface/downhole treating pressure measurement is now a well-established method for the study of hydraulic fracturing operations, although the optimal method of converting the measured data into information about the fracture remains unclear. In addition, Diagnostic Fracture Injection Tests (DFIT) become one of the most preferable cost and time efficient pressure transient tests for ultra-low permeability reservoirs, mainly shales. After injection of small amount of fluid into the formation and creating mini fracture around the near wellbore, the natural decline of the pressure is observed to identify closure of the fracture system during the falloff period in DFIT analysis. There are two distinct regions in falloff data which are Before Fracture Closure and After Fracture Closure regions. There have been various methodologies developed to analyze each region to determine fracture and reservoir parameters, and all can be categorized in two main methods; Before Closure (Pre-Closure) and After Closure

Analysis. In Before Fracture Closure analysis, fall-off data is analyzed for determination of fracture closure parameters (closure pressure and closure time), fluid efficiency, formation leak-off coefficient and leak-off type such as pressure-dependent permeability, fracture height recession or transverse storage, fracture tip extension after closure, or normal leak-off. Fracture closure pressure is the most important parameter to be identified correctly, because both before and after closure analysis mainly dependent on this parameter. Conventional tangential methodologies for DFIT analysis still have uncertainty about estimation of fracture closure and time.

The objective of this research is to develop a new technology that is applicable for both conventional and unconventional reservoirs to decrease uncertainty not only in commonly used conventional fracture diagnostic techniques such as G-function, log-log analysis, square-root-time, to identify fracture and reservoir parameters, but also in the level of interwell connectivity in conventional reservoirs. This research ultimately aims to improve the overall efficiency of hydraulic fracturing designs, treatments in unconventional reservoirs and also the enhanced oil recovery in conventional reservoirs. There are three main areas that have been investigated in this dissertation and they can be categorized as below;

1) Hydraulic Fracturing Operations and DFITs in Vertical Wells
2) Hydraulic Fracturing Operations and DFITs in Horizontal Wells
3) Inferring Interwell Connectivity in Waterflooding operations.

1.2 Organization of the Dissertation

The dissertation is organized as follow. Chapter 1 introduces the fundamentals of mathematical transformations and it explains different types of transformations, their advantages and disadvantages. Chapter 2 reviews the previous work done specifically by wavelet transformation in various industries and the methodologies. Chapter 3 review the discrete wavelet transformation theory and develops the methodologies had been used in this dissertation. Chapter 4 through 6 demonstrate three main investigated areas related to different operations and application of the new diagnostic tool to real field data one by one. Chapter 7 finally concludes the dissertation.

1.3 Overview of Transformations

As explained earlier, most of the raw signals in nature are function of time, and represented in time-domain. If we plot those signals we can obtain their time-amplitude representation. However, this type of representation is not always the best way of obtaining necessary information from the signal. Most distinguished information such as discontinuities usually are hidden in the frequency spectrum of the signal. Therefore, it is essential to represent the signal in its frequency spectrum to reveal hidden information. Mathematical transformations are the essential tools for new representation of a signal (vector). Therefore, it is necessary to use the most appropriate transformation type to obtain detailed information from the signal depending on the particular application. There are three main transformation types (Strang, 1996);

I. Lossless-Orthogonal-Transforms (orthogonal and unitary matrices): A lossless unitary transform is like a rotation. The transformed signal has the same length as the original. The same signal is measured along a new perpendicular axes.

II. Invertible-Biorthogonal- Transforms (invertible matrices): lengths and angles may change during this transform. Even though, the new axes are not necessarily perpendicular, no information is lost.

    Orthogonal wavelets give orthogonal matrices and unitary transforms, whereas biorthogonal wavelets give invertible matrices. Both transformations have perfect reconstruction without having any information loss (noise). They both just move the information around and separate out the noise and decorrelate the signal.

III. Lossy Transforms (not invertible): Unlike other transforms, invertibility is lost in lossy transformation. For example, compression is an irreversible transform where it destroys the small components of the signal.

Most well-known methodology to find frequency content of a signal is Fourier Transform. Hilbert transform, short-time Fourier transform, Wigner distribution, Radon transform, wavelet transform are some of the others. Discrete Fourier Transform (DFT) decompose a signal into sinusoidal basis functions of different frequencies and no information is lost in this transformation. Also, in wavelet analysis, Discrete Wavelet Transform decomposes a signal into a set of mutually orthogonal wavelet basis functions. Wavelet functions are dilated, translated, and scaled versions of a common function (ψ) known as mother wavelet. Both DFT and DWT are invertible, and the original signal can be completely recovered from its transformed representation.

1.4 The Fourier Transform

Fourier (1822) showed that any periodic function can be expressed as an infinite sum of periodic complex exponential functions. His discovery was generalized first to non-periodic functions, and then periodic or non-periodic discrete time signals. In 1965, a new algorithm called Fast Fourier Transform (FFT) was developed and Fourier Transform became more popular. Fourier Transform decomposes a signal to complex exponential functions of different frequencies. It can be defined by the following two equations:

$$X(f) = \int_{-\infty}^{\infty} x(t) e^{-2j\pi f t}\, dt \text{ and} \tag{1.1}$$

$$x(t) = \int_{-\infty}^{\infty} X(f) e^{2j\pi f t} df. \tag{1.2}$$

The integration in the equation (1) is in time, which means the integral is calculated for every value of "f" corresponds to all time instances. The signal has the frequency component "f" at all times (for all "f" values), then the result obtained by the Fourier transform make sense. It will not be applicable for non-stationary signals which has time varying frequency. Fourier transform tells whether a certain frequency component exits or not. This information is independent of where in time this component appears.

In addition, Fourier transformation is reversible transform which means it is possible to go back and forward between the raw data and processed (transformed) data. However, only one of the information is available at any given time, in other words, no frequency information is available in the raw time-domain signal, and no time information is available in the Fourier transformed processed signal. If a signal is stationary, in other words, if the frequency content of the signal does not change by time then the time information is not required. On the other hand, non-stationary signals have various frequencies at different time intervals, so it is important to know the time interval of each frequency occurs.

Most of the biological signals such as ECG (electrical activity of the heart, electrocardiograph), EEG (electrical activity of the brain, electroencephalograph), and EMG (electrical activity of the muscles, electromyogram) are all non-stationary signals. Fourier transformation can obtain the frequency components of these signals, however, it is not capable of giving the time-frequency representation.

1.5 Short Time Fourier Transform (STFT)

Unlike Fourier Transform, Short Time Fourier Transform (STFT) divides the signal into small enough segments where these segments can be assumed to be stationary. A window function *"w"* is chosen with a width same size of the segment of the signal where it is stationary and STFT can be calculated as

$$STFT_X^{(w)}(T,F) = \int_{-\infty}^{\infty} [x(t)\, w^*(t-t')]\, e^{-j2\pi ft} dt. \tag{1.3}$$

Narrow windows give good time resolution but poor frequency resolution. On the other hand, wide windows give good frequency but poor time resolution, also wide windows may violate the condition of stationary. This time and frequency resolution problem is a result of Heisenberg uncertainty principle and this issue exists regardless of the transform used. This resolution problem is the main reason of transition from STFT to Wavelet Transform.

1.6 Wavelet Transform

Wavelet transform is a mathematical tool for data space transformation, in which a function or signal can be expressed in various basis sets. Wavelet transform decomposes a signal into a set of functions which are orthonormal basis functions. The set consists of a single function (ψ) also called "*mother wavelet*", along-with the scalings *(s)* and translations *(u)* of that mother function called wavelet functions. Wavelets (Haar, 1910) are pulse-like functions with a limited duration and frequency. The mother wavelet is a function having zero average, and can be expressed as

$$\int_{-\infty}^{+\infty} \psi(t)dt = 0. \tag{1.4}$$

The wavelet transform of a generic function *f(t)* at scale *(s)* and position *(u)* is computed by

$$\mathcal{W}[f(u,s)] = \int_{-\infty}^{+\infty} f(t)\, \psi_{u,s}(t)dt. \tag{1.5}$$

Equation (1.5) basically represents the correlation of function *f(t)* to a set of basis functions of the mother wavelet ($\psi_{u,s}$). Mother wavelet ($\psi_{u,s}$) can be mathematically expressed in terms of scaling (*s*) which is associated with the wavelet's frequency and translation (*t-u*) which is associated to its position in time as

$$\psi_{u,s}(t) = \frac{1}{\sqrt{s}}\psi\left(\frac{t-u}{s}\right). \tag{1.6}$$

Then, the wavelet transform of that mother wavelet at scale *(s)* and translations *(t-u)* becomes

$$\mathcal{W}[f(u,s)] = \frac{1}{\sqrt{s}}\int_{-\infty}^{+\infty} f(t)\, \psi\left(\frac{t-u}{s}\right)dt. \tag{1.7}$$

There are two types of wavelet transformations based on wavelet orthogonality: continuous wavelet transform and discrete wavelet transform.

Orthogonal wavelets can be used for discrete wavelet transform development, whereas non-orthogonal wavelets are used for continuous wavelet transform. In other words, discrete wavelet transform decomposes the signal into discrete set of wavelets that are orthogonal to its translations and scaling. To decompose the signal, it is required that the scaling function to be orthogonal to its discrete translations to construct the wavelets. These set of wavelets form the orthonormal basis.

1.6.1 The Continuous Wavelet Transform (CWT)

In order to overcome the resolution problem, the Continuous Wavelet Transform (CWT) was developed as an alternative method to Short Time Fourier transform (STFT). Both STFT and wavelet analysis are done in a similar way, the signal is first multiplied with a function (wavelet or window function) and then the transform is computed separately for different segments of the time-domain signal. There are two main differences between these two methods:

1) The Fourier transforms of the windowed signal is not taken, so single peak will be seen corresponding to a sinusoid, i.e., negative frequencies are not computed.
2) The width of the window is changed as the transform is computed for every single spectral component, which is probably the most significant characteristics of the wavelet transform.

The continuous wavelet transform is defined as

$$CWT_x^{\psi}(\tau, s) = \Psi_x^{\psi}(\tau, s) = \frac{1}{\sqrt{|s|}} \int x\,(t)\psi^{*}\left(\frac{t-\tau}{s}\right) dt, \tag{1.8}$$

where, τ is translation, s is scale, and ψ is transforming function, or mother wavelet.

Unlike in STFT, there is no frequency information, instead, scale which is reciprocal of frequency is defined in wavelet transformation (1/frequency). Similar concept of scales in maps, high scales (low frequencies) corresponds to a non-detailed view, to a global information of a signal (usually spans the entire signal) whereas low scales (high frequencies) corresponds to a detailed view, information of a hidden pattern in the signal. Discrete Wavelet Transformation (DWT) that is the main focus of this research will be explained in more details within Chapter 3 Methodology of this dissertation.

CHAPTER II

REVIEW OF PREVIOUS WORK

This chapter reviews the previous studies had been done associated with wavelet analysis, conventional fracture closure diagnostic methodologies and interwell connectivity in waterflooding operations.

Wavelet Analysis

Several studies have examined the use of wavelets by different methodologies for interpretation of various data to identification of sources and types of various phenomena in many industries. In health sciences, one of the most well-known application of wavelets is processing the monitored brain electrical activity represented by electroencephalogram (EEG) signal to identify many neurological diseases, brain disorders such as schizophrenia, obsessive compulsive disorder, and epilepsy. EEG signal consists of several underlying oscillating frequency components e.g. alpha frequency, beta frequency and also a noise component superimposed on these oscillating frequencies. Adeli *et al*. (2002) examined the EEG signals by wavelet transformation for seizure detection and epilepsy diagnosis. Faust *et al.* (2014) summarized significant published research on EEG feature extraction by both CWT and DWT techniques in EEG signal analysis. Saritha *et al*. (2008) used wavelet transformation on ECG signals to describe frequency content of the hearth activity. Abnormalities and the waveforms corresponding to those abnormalities were studied by wavelet coefficients to identify specific function of the myocardial tissue. Another application of wavelet analysis is the interpretation of various data to identification of sources and types of various phenomena such as electrochemical noise (EN) data for analysis of corrosion type (Smith, Macdonald, 2005). Another study area of wavelets is the acoustic emission (AE) data for detection of structural damage of rock specimens under uniaxial compressions (Kang, 2008).

In addition to other industries, there has been different applications of wavelet transformation in petroleum industry. The first application of wavelets in petroleum industry was performed on seismic signal processing in 1982 by Morlet. Because wavelet transform provides information related to relationship between the attenuation of the seismic waves and the time-thickness of the formations, it was used in hydrocarbon detection by Burnet and Castagna in 2003. Prokoph (2000) used wavelet analysis to analyze well-log data from deep marine sediments. Due to the lack of obvious transitions between marine sediment facies, conventional well-log analyses are not able to detect those discontinuities. However, Prokoph *et al.* demonstrated the successful application of wavelet analysis of gamma-ray log data to localize discontinuities in source rock evaluation/characterization. Panda *et al.* (2000) applied wavelet transformation to permeability data to determine spatial distribution of permeability by analyzing the location of layer boundaries and local discontinuities. Panda et al. also studied permeability data to denoise and upscale the geological models by wavelets. Another study was conducted by Soliman *et al.* in 2003 where pressure-transient data from drawdown tests, buildup tests, and minifrac tests were analyzed. The signal produced by a pressure-transient test is expected to have a varying frequency over time as the test encounters various effects in the wellbore and the formation. Therefore, wavelet transformation that is the most appropriate technique for non-stationary signals was used in that study, and results demonstrated two main anomalies in the pressure data. They were detected as wellbore/ tool events and reservoir events. In addition to detecting discontinuities, another application of wavelet transformation is data compression. In order to improve storage efficiency of MWD systems, Bernasconi *et al.* (1999) used wavelet transform to compress excess MWD data by 15:1 compression ratio without any data degradation.

Installation and applications of Pressure Downhole Gauges (PDG) have increased due to their capabilities to record long term not only pressure and temperature but also flow rate, phase flow rate, resistivity and etc. that is very beneficial information for reservoir management. PDGs make it possible to monitor well and the reservoir conditions in real time and this long-term surveillance provides necessary information for predictions and mitigate any problems. However, compared to conventional data from pressure transient tests, PDGs record large amount of data over a long period of time which makes it impossible to process and interpret the entire data altogether, it definitely requires special processing and interpretation techniques. Athichanagorn proposed a multistep technique in 1999 for analyzing long-term continuous pressure and rate data using wavelets which consist of outliers removal, denoising the data, transient identification, data reduction and etc. (Athichanagorn, 1999).

DFIT

The natural decline of the pressure is observed to identify closure of the fracture system during the falloff period. There are two distinct regions of falloff data which are Before Fracture Closure and After Fracture Closure regions. There have been various methodologies developed to analyze each region to determine fracture and reservoir parameters, but all can be categorized in two main methods; Before Closure (Pre-Closure) and After Closure Analysis. Before Fracture Closure fall-off data is analyzed for determination of fracture closure parameters (closure pressure and closure time), fluid efficiency, formation leak-off coefficient and type (pressure-dependent permeability, fracture height recession or transverse storage, fracture tip extension after closure, or normal leak-off). Fracture closure pressure is the most important parameter to be identified correctly, because both before and after closure analysis mainly dependent on this parameter. There has been several Before Closure models to analyze pre-closure period since the first model by Nolte (1997), semi-log derivative (G.dp/dG) model by Barree et al. (1996), $(\Delta t dp/d\Delta t)$ log-log model by Craig and Blasingame (2006) the holistic approach by Barree et al. (2009), and the variable fracture compliance method by McClure et al. (2014). In addition to Before Closure models, Marongiu-Porcu et al. (2011) presented a more comprehensive model combining before and after closure models to determine both fracture parameters and reservoir permeability.

One of the interests of this research is the Before Closure Analysis of the fall-off data to identify fracture closure time and closure pressure by wavelet transformation method. Unlike other methods, wavelet analysis does not require any assumptions regarding to fracture geometry, and it is based on the concept of intermittent fracture propagation and closure phenomena.

Interwell Connectivity

Inter-well connectivity (IWC) is commonly measured using various physics-based methods such as simulations, tracers, heuristics and semi-analytical models, and signal processing techniques. Different signal processing techniques such as Spearman's method (Heffer et al., 1997; Refunjol and Lake, 1997; Soeriawinata and Kelkar, 1999) were used extensively to correlate the rate in producers to injector wells. Other techniques that are based on multivariate linear regression analyses such as capacitance-resistance model (Albertoni and Lake, 2003; Yousef et al., 2006) were also used in IWC studies. Machine learning is another popular approach that several researchers have used to reveal the connections between wells. Tian and Horne (2016) proposed a modified Pearson's correlation and machine learning approach to identify IWC between wells. Kaviani (2009) and Kaviani and Valko (2010) used a multiwell productivity index (MPI) to predict IWC in a homogeneous reservoir. Also, exploratory data analysis (Jansen and Kelkar, 1996), extended Kalman filter (Liu et al., 2009; Zhai et al., 2009), neural network (Panda et al., 1998), and applying the multivariate linear regression analysis (Dinh and Tiab, 2008) are among other techniques that were used to reveal the inter-well connectivity of wells.

CHAPTER III

METHODOLOGY

This chapter reviews the components of the developed diagnostic tool and explains the theory of each component. The first component of the developed methodology is the discrete wavelet transformation, which decomposes the treatment pressures and rates into various resolution levels, aka Multiresolution Analysis (MRA). In addition, other components can be listed as; Change Point Detection (CPD), pseudo-frequency, distribution of signal energy, and Energy Density Plots (EDP).

3.1 Discrete Wavelet Transform (DWT)

Signals are either analog, continuous in time, or discrete and occur at discrete time intervals in nature. Wellbore pressure data can be treated as a signal which is continuous in its nature but is represented by discrete time intervals depending on the resolution of the gauge used for the pressure measurements. Even though most of the signals have discontinuities within them, those discontinuities are not always clearly identifiable in time-domain. To reveal that hidden information, it requires either frequency or scale domain representation of the signal. Transformation from time-domain to wavelet, or scale domain is accomplished by Wavelet Transformation (Allen, Mills 2004).

Among two main wavelet transformations, Discrete Wavelet Transformation of pressure signals are investigated in this dissertation. The signal to be analyzed is required to be of dyadic length (2^j), in other words, the mother wavelet needs to be translated and shifted by powers of two. Therefore, the scale parameter (s) is replaced by 2^j, and the translation parameter (u) is replaced by ($k2^j$) in general wavelet set of basis function and DWT can be calculated as

$$\psi_{j,k}(t) = \frac{1}{\sqrt{2^j}} \psi \left(\frac{t - k2^j}{2^j} \right). \tag{3.1}$$

Discrete wavelet transformation of a signal is basically filtering the signal by passing it thorough high pass and low pass filters to obtain high-frequency and low-frequency components of the signal. High-frequency component of the signal, also called detail information, represents the discontinuities and singularities, whereas low-frequency component represents the coarse approximation of the original data.

High-frequency, low scale detail coefficients (cD) and low-frequency, high scale approximation coefficients (cA) at level j can be calculated as

$$cD_j = \sum_{n=0}^{\infty} f(n)\, \psi_{j,k}(n) = \sum_{n=0}^{\infty} f(n)\, \frac{1}{\sqrt{2^j}}\, \psi \left(\frac{n - k2^j}{2^j} \right) \; and \tag{3.2}$$

$$cA_j = \sum_{n=0}^{\infty} f(n)\, \emptyset_{j,k}(n) = \sum_{n=0}^{\infty} f(n)\, \frac{1}{\sqrt{2^j}} \emptyset \left(\frac{n - k2^j}{2^j} \right). \tag{3.3}$$

Application of high-pass and low-pass filters to a generic function *f (t)* via wavelet transform is defined as wavelet decomposition. Scaling a function has an inverse effect in the frequency domain, when ψ is scaled by2^j, the time resolution decreases while the frequency resolution decreases (Ladd, 1993). Therefore, filtering a signal through high and low-pass filters changes the resolution of the signal. The amount of detail information within the signal can be captured by decomposing the signal into various levels. In order to have further decomposition, approximation coefficients that are the output of the low-frequency filter are passed through high and low-frequency filters again to obtain signal decomposition at next level. This process may be repeated up to a maximum of j levels, where j is exponent of the dyadic length (2^j) of the signal. Breaking down a signal into many lower-resolution components is called multiresolution analysis, and wavelet decomposition tree can be seen in Figure 3.1 (Mallat 1989).

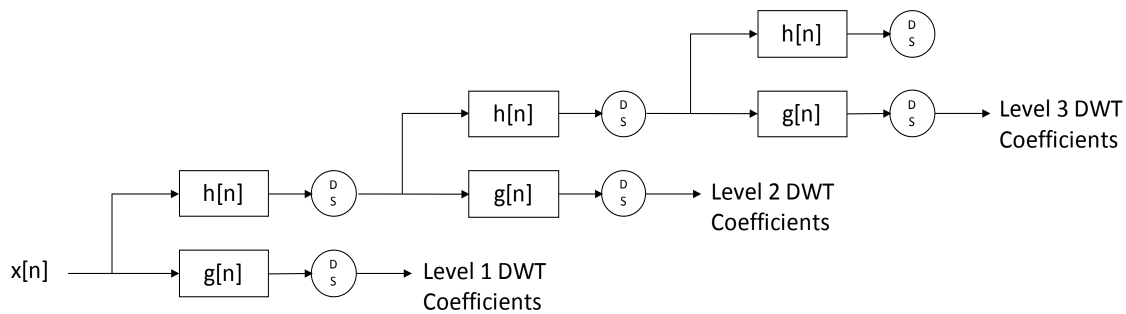

Figure 3.1 Discrete wavelet decomposition tree after Mallat (1989).

3.2 1-D Discrete Wavelet Transformation (DWT)

One-dimensional DWT is a linear transformation and it operates on real valued vectors whose length is dyadic. 1-D DWT results in transforming the original vector into a new vector of the same length. DWT is invertible and orthogonal, so the inverse transform is the transpose of the transform and it is possible to have perfect reconstruction without having any information loss. Therefore, it can be said that wavelet transformation is like a rotation in function space from time domain to wavelet/scale domain. The unit vectors (e_i) of wavelet transformation are the basis functions; mother wavelet (ψ) and wavelet functions (Press, 1992).

3.3 Construction of Wavelet Systems

As mentioned earlier, there are two sets of functions in DWT calculations which are the scaling functions and wavelet functions. Scaling function is $\emptyset(x)$ is the solution to a dilation equation (Equation (3.4))

$$\emptyset(x) = \sum_{k=-\infty}^{\infty} a_k \emptyset\,(Sx - k), \tag{3.4}$$

where S is the dilation factor, in this study of DWT S=2, and a_k are the filter coefficients. Filter coefficients are derived under special conditions for the scaling functions. These constrains can be listed as follows:

1) The area under the scaling function is normalized to unity;

$$\int_{-\infty}^{\infty} \emptyset(x)dx = 1 \;\; and \tag{3.5}$$

$$\sum_{k=-\infty}^{\infty} a_k = 2. \tag{3.6}$$

2) Scaling function and its translates are required to be orthonormal;

$$\int_{-\infty}^{\infty} \emptyset(x)\emptyset(x+l)dx = \delta_{0,l,} \tag{3.7}$$

where $$\delta_{0,l} = \begin{cases} 1, & l = 0 \\ 0, & otherwise, l \neq 0 \end{cases}$$

$$\sum_{k=-\infty}^{\infty} a_k a_{k+2l} = 2\delta_{0,l.} \tag{3.8}$$

3) Wavelet $\psi(x)$ (Equation (3.1)), and the scaling function are required to be orthogonal;

$$\psi(x) = \sum_{k=-\infty}^{\infty} (-1)^k a_{N-1-k} \emptyset(2x - k), \tag{3.9}$$

$$< \emptyset(x), \psi(x) >= \int_{-\infty}^{\infty} \sum_{k=-\infty}^{\infty} a_k \emptyset(2x-k) \sum_{l=-\infty}^{\infty} (-1)^l a_{N-1-l} \emptyset(2x-l) dx, and \qquad (3.10)$$

$$= \frac{1}{2}(-1)^k a_k a_{N-1-k,} \qquad (3.11)$$

$$= 0.$$

$a_k\ and\ (-1)^k a_{N-1-k}$ are the high and low frequency filter coefficients in Equation (3.9) and they form the pair of quadrature mirror filters.

4) Any function of order of P, can be approximated by scaling function as

$$f(x) = \propto_0 + \propto_1 x + \propto_2 x^2 + \cdots + \propto_{P-1} x^{P-1}. \qquad (3.12)$$

This approximation can be represented by Equation (3.13);

$$f(x) = \sum_{-\infty}^{\infty} c_k \emptyset(x-k). \qquad (3.13)$$

The wavelet orthogonality condition also can be defined for the function *f (x)* as

$$< f(x), \psi(x) > = \sum_{-\infty}^{\infty} c_k < \emptyset(x-k), \psi(x) > \equiv 0. \qquad (3.14)$$

Then, the approximation by scaling functions becomes

$$\propto_0 \int_{-\infty}^{\infty} \psi(x) dx + \propto_1 \int_{-\infty}^{\infty} \psi(x) x dx + \cdots + \propto_{P-1} \int_{-\infty}^{\infty} \psi(x) x^{P-1} dx \equiv 0. \qquad (3.15)$$

Equation (3.15) is valid for all $\propto_j$ $(j = 0,1,2,3 \ldots, P-1)$. For $\propto_1 = 1$ and all other$\propto_j = 0$;

$$\int_{-\infty}^{\infty} \psi(x) x^l dx = 0\,, \qquad l = 0,1,2,3, \ldots, P-1. \qquad (3.16)$$

Therefore, the final condition for filter coefficients becomes;

$$\sum_{k=-\infty}^{\infty} (-1)^k a_k k^l = 0, \qquad l = 0,1,2,\dots,P-1). \tag{3.17}$$

The filter coefficients are defined by Equations (3.6), (3.8), and (3.17), they form the scaling function $\emptyset(x)$ for different wavelet systems. Some examples of scaling functions and wavelet functions are shown in (Figure 3.2).

Daubechies wavelet system and construction of scaling functions will be discussed in the following section.

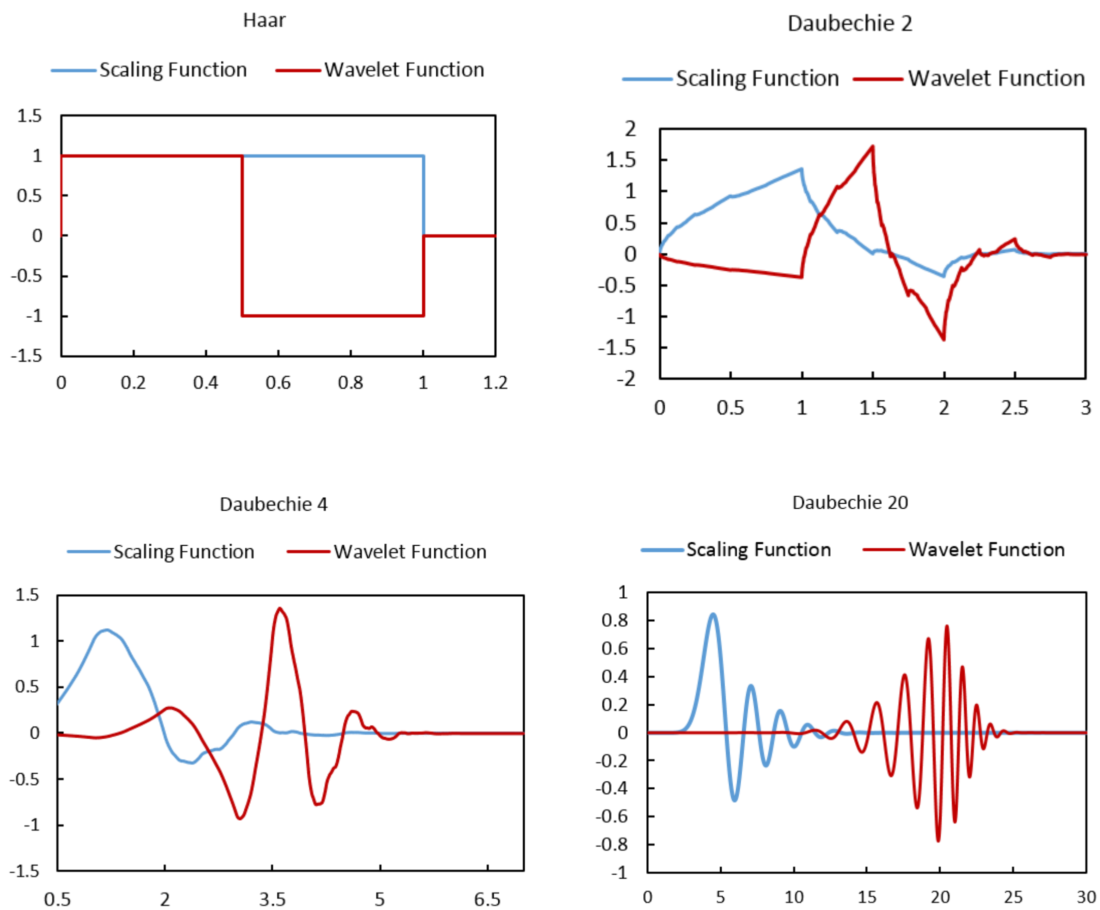

Figure 3.2 Scaling functions and wavelet functions.

3.4 Daubechies Wavelets (dbN)

As it was explained earlier, orthonormal wavelets are required for discrete wavelet transform. Therefore, selection of an appropriate wavelet for decomposition and best representation by coefficients is very crucial. Wavelet families are classified by their basis functions that are based on the number of nonzero elements, in other words their compact size support and the number of vanishing moments. The size support of a wavelet indicates the length of its filter and the vanishing moment of a function is related to how that function decays toward infinity, to its rate of decay (Liu, 2010). Having fewer nonzero elements within the basis function makes it easier to capture irregularities in the function. Therefore, Daubechies wavelets were selected for discrete wavelet analysis, because they have the minimum size support for a given number of vanishing moments, and they can represent more complex functions (Daubechies, 1992).

Daubechies family is a hierarchy of wavelets that are classified by number of their vanishing moments. The simplest wavelet in hierarchy is Daubechies 1, also called Haar wavelet, and its both scaling function and wavelet function are discontinuous. All the other wavelets within the hierarchy (db2, db4, db7, etc.) are continuous and compactly supported, also the smoothness of their scaling function and wavelet function increase with the number of vanishing moments (Boggess, 2009). The wavelet function used in this research is Daubechies 4 (*db4*) which is the simplest and most localized Daubechies wavelet within the family and it has only four filter coefficients and they are highly localized in time.

3.4.1 Construction of db4 scaling function and wavelet

The design of Daubechies 4 orthogonal wavelet system includes the set of constrains on filter coefficients. These constrains are expressed as

$$a_0 + a_1 + a_2 + a_3 = 2, \tag{3.18}$$

$$a_0^2 + a_1^2 + a_2^2 + a_3^2 = 2, \tag{3.19}$$

$$a_0 - a_1 + a_2 - a_3 = 0, and \tag{3.20}$$

$$-a_1 + 2a_2 - 3a_3 = 0. \tag{3.21}$$

The filter coefficients are the solutions of the set of equations from (3. 18) to (3.21) and can be expressed as

$$a_0 = \frac{1+\sqrt{3}}{4\sqrt{2}}, \qquad a_1 = \frac{3+\sqrt{3}}{4\sqrt{2}}, \qquad a_2 = \frac{3+\sqrt{3}}{4\sqrt{2}}, and \qquad a_3 = \frac{1+\sqrt{3}}{4\sqrt{2}}. \tag{3.22}$$

There are two solutions to Equations (3.18) - (3.21); the first solution gives the scaling filter coefficients whereas the second solution gives the wavelet filter coefficients which are the reflection of scaling filter coefficients.

These four wavelet filter coefficients (a_0, a_1, a_2, a_3) are highly localized in time. Transformation matrix, $[W]$ of db4 filter coefficients can be defined as

$$[W] = \begin{bmatrix} a_0 & a_1 & a_2 & a_3 & 0 & 0 & 0 & 0 & 0 & 0 & 0 \\ a_3 & -a_2 & a_1 & -a_0 & 0 & 0 & 0 & 0 & 0 & 0 & 0 \\ 0 & 0 & a_0 & a_1 & a_2 & a_3 & 0 & 0 & 0 & 0 & 0 \\ 0 & 0 & a_3 & -a_2 & a_1 & -a_0 & 0 & 0 & 0 & 0 & 0 \\ 0 & 0 & 0 & 0 & 0 & 0 & \dots & 0 & 0 & 0 & 0 \\ 0 & 0 & 0 & 0 & 0 & 0 & 0 & a_0 & a_1 & a_2 & a_3 \\ 0 & 0 & 0 & 0 & 0 & 0 & 0 & a_3 & -a_2 & a_1 & -a_0 \\ a_2 & a_3 & 0 & 0 & 0 & 0 & 0 & 0 & 0 & a_0 & a_1 \\ a_1 & -a_0 & 0 & 0 & 0 & 0 & 0 & 0 & 0 & a_3 & -a_2 \end{bmatrix}. \tag{3.23}$$

There are two filters in the transformation matrix $[W]$, first one is a smoothing filter (a, a_1, a_2, a_3), which is moving average of four points, whereas second filter, $(a_3, -a_2, a_1, -a_0)$ is the quadrature mirror filter of smoothing filter. The results in the output of smoothing filter represents the data's smooth/approximation information, and results of high-pass filter represents the data's detail information.

To have a perfect reconstruction of the original vector/data/signal from approximation and detail information, transformation matrix, $[W]$ is required to be orthogonal, in other words, the transpose matrix is the inverse of $[W]$. Then, the transpose of transform matrix $[W]^{-1}$ can be expressed in terms of filter coefficients as

$$[W]^{-1} = \begin{bmatrix} a_0 & a_3 & 0 & 0 & 0 & 0 & 0 & 0 & 0 & -a_2 & a_1 \\ a_1 & -a_2 & 0 & 0 & 0 & 0 & 0 & 0 & 0 & a_3 & -a_0 \\ a_2 & a_1 & a_0 & a_3 & 0 & 0 & 0 & 0 & 0 & 0 & 0 \\ a_3 & -a_0 & a_1 & -a_2 & 0 & 0 & 0 & 0 & 0 & 0 & 0 \\ 0 & 0 & a_2 & a_1 & 0 & 0 & \dots & 0 & 0 & 0 & 0 \\ 0 & 0 & a_3 & -a_0 & 0 & 0 & 0 & a_0 & a_3 & 0 & 0 \\ 0 & 0 & 0 & 0 & 0 & 0 & 0 & a_1 & -a_2 & 0 & 0 \\ 0 & 0 & 0 & 0 & 0 & 0 & 0 & a_2 & a_1 & a_0 & a_3 \\ 0 & 0 & 0 & 0 & 0 & 0 & 0 & a_3 & -a_0 & a_1 & -a_2 \end{bmatrix}. \qquad (3.24)$$

After calculating wavelet coefficients by transforming a pressure signal, a potential challenge is relating wavelet coefficients' trend to different events occurring within the reservoir or during the execution of the fracturing jobs in the real-time analysis. Correlating different events with a specific frequency band is a crucial step in wavelet analysis. Each decomposition level indicates a specific frequency band, and this frequency range decreases by half at each decomposition level. Since the analyzed signal needs to be in dyadic length (2^j) for DWT, the theoretical maximum possible decomposition level (DL) can be determined by

$$DL_{max} = \log_2 N, \tag{3.25}$$

where N is signal length (Lei, 2013). However, it is more important to determine the optimum decomposition level to be analyzed.

3.5 Pseudo-frequency

While Fourier transformation gives the frequency spectrum of a given signal, discrete wavelet transformation provides the scale spectrum. Significant advantage of wavelet transformation is separating a group of frequencies and knowing their occurrence time. In order to know the frequency band of each decomposition level, the relationship between scale and frequency, which is the corresponding frequency of each scale at each level, should be known. The frequency that is associated with the wavelet at the specific scale "a" is called pseudo-frequency (Abry, 1997) and it is calculated as

$$F_a = \frac{F_c}{\Delta\, a}, \tag{3.26}$$

where F_a is the pseudo-frequency related to the scale a with the unit of Hz, Δ is the sampling period, and F_c is the center frequency or dominant frequency of a wavelet in Hz. F_c is defined as the frequency with the highest amplitude in the Fourier transform of the wavelet function. Some examples of the center-frequency of the wavelets can be seen in Figure 3.3. Center-frequency of Daubechies 4 wavelet (*db4*) is 0.71 Hz.

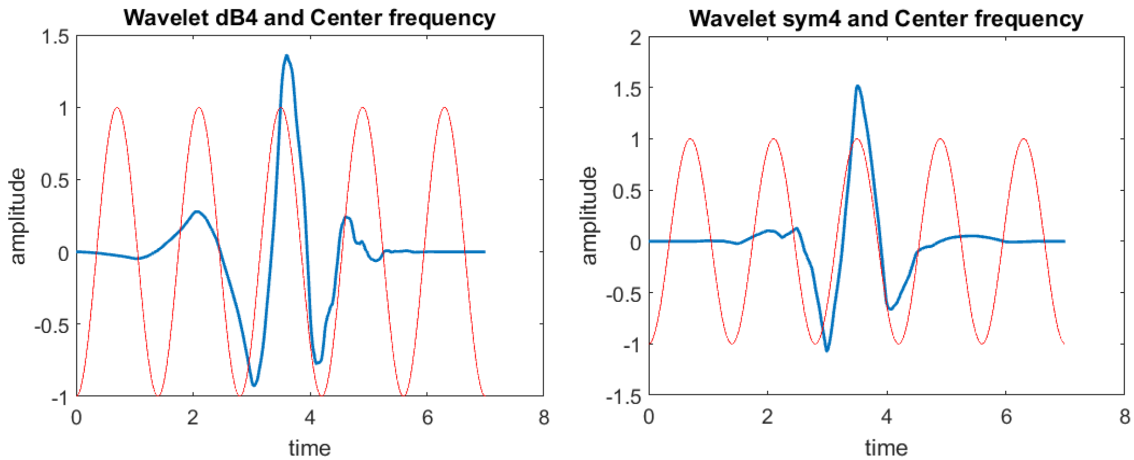

Figure 3.3 Daubechies 4 and Symlet 4 wavelets and their center frequencies.

Based on the sampling rate, the type of the wavelet used (db4), and the level scale one may obtain the frequencies at each level in Table 3.1 using Equation (3.26). This table shows the frequency bands that each decomposition level captures by Daubechies 4 wavelet and it is used to distinguish various fracturing events and their frequency bands.

Table 3.1 Pseudo-frequency decomposition of Daubechies4 wavelet (db4) (Sampling Rate=1 sec)

Decomposition Level, (j)	Scale, a (2^j)	Fa (Hz)	Period sec	Period min
0	1	0.71	1.41	0.023
1	2	0.355	2.82	0.047
2	4	0.1755	5.63	0.094
3	8	0.08875	11.27	0.188
4	16	0.044375	22.54	0.376
5	32	0.022188	45.07	0.751
6	64	0.011094	90.14	1.502
7	128	0.005547	180.28	3.005
8	256	0.002773	360.56	6.009
9	512	0.001387	721.13	12.019
10	1024	0.000693	1442.25	24.038

3.6 Energy Density Plots

Pressure measurements are collected in the time domain, and the techniques such as Fourier Transform and wavelet analysis are used to convert information into the frequency/wavelet domain. The main reason to analyze pressure data in wavelet domain is to provide more information under visual inspection that would be unavailable in the time domain. For example, transients in the time domain might be difficult to determine visually, due to the overlapping of noise events, but, in the frequency/scale domain, the amplitude of the transients are associated with the specific frequency of the phenomenon involved, and thus can be easily recognized/determined. Therefore, Fourier Transform analysis is very beneficial in determining the corresponding frequency of each occurring transient. However, during Fourier Transform analysis, all the time information of transients occurred is lost. On the other hand, wavelets allow for the collection of frequency information on a number of scales, and they preserve time information about the occurrence of transients. Representation of any data in the frequency domain can be achieved by Power Spectrum Density (PSD). PSD shows the strength of the variations (energy) as a function of frequency. PSD is one of the most widely used methodology to define corrosion type and corrosion rate from Electrochemical Noise (EN) data. Smith et al. (2005) used wavelet transform to detect corrosion type and they utilized wavelet coefficients as Energy Density Plot (EDP) approach.

During Discrete Wavelet Transform, the total energy of the signal is partitioned into all spectral components (i.e., different resolution levels of the signal). Therefore, DWT conserves the energy of the signal. Parseval's theorem relates the energy of the signal to the energy in each of the components and their wavelet coefficients (Burrus, 1998). For a discrete signal of length N, with the data points a_i, the total energy of the signal can be given by

$$E = \sum_{i=0}^{N-1} |a_i|^2. \qquad (3.27)$$

Also, energy of the details and approximations at level l can be presented as

$$E_i^d = \sum_{j=1}^{M} \left|d_{ij}\right|^2, i = 1,2, \ldots\ldots, l \text{ and} \qquad (3.28)$$

$$E_l^a = \sum_{j=1}^{M} \left|a_{lj}\right|^2, \qquad (3.29)$$

where *i* is the wavelet decomposition level up to *l*. M is the number of the coefficients of details, approximations at each decomposition level. E_i^d is the energy of the detail coefficients at decomposition level *l* and E_l^a is the energy of the approximates at decomposition level *l* (Smith, 2005). In Smith's study, the ratio of the details' energy to signal's total energy is defined as fraction of total energy and the plot of it (EDP) is used to gather information about relative energies associated with different levels.

Figure 3.4 shows an example of EDP. In the figure, the horizontal axis represents the energy of each decomposition level, and the vertical axis shows the fraction of the energy at that level to the total energy of the signal. This plot is generated by dividing Equation (3.28) by Equation (3.27).

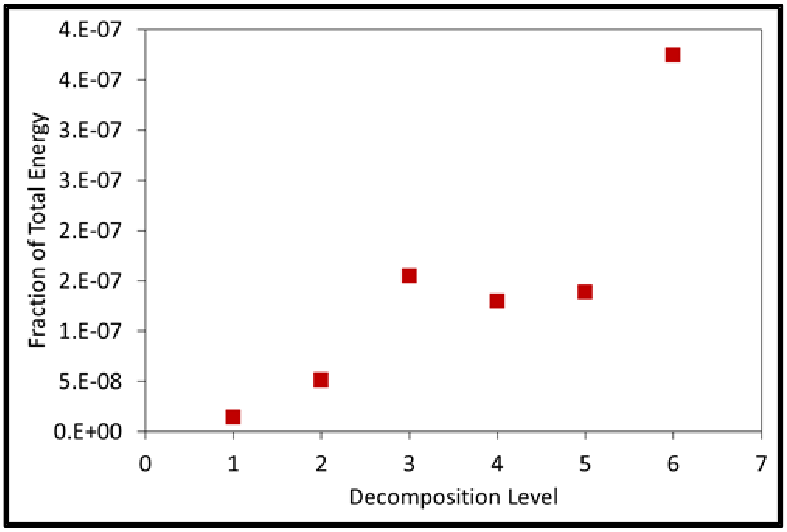

Figure 3.4 Energy Density Plot (EDP).

The energy of the signal is computed by conducting the wavelet transform of the signal and computing the energy of each detail coefficient track. Because each detail coefficient track represents a range of frequency, energy of each detail coefficient track (frequency band) represents the quantity and strength of the events in that frequency band, thereby localizing the events to a certain frequency band. The fractions of the total energy are computed by dividing the energy in each track by the original signal energy. The Energy Density Plots (EDP) are then constructed by plotting the fraction vs detail level to find trends in the energy of detail coefficients. Aballe *et al.* (1999) used this technique for the corrosion process to analyses the noise from electrochemical data. Using the same methodology, Smith and Macdonald (2005) showed that the percentages of the energy from the detail coefficients could reveal unexpected changes in the signal recording.

CHAPTER IV

FIELD DATA APPLICATIONS

This chapter presents applications and interpretations of four hydraulic fracturing operations field data, and two DFITs field data, total of six analysis by wavelet transformation.

4.1 HYDRAULIC FRACTURING INJECTION FIELD CASES

This section demonstrates a successful application of Wavelet Analysis to fracturing pressure data across various conventional and unconventional formations to evaluate post treatment data and enhance future stimulation practices. This methodology was compared to the proven Moving Reference Point (MRP) technique developed by Pirayesh *et al.* (2013), to improve the understanding of wavelet analysis. As a fracturing diagnostic tool, the wavelet analysis technique can also be used as companion diagnostic tool alongside previously published methods (such as MRP etc.).

4.1.1 Problem Statement

Wavelet analysis of a signal is the mathematical decomposition of that signal into orthogonal wavelet components. The level of decomposition is chosen to discern high and low-resolution parts of the signal. The process represents the signal as a sum of translations and scalings of the chosen wavelet to obtain coefficients of each wavelet.

Fracturing treatment pressure signals occur at various frequencies with finite durations that makes it possible to divide the pressure signals into many components and analyze them individually by wavelet transformation. Discrete Wavelet Transformation by Daubechies wavelets was implemented on fracture propagation pressure to various resolution levels to reveal necessary information within the data. The detail coefficients were analyzed by examining the anomalies at various resolution levels.

Wavelet analysis was performed on various shale and conventional fracturing data. Some interesting patterns are readily discernable from the wavelet detail coefficients. For instance, during the injection of proppants, there is an amplitude change in the detail coefficients at the exact moment when the proppant contacts the formation surface. This is expected because wavelet analysis is sensitive to any discontinuity in the system. Furthermore, such amplitude changes are also observed in the analyzed pressure data corresponding to tip screen-out and near wellbore sand-out events. Comparing such events along-side the MRP method paves the way for early detection of screen-out events. A comparison with the MRP technique is also provided in this study. This method reduces the uncertainty in analysis of Nolte-Smith and MRP method by providing an independent estimate of fracture propagation characteristics.

There have been publications discussing wavelet transformations of various formation and reservoir parameters (permeability, reservoir pressure, etc.), and discussing the application of wavelets for noise reduction and data smoothing. However, this is the first study mainly about wavelet analysis of fracture injection pressure data to understand and detect anomalies during various completion treatments. Ultimately, this technique helps to improve treatment designs and efficiency by analyzing fracture and formation behavior of the treatment and enhance decision making during execution, by providing early screen-out detections.

4.1.2 Methodology of Data Analysis

To analyze and reveal anomalies caused by discontinuities within the hydraulic fracturing pressure, one-dimensional discrete wavelet analysis of fracture propagation pressure was performed by implementing discrete wavelet transform algorithm. First, single-level wavelet decomposition of the pressure signal was performed by using Daubechies wavelets that generates the high frequency detail coefficients (*cD1*) and low frequency approximation coefficients (*cA1*) at level 1. As it was discussed earlier, approximation and detail coefficients are the results of high-pass and low-pass filtering processes, and each filtering process eliminates every other data point of the signal. This process is called subsampling and it decreases the sample number by half. After filtering, the original signal can be represented by half of the data points which results in half the time resolution and a double the frequency resolution of the previous level (Valens, 1999).

In order to be able to time localize the anomalies in the signal, time resolution of both the coefficients and the original signal should be same, so the reconstruction of details (*d*) from detail coefficients (*cD*) by upsampling process was required in our analysis. Then, multi-level decomposition of signals was performed to get a hierarchical set of approximations and details of the pressure signal up to an appropriate level, at which useful information can be revealed. Figure 4-1 demonstrates the details and approximation from a multi-level decomposition of pressure data from a hydraulic fracturing treatment up to level-3. Each level captures different level of information from the pressure signal, the higher the level, the detailed the information is, and the original pressure signal (s) is the summation of approximation at level-3 (*a3*), details at level-3 (*d3*), level-2 (*d2*), and level-1 (*d1*). As it can be seen from Figure 4.1 that, detail coefficients demonstrate a peak where an anomaly located within the pressure signal. Even though this anomaly cannot be seen from time-domain representation of the original pressure signal, wavelet transformation unveils this hidden information by sharp changes in detail coefficients. Also, time localization is available within wavelet analysis, therefore it is possible to detect exact time of any discontinuity within the signal.

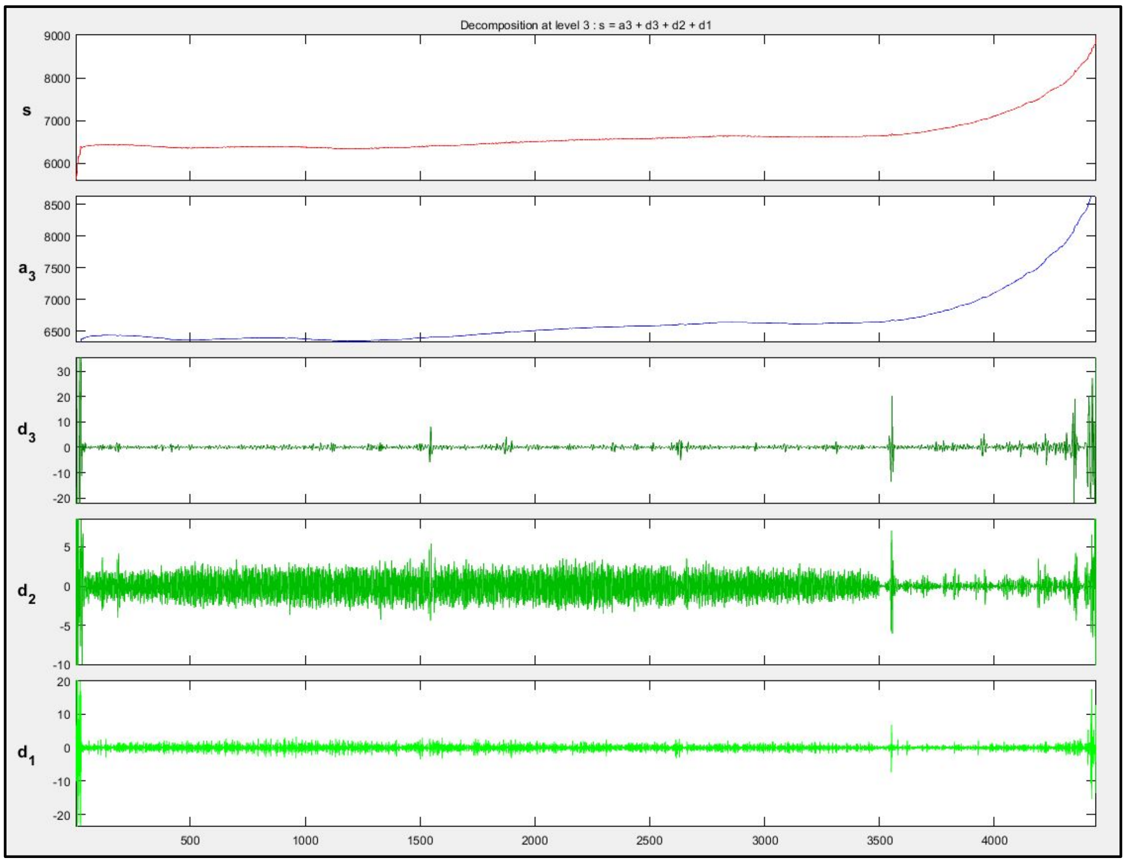

Figure 4.1 Decomposition of fracture propagation pressure at level 3.

Next example presents the application of wavelet analysis on fracture propagation pressure from Cotton Valley tight sandstone and Travis Peak sandstone hydraulic fracturing treatments, two FracPack examples, along with examples from Marcellus and Eagle Ford shale horizontal well fracturing treatments. The findings from wavelet analysis are also compared to MRP method for further evaluation and validation of the diagnostic results. The results demonstrate applicability of wavelet analysis as a diagnostic tool for early detection of key hydraulic fracturing anomalies such as near wellbore screen-out, tip screen-out and fracture fluid loss due to formation heterogeneity.

4.1.3 Field Example 1: Cotton Valley Formation

This example, as shown in Figure 4.2, represents the screen-out during the treatment at around 184 minutes. As discussed earlier in the methodology, details were calculated at various levels by Daubechie7 (db7) and level 3 details (d3) were found to be the most appropriate for detecting any changes in the fracturing system for this case.

Wavelet analysis captured several discontinuities in the fracture propagation pressure from time 112 to 190 minutes. As represented in Figure 4.3, there are two main visible anomalies (peaks) shown by the d3 details at various instances during the fracture treatment. The first peak occurs around 138 minutes, which corresponds to the start of the proppant ramp up schedule ((Figure 4.4 (a)). The minute difference in the start of the proppant ramp up from the actual treating plot and the wavelet analysis, can be attributed to the travel time (about 2 minutes) of the proppant from the sand auger to the wellhead (Figure 4.4(b)). Then at the 171 minutes, the second spike anomaly occurs, which in this case is the first visible sign of a screen out effect.

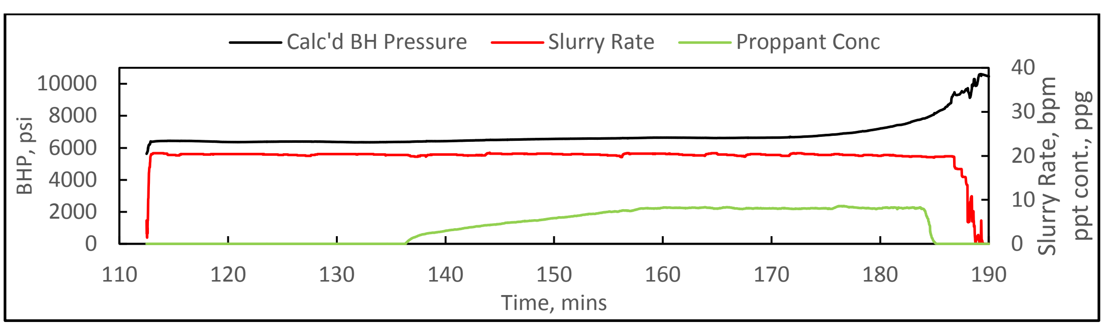

Figure 4.2 Example 1 Cotton Valley formation treatment schedule.

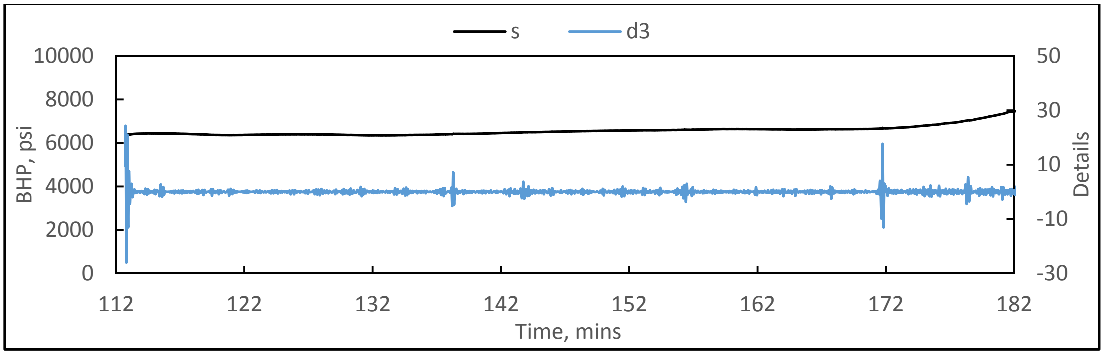

Figure 4.3 Example 1 Cotton Valley formation wavelet analysis vs. BHP.

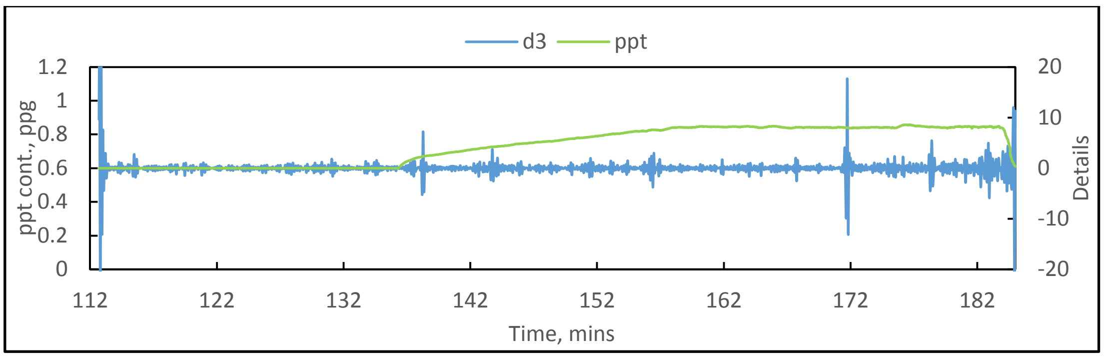

(a)

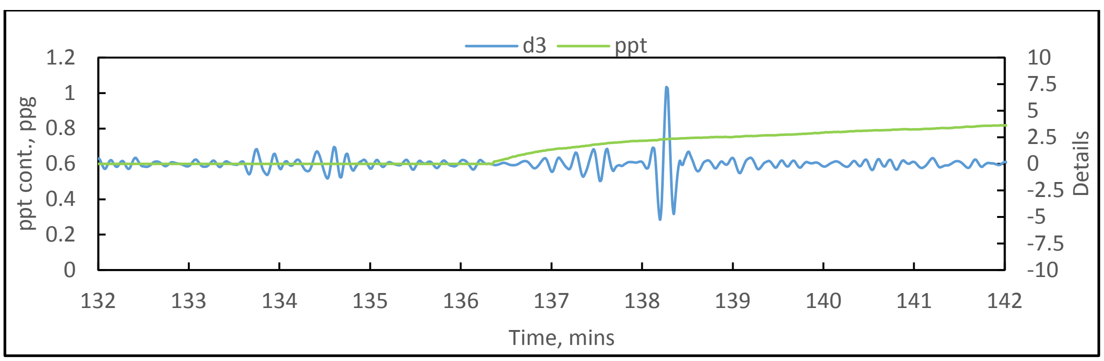

(b)

Figure 4.4 (a) Example 1 Cotton Valley formation wavelet analysis vs. proppant concentration (b) zoom.

According to MRP method application to Cotton Valley sand by Al- Husain et al., e-time plot detected sanding out symptoms at approximately 174 min. (Figure 4.5 (a)). This is based on 200 period-point moving average of the calculated e values of 1 that is an indication of dilation and sanding out (Pirayesh *et al.*, 2015).

In comparison, wavelet analysis is capable of detecting the same pressure anomaly 2 minutes earlier which equates to almost 13 minutes prior to actual screen-out observation by the operator at 184 minutes (Figure 4.5 (a) and Figure 4.5 (b)). Confirming the validity of wavelet analysis as a fracture diagnostic tool for early screen-out detections in Cotton Valley formation.

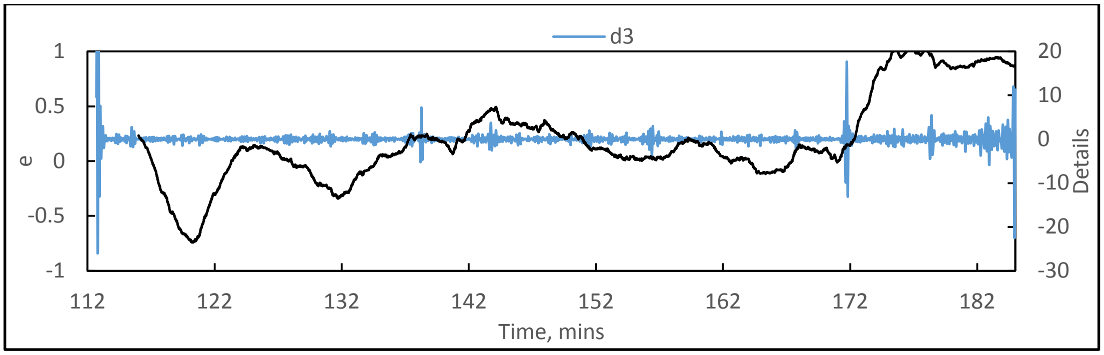

(a)

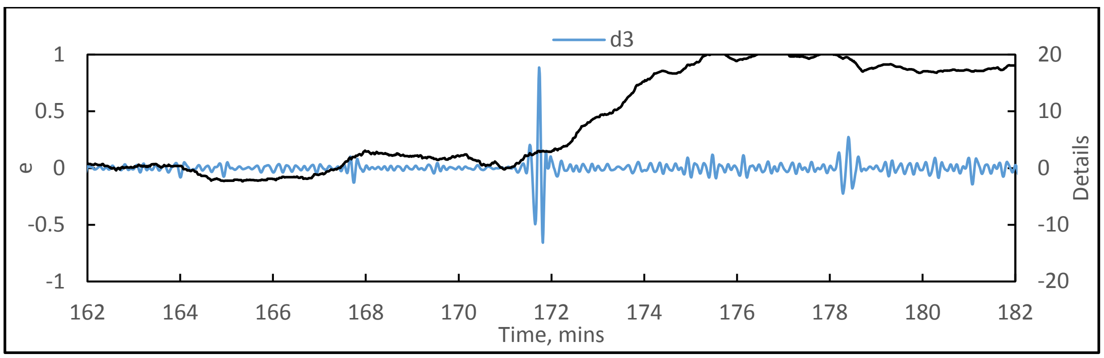

(b)

Figure 4.5 (a) Example 1 Cotton Valley formation comparison of wavelet analysis vs. MRP method (b) zoom.

4.1.4 Field Example 2: Travis Peak Formation

This example references a multilayer shale Travis Peak formation. According to Al-Husain et al. two major fracture height growths are present, and they can be identified by cycles of rapid fracture height growth (represented by e value less than zero) in Figure

4.6. In wavelet analysis the corresponding large amplitude changes can be related to potential severe fluid loss by the impact of natural fractures in the reservoir. However, unlike the fluid loss, the effect of dilation of the fractures due to high fluid efficiency and shale ductility cannot be seen in wavelet analysis because there are no high amplitude changes that correspond to those events. As it can be seen from Figure 4.7(a) that, *d5* details demonstrate spikes when MRP method shows severe fluid loss trend (such as between 80 to 88 mins, and 100 to 109 mins). However, this correlation is not applicable once proppant is introduced to the fluid system at approximately 110 mins. This is because proppant attenuates the effect of fracture behavior in the pressure signal, which is required to perform wavelet analysis at different details' scale (such as in Figure 4.7 (b)) in order to compute further analysis.

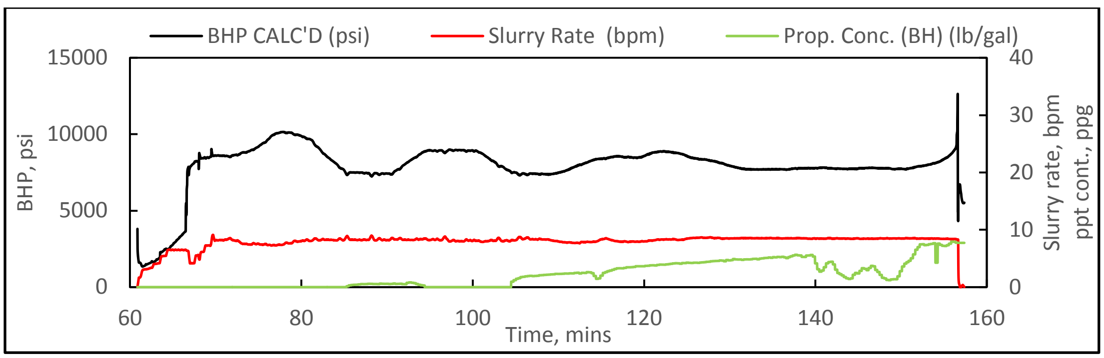

Figure 4.6 Example 2 Travis Peak formation treatment schedule.

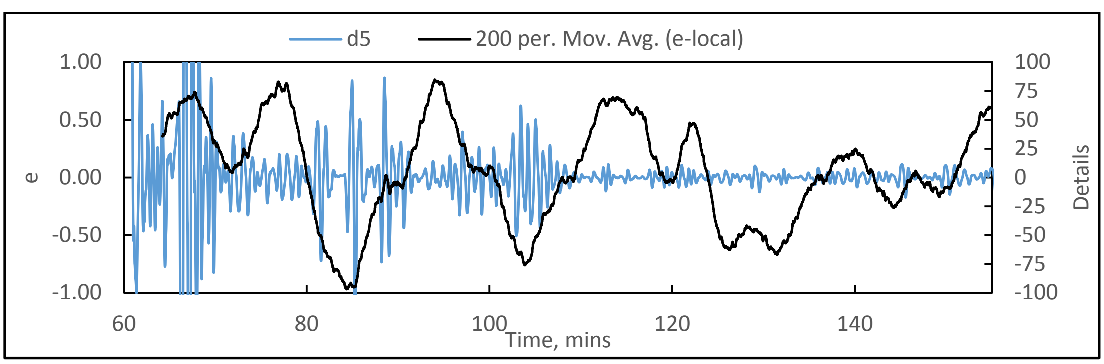

(a)

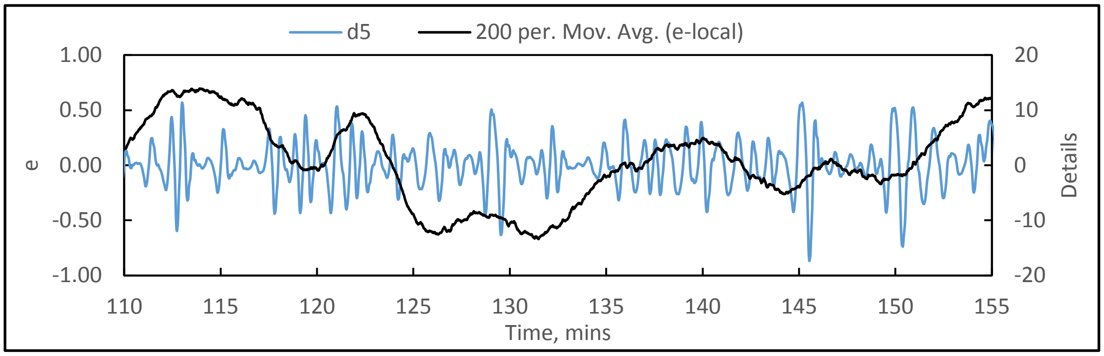

(b)

Figure 4.7 Example 2 Travis Peak formation comparison of wavelet analysis vs. MRP method (b) zoom.

4.1.5 Field Example 3: High Permeability Gas Well Frack-Pack

In this high permeability gas well FracPack example (Figure 4.8), wavelet details demonstrate significant amplitude change at 10 minutes compared to overall trend. In this particular case, fracture packing/tip screen-out initiates at time approximately 11 min. as indicated by the e value reaching to 1 (Pirayesh, et al 2015) in MRP method. Wavelet analysis also demonstrates (Figure 4.9, Figure 4.10) significant change in details amplitude at 10 minutes that validate the wavelet analysis application on FracPack treatments.

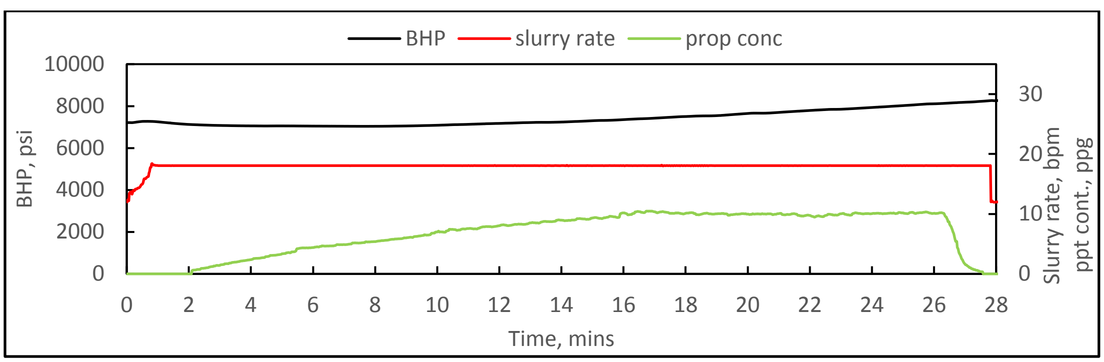

Figure 4.8 Example 3 high permeability gas well frack-pack treatment schedule.

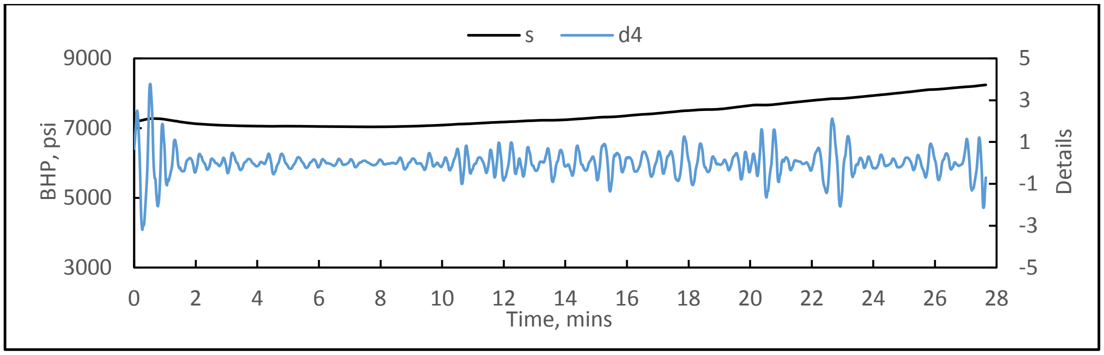

Figure 4.9 Example 3 high permeability gas well frack-pack wavelet analysis vs. BHP.

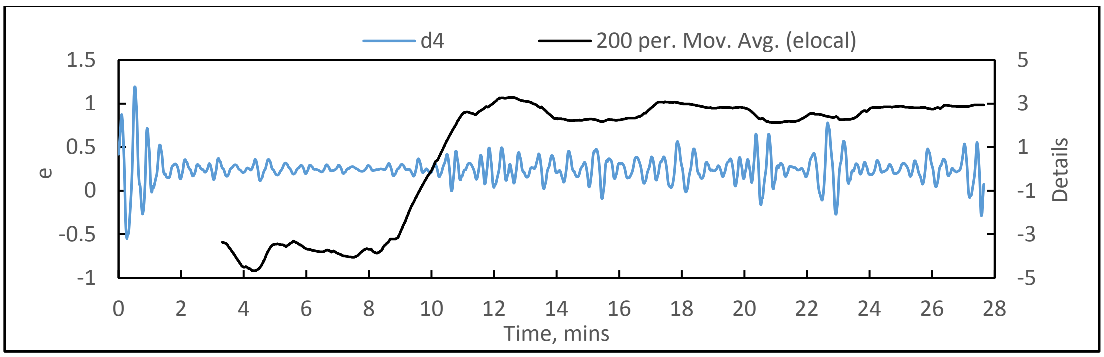

Figure 4.10 Example 3 high permeability gas well frack-pack wavelet analysis vs. MRP method.

4.1.6 Field Example 4: Eagle Ford Shale Formation

This example demonstrates analysis of a hydraulic fracturing treatment (Stage 9) of a 3,800 ft. long horizontal well in Eagle Ford shale (Figure 4.11). Wavelet analysis captures various discontinuities within the pressure signal as a result of natural fractures in the formation. Soliman et al. (2014) identified three major heterogeneities intersecting hydraulic fractures by MRP method as shown in Figure 4.12. There is a relationship in the amplitude of the wavelet details and the MRP e values in results to severe fluid loss and dilation pattern. Even though a correlation is present, there is a potential effect of continuous rate fluctuation on the wavelet analysis. Therefore, further analysis would be required to determine the overall impact of heterogeneity on pressure signal and fracture behavior.

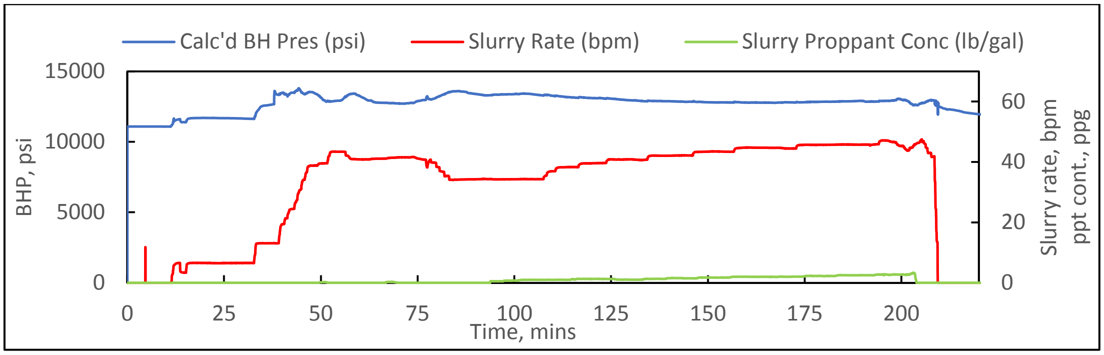

Figure 4.11 Example 4 Eagle Ford formation treatment schedule.

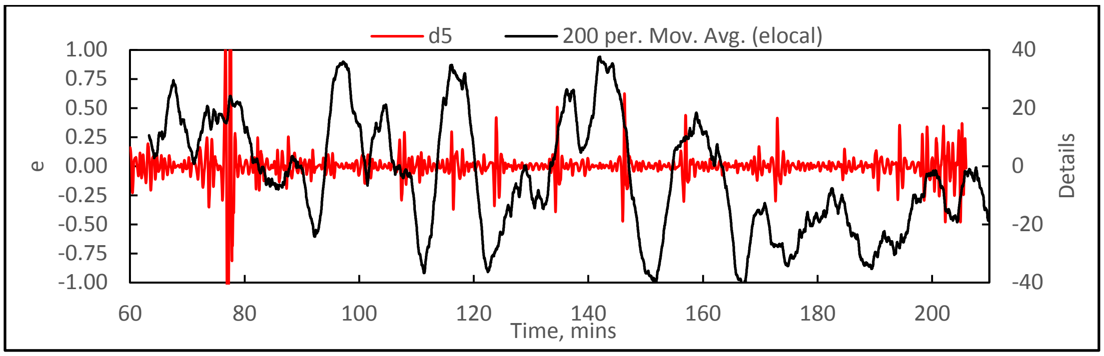

Figure 4.12 Example 4 Eagle Ford formation wavelet analysis vs. MRP method.

4.1.7 Discussions and Conclusions

Based on the results of the completed analysis in different formations, it is evident that wavelet analysis can be used as an effective fracture treatment diagnostic tool that aids the identification of potential hydraulic fracturing problems and fracture behavior anomalies. Furthermore, it provides an independent means of analyzing pressure data. One of the advantages of wavelet analysis is the early detection of screen-out and tip-screen-out anomalies. As it was analyzed in Cotton Valley example, wavelet analysis can capture early signs of a screen-out from pressure data prior to real-time diagnostics based on pressure increase monitoring. This extra time could be an advantage to initiate risk mitigations and troubleshooting techniques to minimize and potentially prevent the negative impact of screen-outs.

Because wavelet analysis is sensitive to any physical changes in pressure signals, once the proppant is introduced to the fracturing treatment system, the results begin to show a significant change in details amplitude as demonstrated in Travis Peak formation field example. Wavelet analysis may also be applicable to identify severe fracturing fluid loss and dilation in conjunction with the MRP method.

4.2 DIAGNOSTIC FRACTURE INJECTION TEST (DFIT) FIELD CASES

In this chapter, DFIT pressure is treated as a non-stationary signal and analyzed by one of the signal processing techniques which is wavelet transformation. The purpose of signal analysis is to extract relevant information from a signal by transforming it. Firstly, the signal is transformed into wavelet domain by Discrete Wavelet Transformation (DWT) to calculate high-frequency wavelet coefficients (details), then change-point detection technique is applied to distinguish major changes within the coefficients trend to determine fracture closure pressure and time.

4.2.1 Problem Statement

DFIT pressure decline data from different wells were analyzed by wavelet transformation. Detail coefficient demonstrates different patterns depending on the formation analyzed and near wellbore activities. This is expected because wavelet analysis is sensitive to any physical changes within the system. From the amplitude changes of the coefficients, wavelet tool demonstrates the fracture closure as a continuing process.

Because wavelet is sensitive to changes in the system, it detects the fracture closure unambiguously by amplitude change, as compared to slope changes in other conventional methodologies. A comparison with some of the most commonly used diagnostic techniques, conventional log-log diagnostic plot, square root time, G-function and its derivative analysis are also provided in this study.

There have been several publications discussing various techniques analyzing DFIT pressure decline in unconventional formations and yet there is relatively high uncertainty in before-closure-analysis. However, this methodology is more sensitive to fundamental changes in the system, so application in detecting closure pressure and time decreases the uncertainty compared to other conventional tangential methodologies.

There has been several Before Closure models to analyze pre-closure period since the first model by Nolte (1997), semi-log derivative (G.dp/dG) model by Barree et al. (1996), ($\Delta t dp/d\Delta t$) log-log model by Craig and Blasingame (2006) the holistic approach by Barree et al. (2009), and the variable fracture compliance method by McClure *et al.* (2014). In addition to before closure models, Marongiu-Porcu et al. (2011) presented a more comprehensive model combining before and after closure models to determine both fracture parameters and reservoir permeability.

The main interest of this chapter is the Before Closure Analysis of the fall-off data to identify fracture closure time and closure pressure by wavelet transformation method. Unlike other methods, wavelet analysis does not require any assumptions regarding to fracture geometry, and it is based on the concept of intermittent fracture propagation and closure phenomena.

4.2.2 Changepoint Detection

Changepoints are times of discontinuities in a time series that can be induced from changes in observation locations, equipment, measurement techniques, environmental changes, and so on (Reeves & Chen, 2007). In other words, a changepoint is an instance where statistical properties before and after this point in time differ. However, these statistical properties of the signal are constant in some sense before and after the change point and demonstrate similar patterns. The concept was first proposed by Page (1954).

Mathematically speaking, for a signal $s_1, s_2, s_3, \ldots s_n$ if a changepoint exists at, then $s_1, s_2, s_3, \ldots s_\tau$ differ from $s_{\tau+1}, s_{\tau+2}, s_{\tau+3}, \ldots s_n$ in some way. These differences may be the changes in: mean, variance or root mean squared values.

Changepoint procedure

Changepoints are computed by minimizing a suitable contrast function using discrete optimization of the sum of appropriate cost function of the segment of the signals. The contrast function V is expressed as the sum of costs of the signal segments in Equation (4.1)

$$V = \sum_{k=0}^{K} cost\left(y_{t_k \ldots t_{k+1}}\right), \tag{4.1}$$

where, K is the total number of changepoints, and y_{t_k} are the segments of the signal. The cost function measures the goodness of fit of each segment. The simplest cost function is the sum of squared residuals after a linear fit.

The procedure starts by dividing the signal into K segments. An estimate of the statistical property (such as variance) is computed. The deviation of the property is determined for each segment; and residuals are computed, which becomes the cost function, and the sum of all cost functions yield the contrast function. Finally, the location of the segments is varied until the cost function is minimized. Bai (2006), Chen and Gupta (1997, 2011) and Truong *et al*. (2018) discussed the topic more in details.

Figure 4.13 shows a signal that was constructed from normally distributed random numbers with a variance of 1 for the first 100 points, a variance of 2 for the next 100 points, and finally a variance of 10 for the last 100 points. Using the methodology described above, two changepoints are detected based on those variance changes i.e. at time = 100 and time = 200 which demonstrates the successful application of the method.

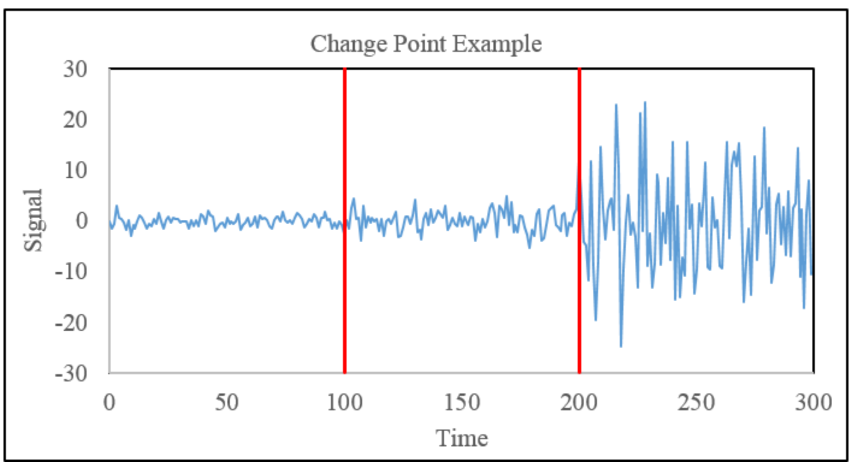

Figure 4.13 Signal with two distinct variance changes. Red lines show the detected change points.

Changepoint Detection of Wavelet Events

After obtaining multiresolution analysis of the fall-off pressure data using Daubechies wavelet, detail coefficients of various levels were analyzed by changepoint detection technique. Changepoint detection was used to identify sudden changes based on the standard deviation changes in the detail coefficients. During fracture closure mechanism, the fundamental changes occurring are due to physical changes in the environment. Once the fracture is fully closed, a change in the variance of details coefficient will occur, and this change will be captured by the change point detection technique. Therefore, the exact time corresponding to the detected change of variance, fracture closure time can be determined. Due to their time-frequency localization property, wavelet transformation can efficiently localize such changes and the changepoint detection can segment the signal in wavelet domain.

Because the change point detection algorithm is designed to search for changes in variance, it works automatically in identifying such changes. This avoids any unwanted bias from the analyst. Moreover, change point detection can also identify other such events that cause vibrational changes.

4.2.1 Application to DFIT: Test 1

Figure 4.14 presents the job chart of the DFIT 1. In this breakdown job 20.18 bbl. of treated water was injected into the formation causing a breakdown of the formation and propagation of the created fracture. The injection was followed by a shut-in (fall-off period) as shown in Figure 4.14.

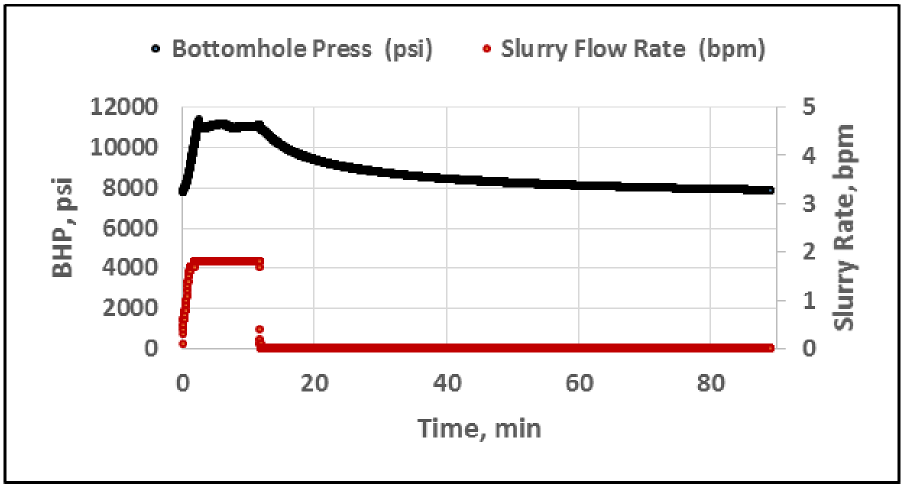

Figure 4.14 Job Chart Breakdown Test.

G-function Analysis

The $G\frac{dp}{dG}$ versus G plot (Figure 4.15 (a)) indicates normal formation behavior with fairly quick closure occurring at closure pressure of about 10,305 psi and at 140 seconds. Also, square-root time analysis indicates a closure pressure of 10,206 psi at 164 seconds (Figure 4.15 (b)).

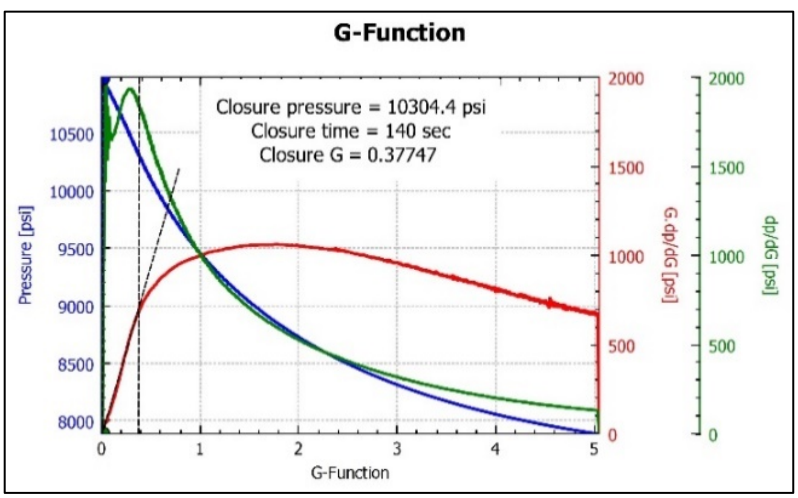

(a)

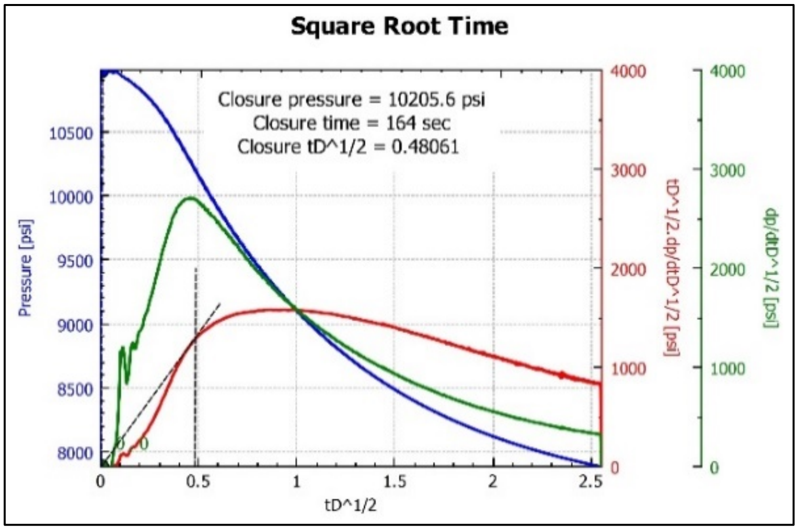

(b)

Figure 4.15 (a) G-function Analysis (b) Square Root Time Analysis of DFIT 1.

Log-Log Plot

Log-Log plot in Figure 4.16 indicates wellbore storage by its significant characteristic unit slope on both pressure difference and pressure derivative curves immediately before closure. Also, the development of a short fracture linear flow line with a slope of ½ on the derivative can be observed (Bachman et al. (2007)). Departure from this ½ slope straight line yields a closure pressure of 10,200 psi at 170 seconds. Also, log-log plot indicates a formation linear flow regime at time 2,000 seconds.

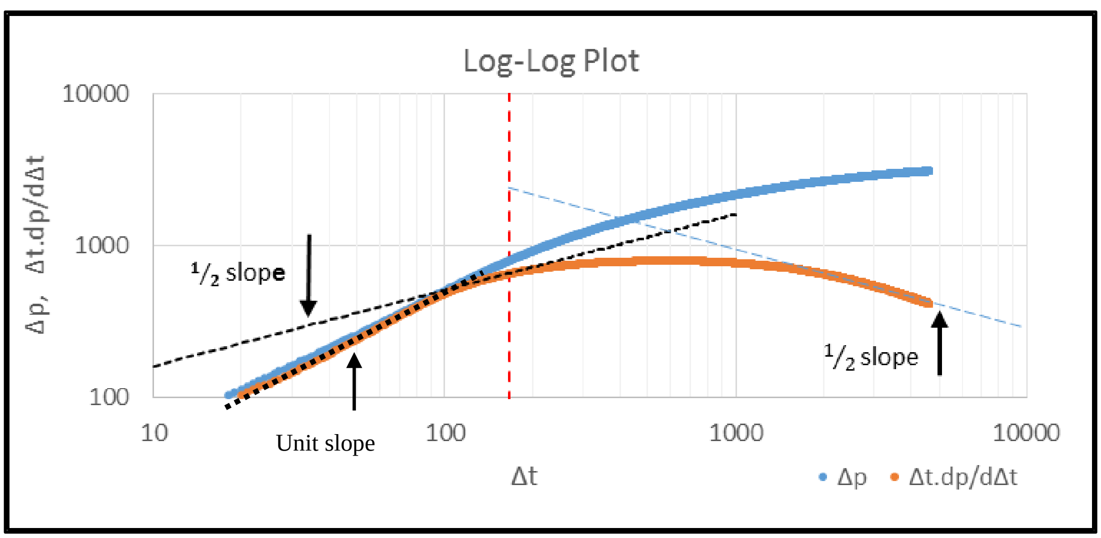

Figure 4.16 Log-Log Plot of DFIT 1.

Wavelet Analysis

As discussed earlier in the methodology, the first step in wavelet analysis was calculation of high-frequency component of the fall-off pressure data, i.e. the detail coefficients (*cD*) which represent any of the physical changes in the system, discontinuities, and singularities hidden in pressure behavior. These physical changes are represented by the amplitude variations in detail coefficients (variance of detail coefficients) at various decomposition levels. It can be seen from Figure 4.17 that, detail coefficients at level 5 (*d5*) demonstrate high amplitude variations at the beginning of fall-off period similar to water-hammer effect, then the variations diminish with time.

Right after the shut-in, fracture starts to leak-off and the fracture closure is initiated. Fracture closure may not be a smooth phenomenon and reduction in width and height is expected to be intermittent. In addition, fracture closure might not be a single event as is usually assumed, but rather than a continuous process wherein the fracture dimensions get smaller during the closure process, this process was discussed by Soliman and Daneshy (1991). The situation can be significantly more complex in case of fractured shale formations, where hydraulic fracture cannot be planar, but very complex.

Because of these intermittent closure events, wavelet transform captures various events and represents the whole closure by variations in detail coefficients. The full closure event can be captured by wavelet analysis, since after the full closure there would not be any physical changes in the system resulting in no amplitude variations in detail coefficients.

As it can be seen in Figure 4.17 (a) and (b), (*d5*) details show a high variation pattern until 10 minutes, and there is no variation after that. After obtaining multiresolution analysis of the fall-off data, in order to find the exact change point locations, overall change of variance was applied to wavelet coefficient (*d5*). The change-point detection methodology captures two main changepoints in detail coefficients, CP1 and CP2 at 1.68 minutes (100 sec) and 9.18 minutes (548 sec), respectively. Variance of (*d5*) before and after CP1 is easily seen in Figure 4.17(a) which demonstrates the detail coefficients variations in a larger details scale compared to Figure 4.17(b).

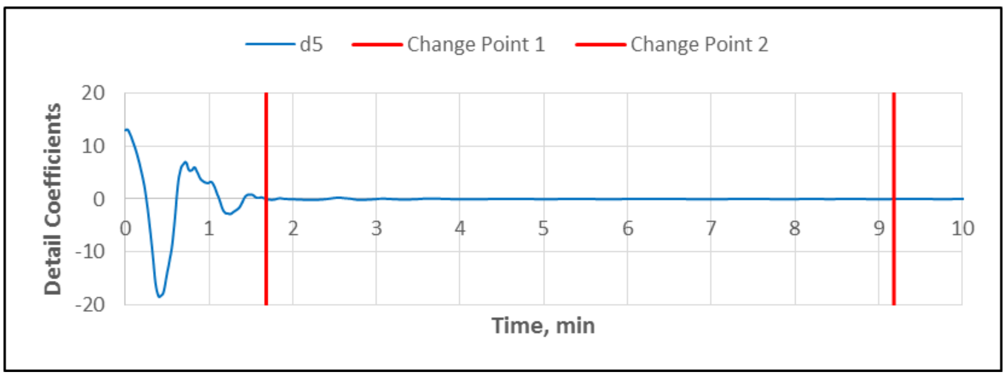

(a)

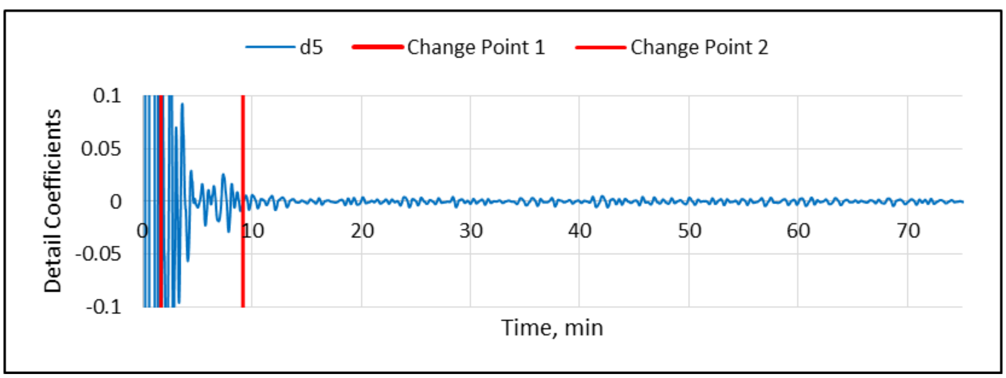

(b)

Figure 4.17 (a) Wavelet Analysis of DFIT 1 (b) zoom.

When we compare all the diagnostic techniques (Table 4.1) to determine fracture closure time and pressure, G-function derivative, Sqrt (t), log-log plot, and wavelet analysis demonstrate very similar results capturing the closure event at CP1. However, unlike other techniques, wavelet analysis reveals more information and captures another event at CP2 which can be explained by the end of full closure of the fracture. In addition, while log-log plot demonstrates the formation linear flow regime at 2,000 seconds, wavelet analysis does not capture that flow transition period by detail coefficients. Wavelet coefficients have smooth and constant trend after 10- minute due to no physical changes in the system.

Table 4.1 Comparison of DFIT 1 Analysis.

		G-function	**Sqrt (t)**	**Log-log**	**Wavelet**
Closure 1	**Closure P. (psi)**	10,305	10,206	10,200	10,487
	Closure t. (sec)	140	164	170	100
Closure 2	**Closure P. (psi)**	-	-	-	9,307
	Closure t. (sec)	-	-	-	548

4.2.2 Application to DFIT: Test 2

Figure 4.18 illustrates the job chart of the DFIT 2. Compared to DFIT 1, this test was a follow up test after a breakdown injection test. In this job approximately 60.5 bbls of treated water was injected into the formation causing the opening of the existed fractures/fissures, creating new fractures and intersecting existed fractures resulting in more complex fracture network. The injection was then followed by a shut-in (fall-off) period as shown in Figure 4.18.

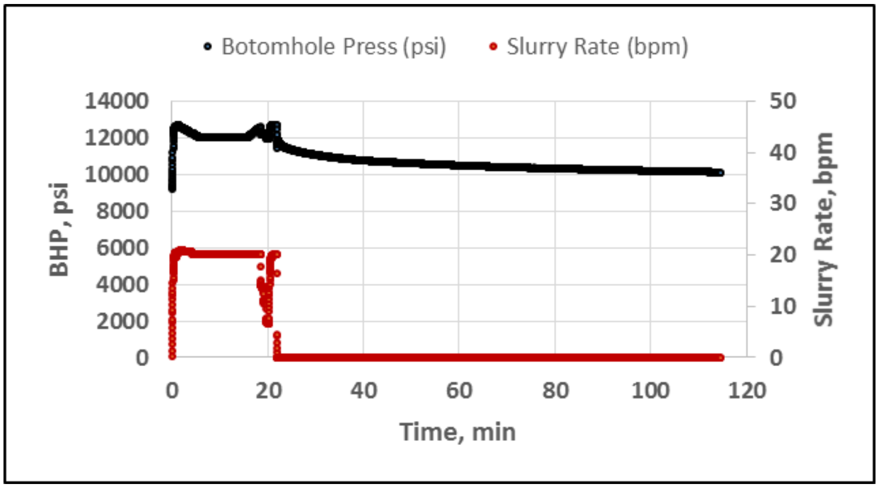

Figure 4.18 Job Chart DFIT 2.

G-function Analysis

According to G-function analysis, there are multiple fracture closure events. The first observation from the analysis is the hump of G-function derivative curve which is a signature of fissure opening. The closure of the first fracture network can be expressed by the deviation of G-function derivative curve from the straight line at 34 minutes (2,036 seconds) or at 44 minutes (2,650 seconds) depending on the interpretation of the analyst (Figure 4.19(a) and (b)). Square root time plot also confirms the same fracture closure parameters at 34 minutes (2,038 seconds)-10,542 psi and at 44 minutes (2,653 seconds) - 10,436 psi.

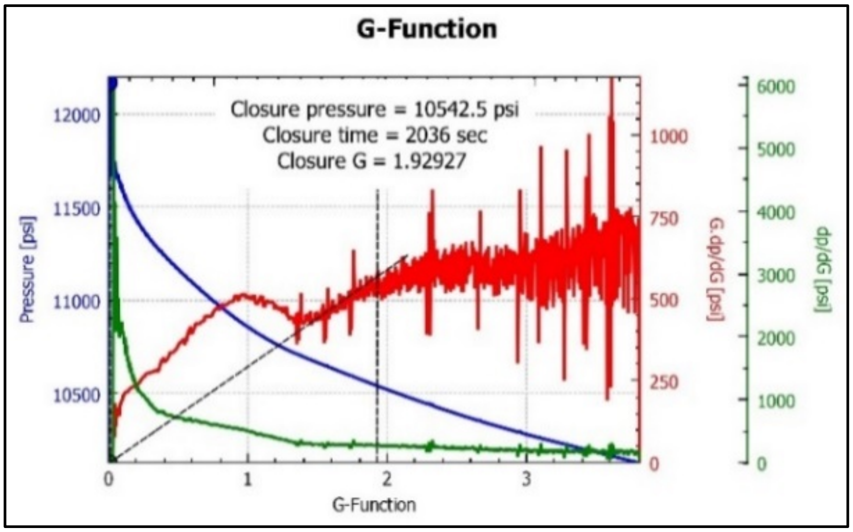

(a)

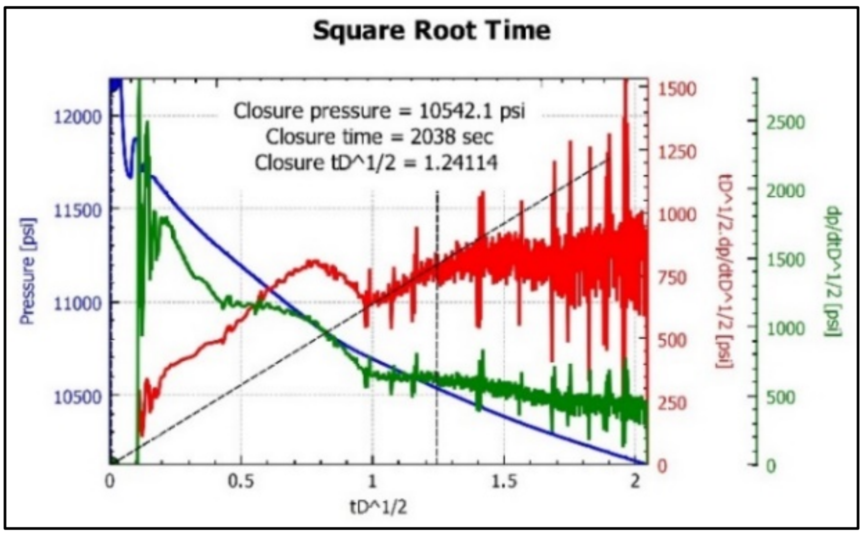

(b)

Figure 4.19 (a) G-function (b) Sqrt (t) of DFIT 2.

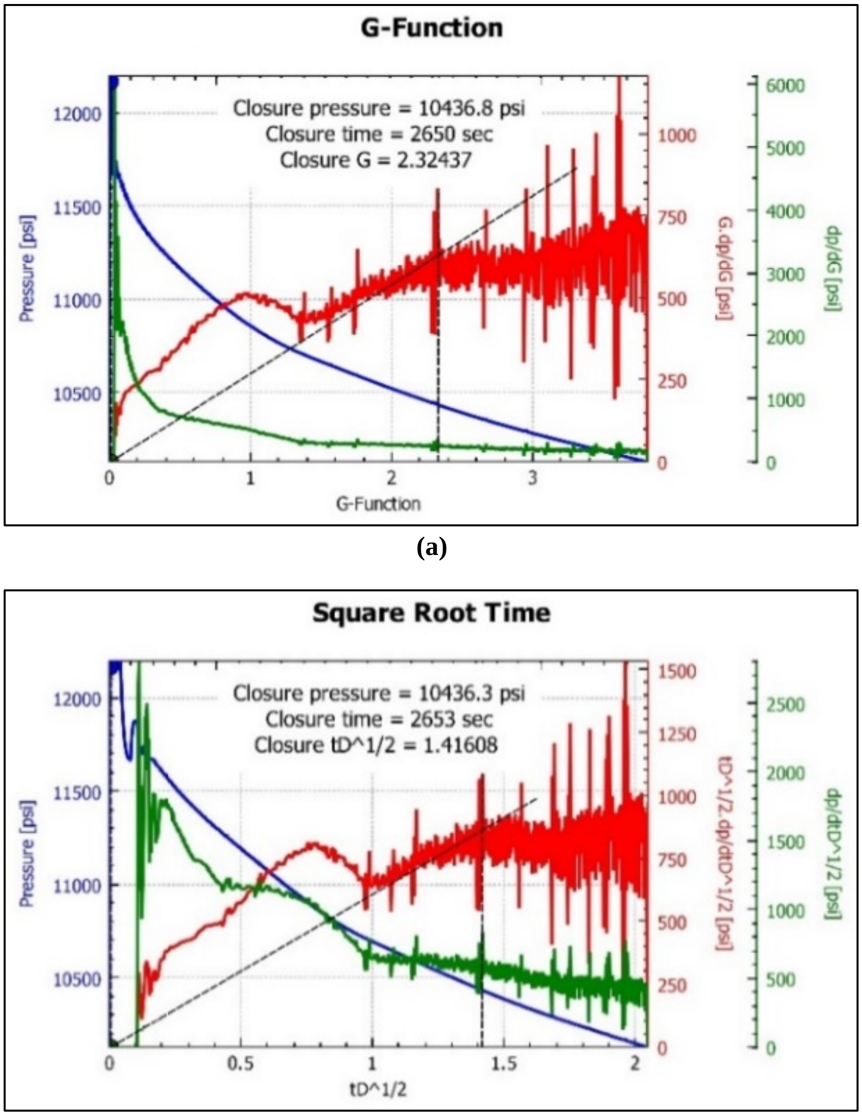

(a)

(b)

Figure 4.20 (a) G-function (b) Sqrt (t) of DFIT 2.

It is also possible to apply G-function and square root of time methodologies and identify another fracture network at time 90 mins (5,400 sec) and obtain closure at 5,415 seconds with closure pressure 10,141 psi. These two tangential methods are very sensitive to localization of the line, departure from this straight line and mainly it depends on the interpretation. Also, smoothing the data could result in different interpretation and it could increase the uncertainty of the analysis.

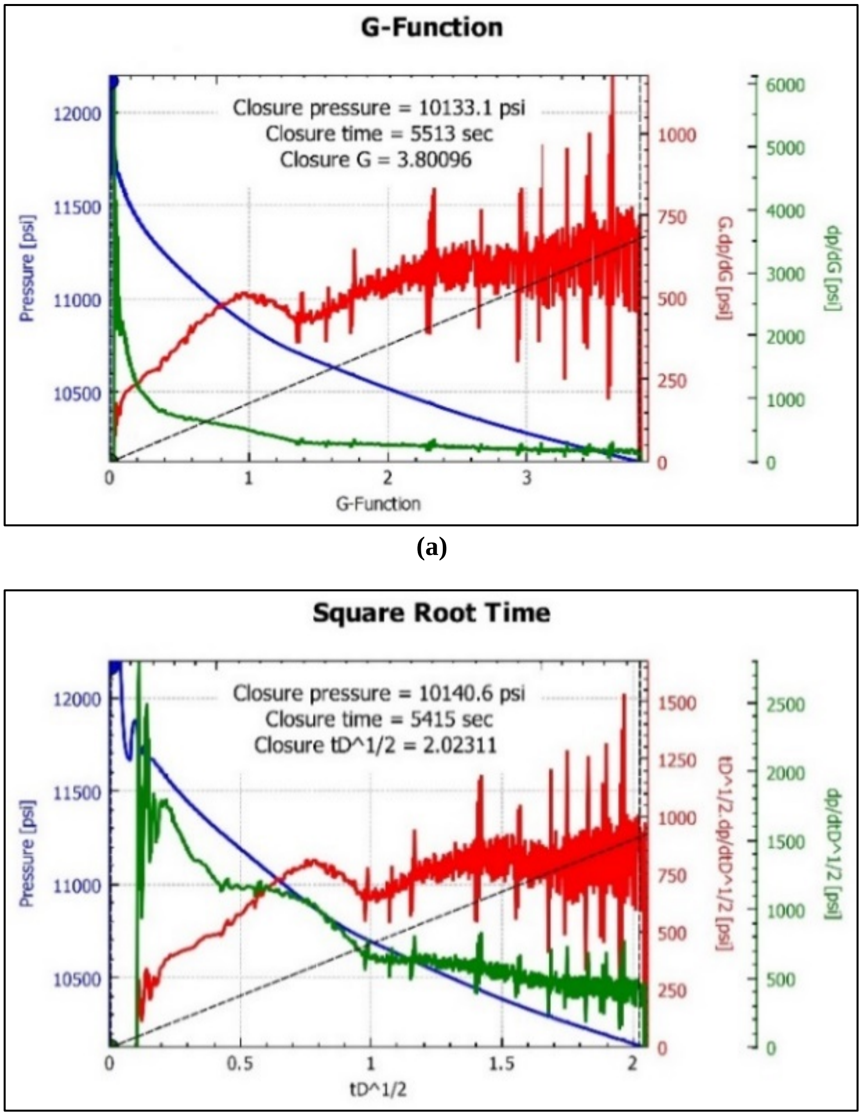

(a)

(b)

Figure 4.21 (a) G-function (b) Sqrt (t) of DFIT 2.

Log-Log Analysis

It can be also seen from log-log plot (Figure 4.22) that, 3 different fracture linear-flow regimes can be determined by ½ slope at three different times. Deviations from first two ½ slopes occurs at 600 seconds and 2,050 seconds, respectively. On the other hand, no deviation from ½ slope is observed during the 3rd fracture linear flow. In addition, log-log plot does not reach to zero slope, or does not deviate from half slope, therefore it can be said that the flow regime is still in the fracture linear flow.

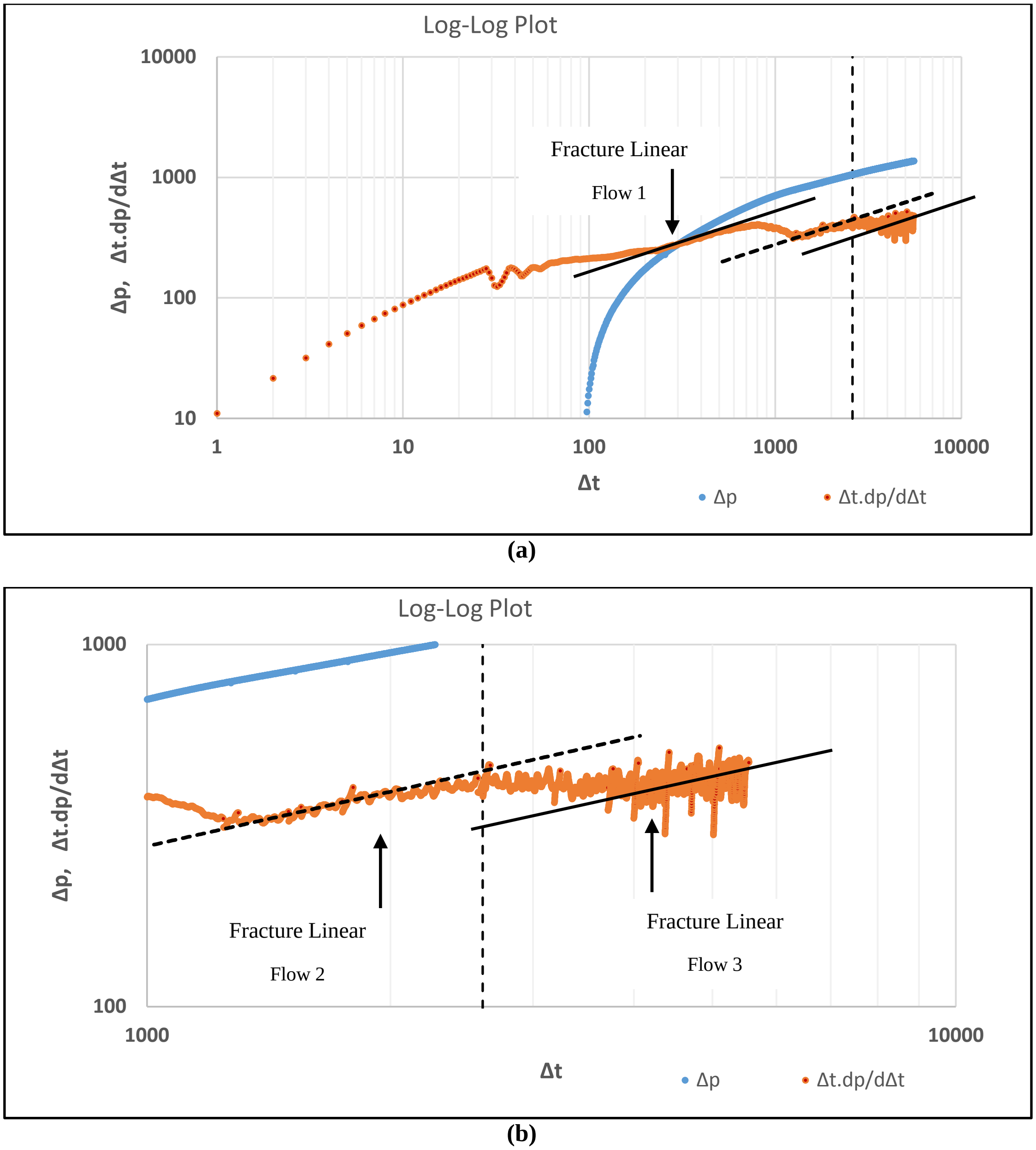

Figure 4.22 (a) Log-Log Plot of DFIT 2 (b) zoom.

Wavelet Analysis

One-dimensional multiresolution analysis of fall-off data was applied by (*db4*) wavelet up to level 3 and (d3) detail coefficients were computed. Applying changepoint detection methodology on these detail coefficients results in four main segments (Figure 4.23 (a) and (b)). Each segment has a different variance as compared to the variance from other segments. Among these changepoints, CP2 (30 min.) and CP3 (43 min.) are identical to closure time captured by G-function analysis. However, wavelet analysis captures more events even after the G-function closure time until CP4. Similar to Test 1, detail coefficients demonstrate variations in their amplitudes even after G-function closure time which represents the progressive fracture closure. Variance of (*d3*) before and after CP1 is easily seen in Figure 4.23 (b) which demonstrates the detail coefficients variations in a larger details scale compared to Figure 4.23(a).

In addition, log-log plot of Test 2 confirms that flow regime continues to be fracture linear with a slope of ½. Therefore, it can be concluded that the events captured by wavelet analysis are not related to changes in the flow regime, but directly related to fracture geometry. This indicates that wavelet analysis successfully captures various fracture network closures that are less subjective and less impacted by the interpretation of the analyst.

It is known that Test 2 was conducted in a naturally fractured reservoir, therefore, having multiple progressive fracture closure events are expected from DFIT analysis. Wavelet analysis is able to detect hidden discontinuities in the pressure signal which are the closure events of intersecting fractures in the system.

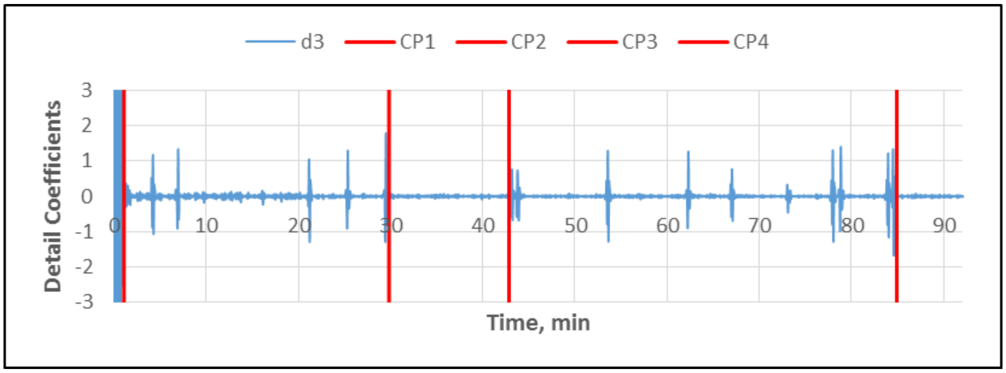

(a)

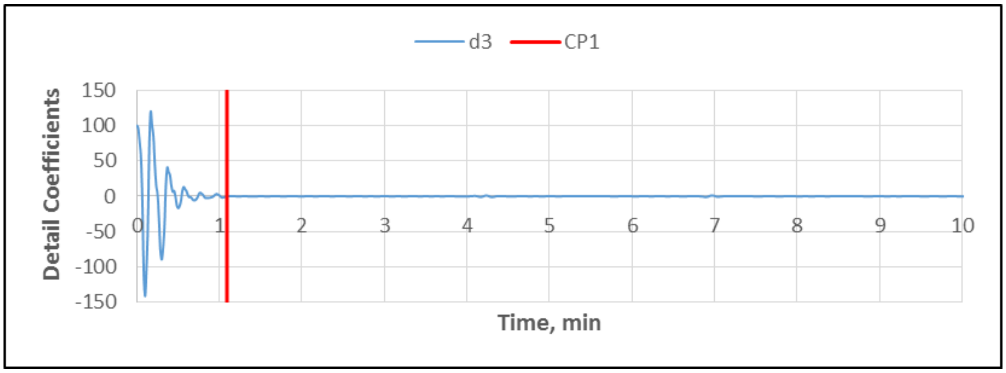

(b)

Figure 4.23 (a) Wavelet Analysis of DFIT 2 (b) zoom.

G-function derivative, square root time, log-log plot and wavelet analysis demonstrate very similar results in terms of fracture closure time and closure pressure (Table 4.2). All four diagnostic techniques agree on the existence of multiple closure events. However, the presented technique, which relies on wavelet and changepoint method, captures the closure events automatically, while other methods depend on the judgement of the analyst and therefore the outcome might be subjective.

In addition to the other tangent-based methodologies, wavelet analysis reveals the hidden progressive fracture events until CP4 and it confirms the presence of multiple fracture networks, i.e. existence of the natural fractures in the formation. Importantly, wavelet detail coefficients show a repeated pattern (Figure 29) until the end, which suggests that all fracture networks have not closed completely. This is further confirmed by the log-log plot, which indicates that the flow regime is still linear fracture flow with a ½ slope.

Table 4.2 Comparison of DFIT Test 2 Analysis.

		G-function	Sqrt (t)	Log-log	Wavelet
Closure 1	**C. Pressure (psi)**	10,541	10,542	10,540	10,592
	C. time (sec)	2,045	2,038	2,050	1,790
Closure 2	**C. Pressure (psi)**	10,437	10,437	10,540	10,449
	C. time (sec)	2,645	2,647	2,050	2,580
Closure 3	**C. Pressure (psi)**	10,133	10,141	-	10,167
	C. time (sec)	5,513	5,415	-	5,100

4.2.3 Discussions and Conclusions

Wavelet analysis was applied to two DFIT Tests that were from different formations. The results from both conventional tangent-based diagnostic methods and wavelet analysis demonstrate very similar results capturing the closure events. However, unlike other techniques, wavelet analysis reveals more information and captures more events during closure which is a result of progressive intermittent fracture closure. Some of the main conclusions of our study are:

Discrete Wavelet Transformation (DWT) captures discontinuities within pressure signal by representing the signal in wavelet-domain which cannot be revealed in time-domain while the outcome is less prone to interpretation errors.

Unlike conventional diagnostic methodologies, wavelet analysis does not require data smoothing which could result in potential misinterpretations.

Change point detection algorithm is designed to detect changes in variance automatically which is less subjective and less impacted by the interpretation of the analyst, so this methodology reduces the uncertainty in DFIT analysis to estimate closure time and pressure.

Wavelet analysis is very sensitive to physical changes in the system, in case of DFIT, these physical changes are related to the intermittent decrease in fracture width and length. Therefore, fracture closure can be identified from wavelet coefficients. Once the fracture network has completely closed, physical changes are minimized, as a result, the detail coefficients show a smooth pattern after closure event. This change in variance is easily detected by change-point technique.

CHAPTER V

UNCONVENTIONAL HORIZONTAL WELLS

In this chapter, the methodology that was explained in Chapter 3 is applied to two operational scenarios in horizontal wells. The first scenario is an analysis of the treatment pressure and slurry rate during hydraulic fracturing treatments of a horizontal well in different stages. The second scenario is the analysis of the fall-off pressure from DFIT. In the first scenario, EDP of pressure and rate are compared to identify any separation between the two plots. It is expected to observe a match between the two EDPs if no other noise is entered the recorded signal from the generated events such as fracture propagation in the rock. In the second scenario, since the only available data is the recorded pressure during the pressure fall-off, EDP is used differently. In that case, the abnormal changes in the EDP trend are identified to select the decomposition levels that need further investigation.

5.1 Analysis of Hydraulic Fracturing Injection Data in Horizontal Wells

In this section, two stages of a horizontal well with multistage fractures in the Marcellus shale are investigated. Existence of natural fractures in Marcellus shale was studied in outcrops of Devonian shales of the Appalachian basin by Engelder et al. (2009). According to their study, two sets of fractures are observed in the outcrops, known as J1 and J2. Both joint sets have significant contributions to hydraulic fracture stimulation depending on the drilling direction of the horizontal wells.

Pirayesh et al. (2013) developed a real-time fracture diagnostic technique called Moving Reference Point (MRP) based on the concept of intermittent fracture propagation. The idea was that the fracture might grow in length and dilates in width during propagation, especially when a fracture intersects a natural fracture. This method showed several advantages over the conventional Nolte-Smith method for analyzing the pressure data. Soliman et al. (2014) used the MRP method to investigate and interpret the fracturing pressure data that is used in this section. Here, we used MRP along with the proposed method to identify the events during fracture propagation.

5.1.1 Case 1 - Marcellus Shale, Stage 1

Figure 5.1 shows the job chart of the stage 1. During this stage execution, the slurry rate is relatively constant around at 90 bpm, as shown in Figure 5.1(a). This stage lasted for 150 min.

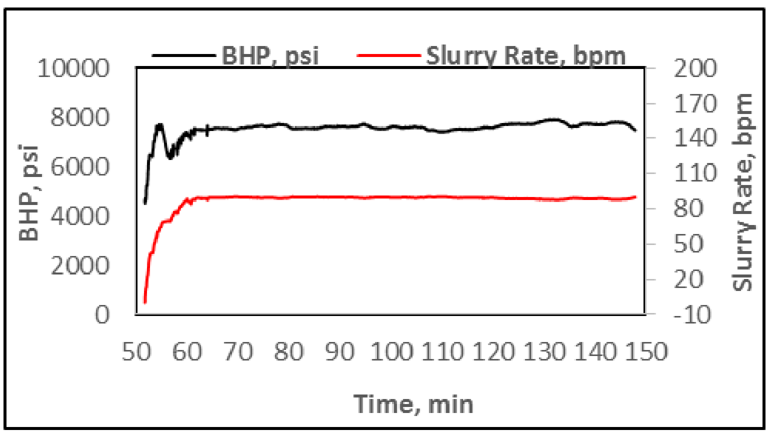

(a)

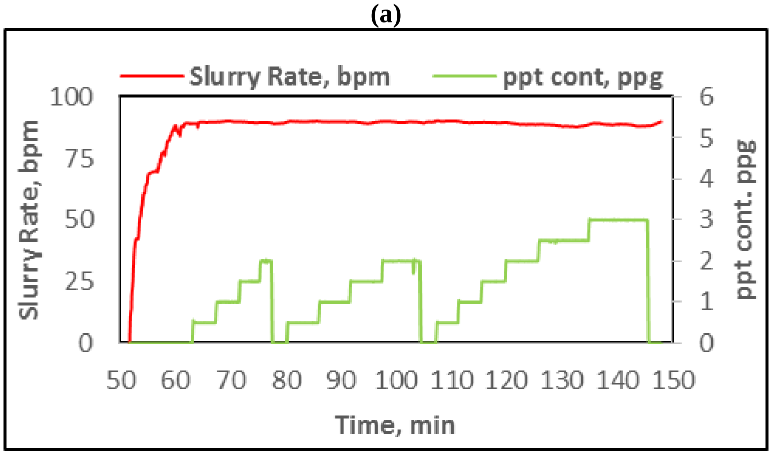

(b)

Figure 5.1 Job chart of Stage 1 a) pressure and rate, b) rate and proppant concentration.

Wavelet Analysis

Firstly, the pressure and rate signals are analyzed using the DWT method. The figure shows the detail coefficients of the pressure signal up to level 9. As can be seen in the following figure, while level 1-5 details (Figure 5.1 (a)) captures the fluctuations in the pressure signal at the beginning (i.e., 50-60 min), lower frequency level details (d6-d9) show events that occur in higher amplitude throughout the job Figure 5.2. For example, *d8* represents a pseudo-frequency of 0.0027 Hz.

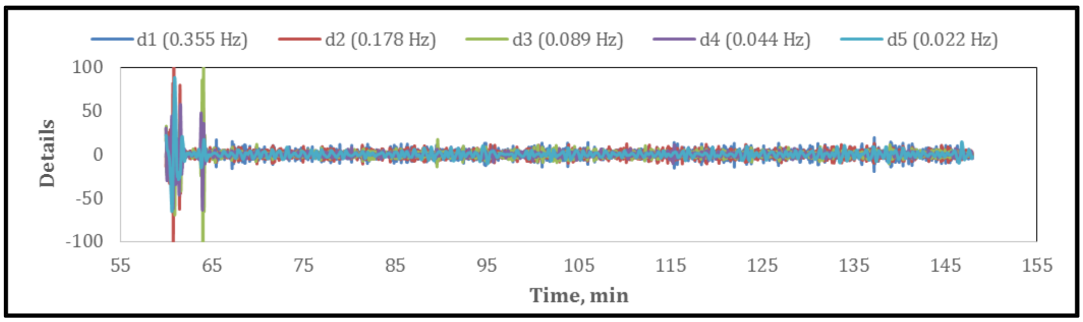

(a)

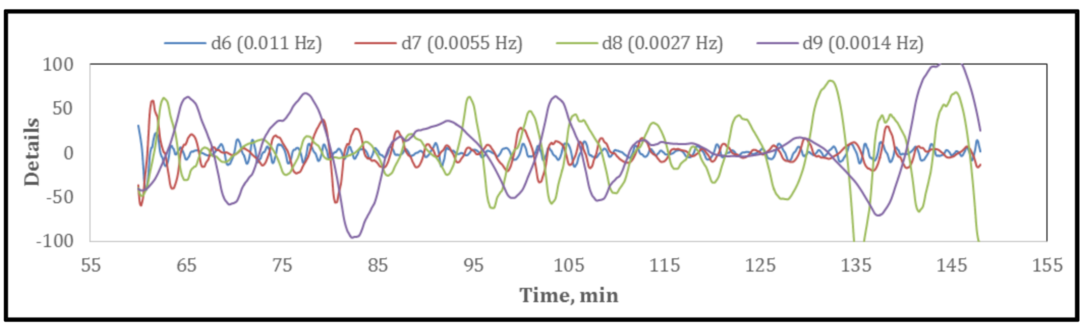

(b)

Figure 5.2 Decomposition of stage 1 BHP. a) High-frequency details (levels 1-5), b) Low-frequency details (levels 6-9).

Similar wavelet decompositions are performed for the slurry rate. By comparing the detail coefficients of treating pressure and slurry rate detail coefficients, useful information can be revealed. For example, if a high-amplitude event is found in both of the detail coefficients of the pressure and rate signals at the same time, then one can conclude that the event is rate-related. In contrary, if the high-amplitude event only happens in the detail coefficient of rate signal then the event can concluded to be rock-related and not rate related.

Energy Density Plot (EDP)

It is beneficial to compare the energy level of the pressure and rate signals for all levels as described earlier to find similarities and differences in the trends. Similarity of detail coefficients of both pressure and rate energy indicates that changes in pressure are caused by changes in rate without contribution from the rock. Therefore, the events are only rate-related. However, departure from similarity in the EDP of pressure and rates indicates rock-related events. Figure 5.3 shows a comparison between the rate and pressure EDPs. As can be seen in the figure, the energy of decomposition levels of pressure and rate match at level 7 and beyond. The frequency band from level 7 to 12 is [0.005547 Hz - 0.000173 Hz], indicating that these low-frequency levels capture the events having more than 3 to 96 min. time period. So, one can conclude that at those frequency bands (d7-d12), events are mostly rate related, and minimum rock-related events are observed. To further investigate this observation, the distribution of energy at level 8 for pressure and slurry rate are plotted in the time domain (Figure 5.4). As can be seen, the changes in the pressure energy occur concurrently with changes in the energy density of the rate signal.

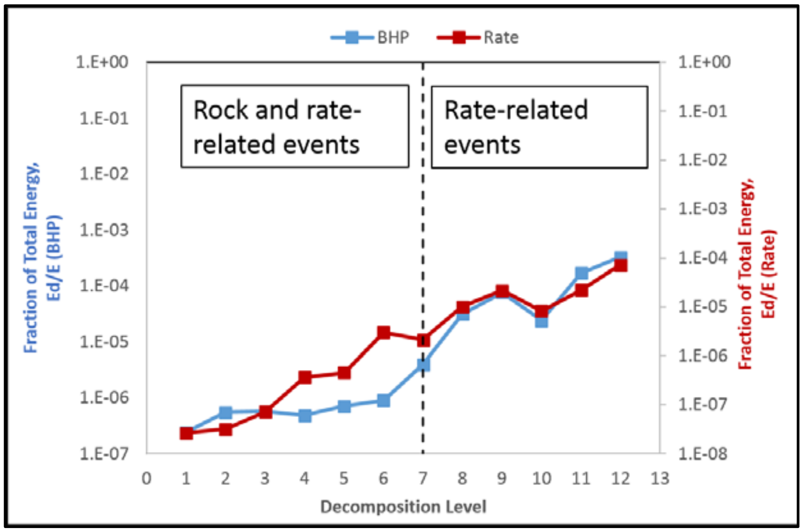

Figure 5.3 Energy Density Plot of BHP & Slurry Rate for Stage 1.

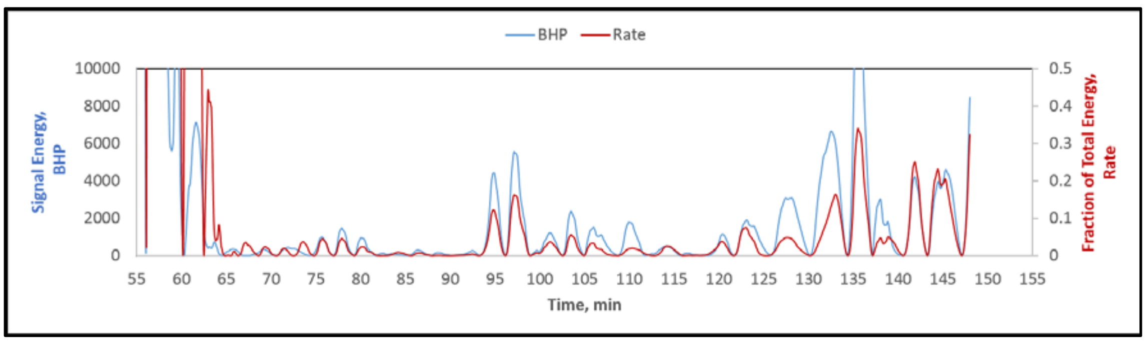

Figure 5.4 Distribution of the signal energy at level-8 for both BHP and Slurry Rate.

A dissimilar trend was observed from the EDP (Figure 5.3) of decomposing levels 1-7, which indicates that the energy deviation in the pressure signal is a result of rock-related events with different frequencies. The maximum difference in the energy of pressure and rate is observed at level 6. In order to localize the events that cause the deviation in time, energy distribution of the pressure and rate signals at level 6 are plotted in Figure 7 for comparison. As shown in the figure, the pressure and rate energies show events, some of those events match each other. The matching events demonstrate a cause and effect relationship between rate and pressure as discussed in the last paragraph.

However, some events show a mismatch at several times during the job. The events that show the mismatches can be categorized into two types. In the first type of events (black colored numbers on Figure 7), the changes in the pressure signal energy happen without any change in the rate signal, while in second type (green colored numbers on Figure 5.5) pressure events correspond to the rate energy fluctuations. To determine the exact type of the event and relate it to physical phenomena (i.e., hydraulic-natural fracture interaction, height growth, etc.), those events are compared to those time intervals with MRP plot.

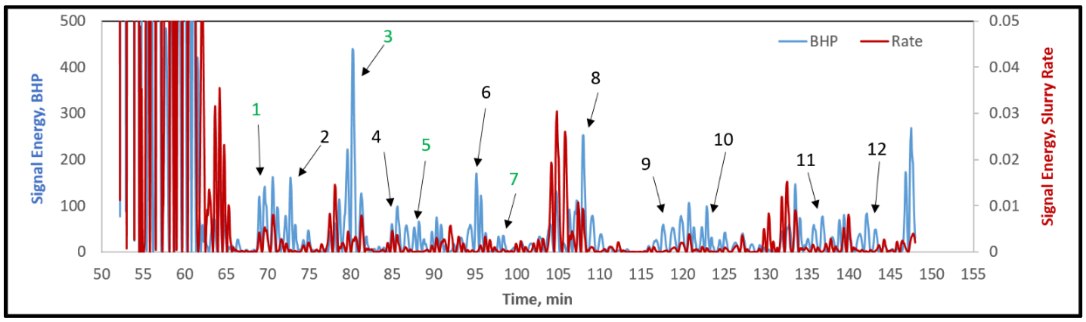

Figure 5.5 Distribution of the signal energy at level-6 for both BHP and slurry rate.

Figure 5.6 shows the results of the MRP methodology for the same data. In the MRP method, the peaks that are in the green arrow show the normal propagation for the fracture, while the point at deeps is an indication of the fracture height growth. Comparing this figure and its events with Figure 5.5, one can distinguish the type of the events. Here we use the same numbering for the events. For example, the first group of events that were observed in the distribution of energy can be matched with the normal propagation of the fracture according to MRP. Point 2 is an example of such an event on both figures. On the other hand, the points in the second group can be matched with the points that are indicated as height growth by MRP. Points 1 and 3 are examples of such points.

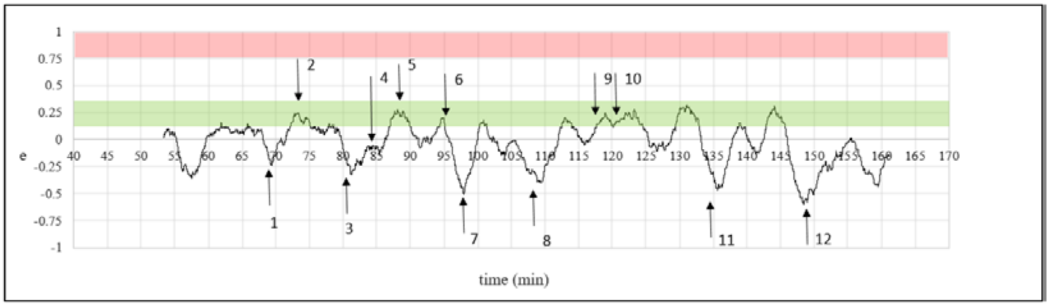

Figure 5.6 Fracture growth exponent plot for Stage 1 (after Soliman et al. (2014)).

5.1.2 Case 2 - Marcellus Shale, Stage 2

Figure 5.7 presents the job chart for the second stage of the same horizontal well in Case 1. One of the purposes of our study is to understand the fracture behavior in real-time from the recording pressure and to understand the wavelet amplitude fluctuations. These wavelet coefficient variations in treating pressure can be due to rate fluctuations or can be directly related to the fracture behavior, such as dilation of the fracture or height growth (Soliman, 2014). Because of this, we consider the injection regions with a relatively constant slurry rate in our analysis that is the injection period between 38- 126 minutes.

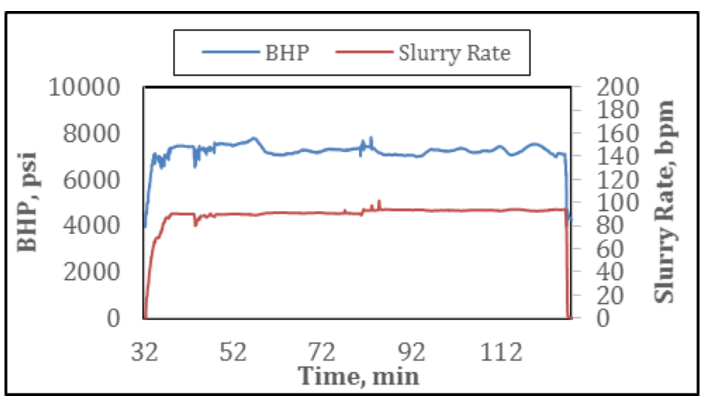

(a)

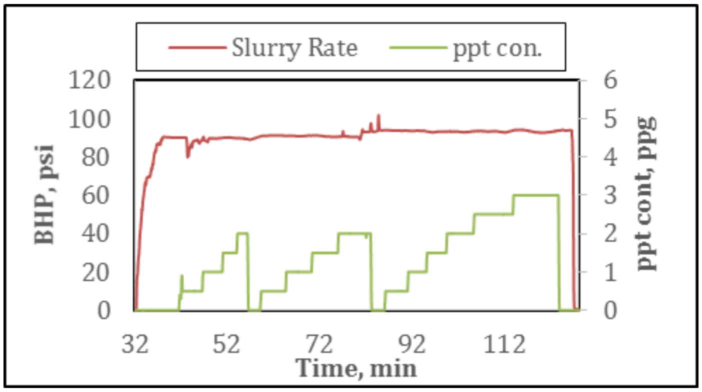

(b)

Figure 5.7 Job chart of Stage 2. a) Pressure and rate, b) rate and proppant concentration.

Wavelet Analysis

The wavelet transformation and the detail coefficients of calculated BHP can be seen in Figure 10. Both figures show that both the high-frequency coefficients (d1-d5) and low-frequency coefficients (d6-d7) capture the slurry rate variations at the beginning of the execution and around 82 minutes; however, level 8 (d8) does not represent those variations, they represent low-frequency events, instead.

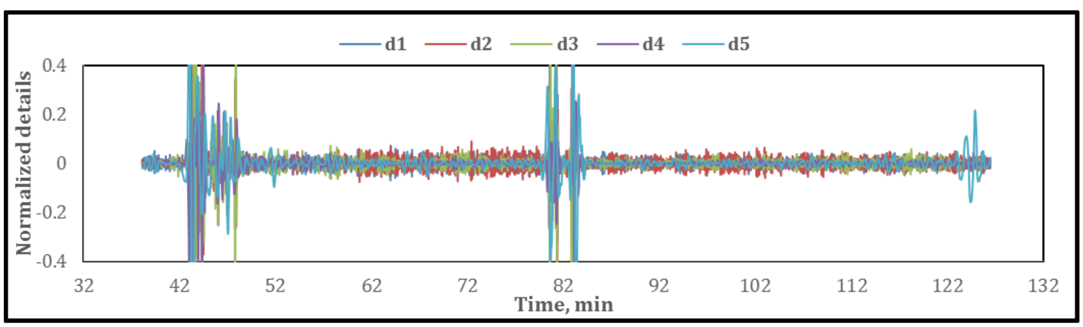

(a)

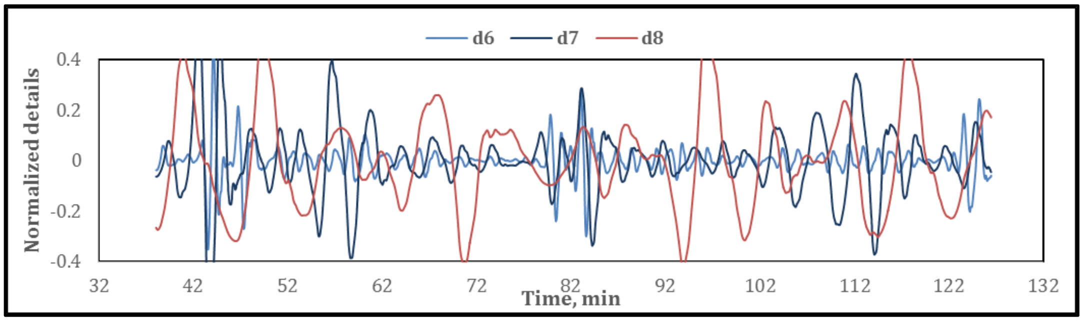

(b)

Figure 5.8. Decomposition of stage 2 BHP. a) High-frequency details (levels 1-5), b) Low-frequency details (levels 6-9)

Energy Density Plot (EDP)

Figure 5.9 demonstrates the comparison of EDP of treating pressure and slurry rate. Two main energy trends are very similar to EDP analysis from Stage 1. The first trend indicates mainly the differences between energy levels in pressure and rate between Level 1 and Level 8. However, in the second trend that happens after Level 8, both pressure and rate energies follow the same trend, which is an indication of no energy contribution from the rock/formation. In other words, the events that wavelet transformation captures at level 8, and higher levels are only rate-related. The frequency range of these rate-related events for this case is 0.002773 Hz. and below. Figure 5.10 demonstrates the energy distribution of BHP and slurry rate at level 11. Both pressure and rate energies change and follow the same trend at the same time intervals. Therefore, it can be said that the events at this frequency range is a result of only rate fluctuations, and there is no energy contribution from the rock.

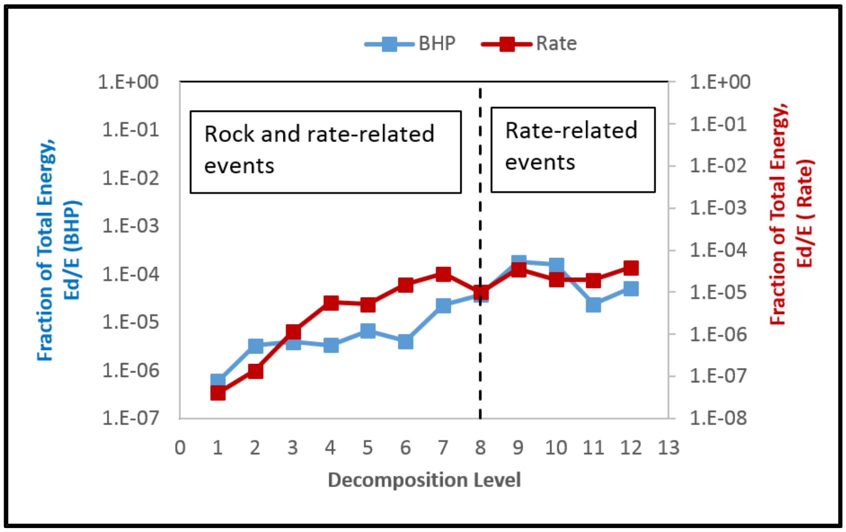

Figure 5.9 Energy Density Plot of BHP & Slurry Rate for Stage 2.

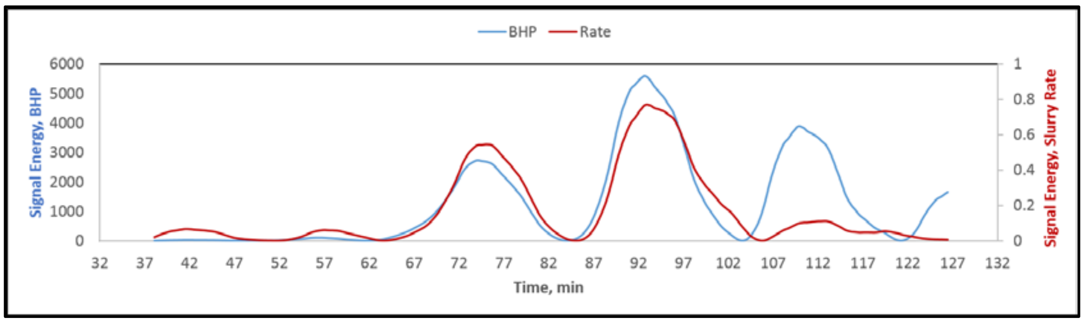

Figure 5.10 Distribution of the signal energy at level-11 for both BHP and Slurry Rate.

It can be seen by looking at the higher frequency band that before level-8, pressure energy and slurry rate plots follow different trends. This deviation in the energy trend is an indication of energy contribution coming from rock-related events within the frequency range of [0.35 Hz-0.002773 Hz.]. Therefore, levels 1-8 captures both rock-related and rate-related events at different frequency levels. The highest energy deviation is seen at level 6, which is the same level in Stage 1. Therefore, we investigated d6 energy distribution to localize events in time. We followed the same approach as in Case 1 and compared energy distribution of d6 of both BHP and slurry rate in time. Level-6 (d6) captures both rate-related and rock-related events at pseudo-frequency of 0.011 Hz. Figure 5.11 demonstrates the localization of only rate-related events by green colored numbers, whereas black colored numbers indicate both rock-related and rate-related events. To determine the exact type of the event (i.e., hydraulic-natural fracture interaction, height growth, etc.), we compared those time intervals with MRP.

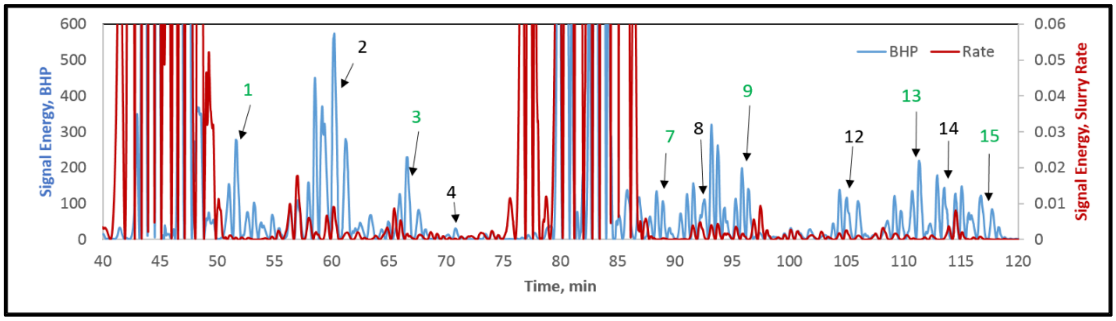

Figure 5.11 Distribution of the signal energy at level-6 for both BHP and Slurry Rate.

In this case, the events represented by green odd numbers are the results of only high-pressure energies. As can be seen in Figure 5.11, there is no energy contribution from rate, and energy of slurry rate at those time intervals are almost zero. Therefore, it can be said that the pressure energy changes are independent of rate energy, so they are only rock-related events. The fracture behavior during those times, which are represented by odd green numbers is identified as normal fracture propagation. Also, the events represented by the black even numbers are a result of both energy changes in pressure and rate. These events are interpreted as rapid height growth by MRP methodology (Figure 5.12). Points 2, 4, 6 are examples of these rock and rate-related events.

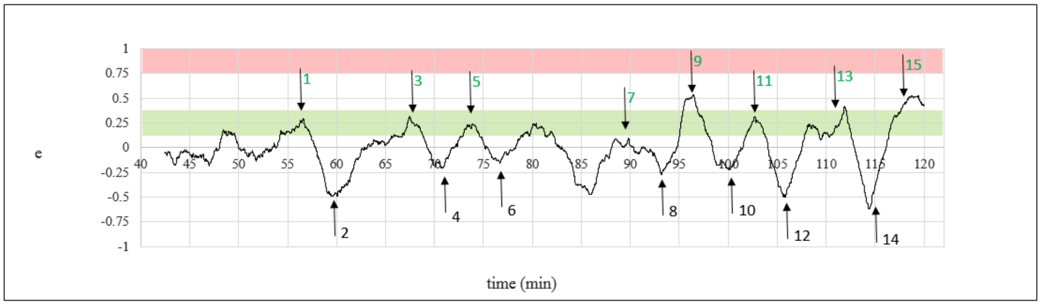

Figure 5.12 Fracture growth exponent plot for Stage 2 (after Soliman *et al*. (2014)).

5.2 Analysis of Diagnostic Fracture Injection Test in Horizontal Wells

The energy density plot that was explained and applied to the hydraulic fracturing job in the last section can be used in other scenarios in hydraulic fracturing. In this section, the application of the proposed approach in diagnostics fracture injection test (DFIT) for identifying fracture closure is presented. In DFIT, a small volume of fluid without proppant is injected at a low rate to create short/mini fractures; then the wellhead is shut-in to allow for the leak off of the pressurized fracturing fluid to the rock. As the fluid leaks off to the formation, net pressure in the fracture continues to drop that causes a decrease in the fracture width. At a certain point, when the fracture surfaces touch each other, the fracture pressure becomes equal to the minimum horizontal stress and recorded as the fracture closure. There are two distinct regions in fall-off data which are before and after closure regions. There have been various methodologies developed to analyze each region to determine fracture and reservoir parameters. Selecting the right point as the fracture closure is crucial in DFIT, especially in ultra-tight formation with horizontal wells and several fractures.

The main difference between the approach that was presented in the previous section for hydraulic fracturing treatment and the one for DFIT is that in this case, only the pressure data is available. Therefore, no comparison can be made between the rate (source) and pressure (effect) signals to identify the events. Thus, one needs to decide and identify the events only from the pressure signal response of the wellbore. We believe that the fracture closure is not a sudden event, but it is progressive and intermittent, in which fracture width and length decreases. Therefore, it should happen in lower frequencies of the signal. Also, a change in the trend of EDP can be useful to identify the energy change due to the noise.

5.2.1 Case 3 – DFIT Example of the Niobrara Shale

Figure 5.13 shows a DFIT in Niobrara Shale. The blue, green, and red lines show the bottom-hole pressure, $\frac{dp}{dG}$ and $G\frac{dp}{dG}$ lines respectively. The duration of injection in this test was 606 sec (~10 min) and the pressure fall off is recorded for 8 days. Also, a downhole gauge was used to record the pressure of this case. As shown in the figure, a closure pressure of 3,379 psi from the G-function plot is estimated at 4 hr. and 38 min.

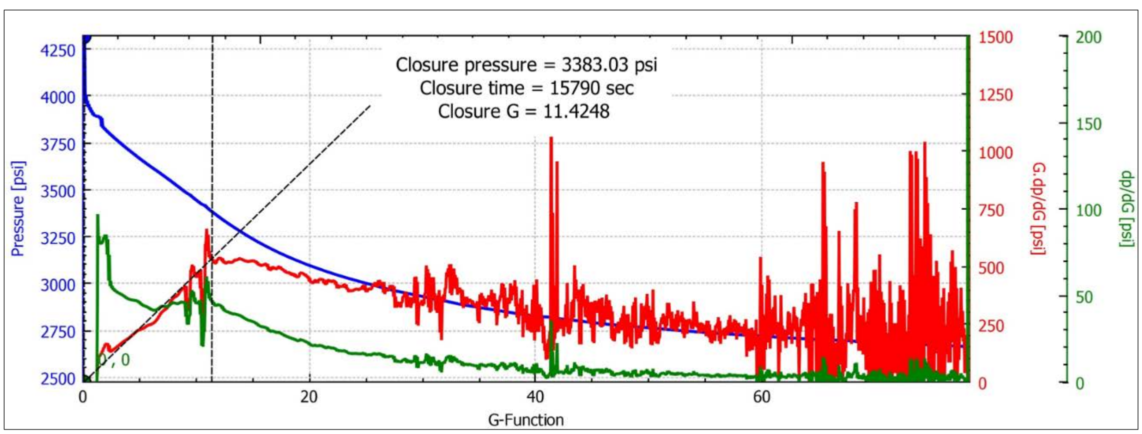

Figure 5.13 G-function analysis of DFIT Niobrara case.

Energy Density Plot (EDP)

Figure 5.14 shows the EDP of the pressure fall-off. There are three energy trends with distinctive EDP slopes. These energy trends are categorized as high, medium, and low frequency ranges for the fall-off pressure signal. Smith and Macdonald (2005) used EDP for analysis of the electrochemical noise data. They were able to differentiate the corrosion types using the percentage of the total signal energy that each of the frequency range contributes. Similar to that study, we aim at identifying the time of the closure and its frequency from EDP. For this purpose, we analyzed each energy trend in EDP individually.

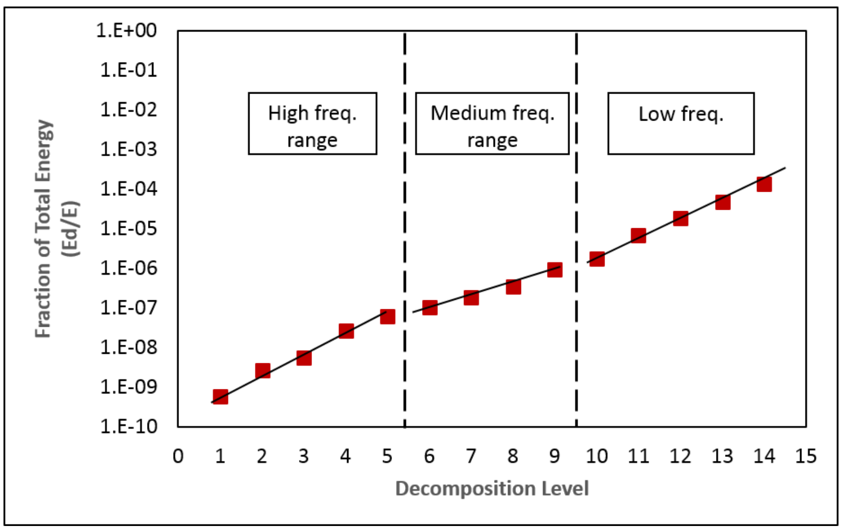

Figure 5.14 Energy Density Plot of pressure fall-off.

Figure 5.15 shows the energy distribution plots of high (levels 1-5), medium (levels 6-9), and low-frequency bands (levels 10-14) for the pressure fall-off. The energy distribution plot of level 4 as a representation of the high-frequency band is shown in Figure 5.15 (a). As can be seen, the energy distribution of the high-frequency range levels (i.e., levels 4 in this example) is almost consistent in time and mask the effect of lower frequency events. Unlike high-frequency levels, medium and low-frequency energy distributions show several trends. For example, four different regions can be distinguished in the medium frequency range, as shown in Figure 5.15(b). These regions are marked as 1, 2, 3, and 4. The energy level in regions 1 and 4 is constant and with region 1 in a higher energy level, while the energy level of region 3 decreases from a higher energy level to a lower energy level and it seems to be a transition between these two levels. Also, in region 2, an increase flowed by a decrease in the energy of the signal is observed that is due to a sudden increase in the recorded pressure at that time and is observed in G-function plot, which we believe it is not a rock related event.

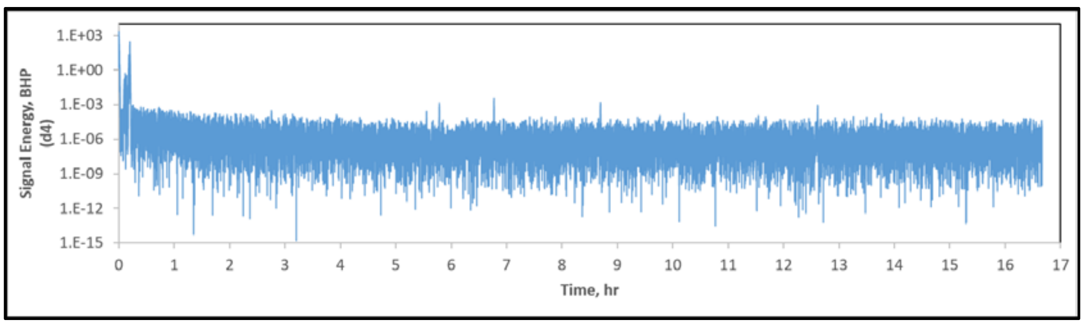

(a)

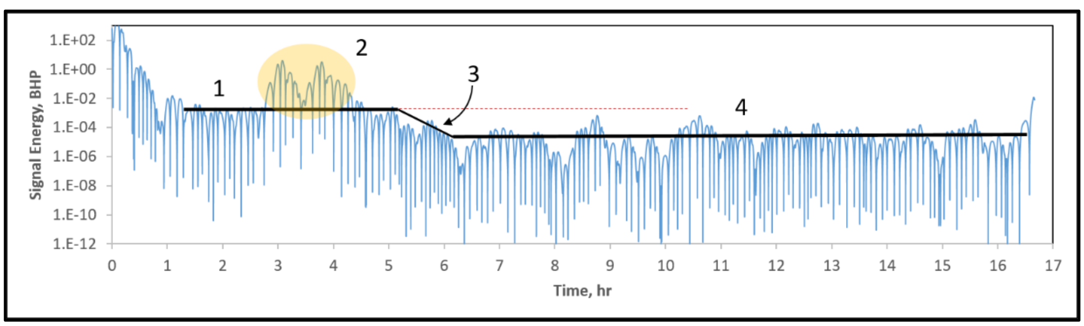

(b)

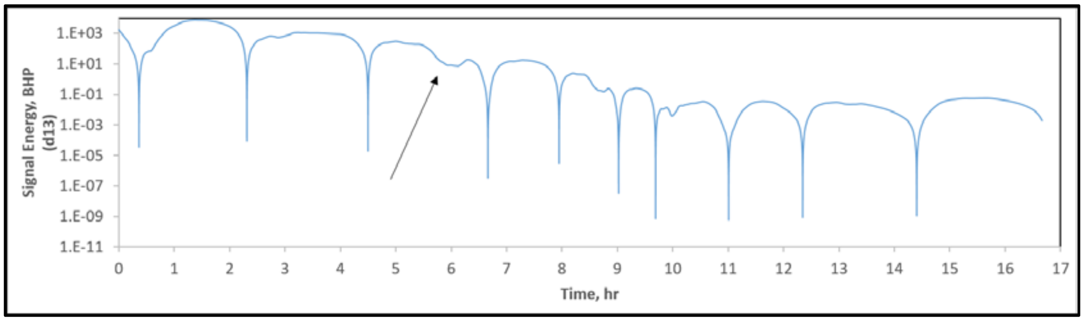

(c)

Figure 5.15 Energy distribution plots of (a) high frequency, (b) medium frequency, (c) low frequency

.

One may relate the trends in region 1 and 4 to the behavior of the fracture in DFIT. As the fracture closes, it continuously loses width and length until it fully closes. Therefore, it is expected that the frequency of the noise that enters the pressure data from a closing fracture to stay in the same energy window while the fracture is open. Also, during closure (i.e., when the surfaces of the fracture touch each other) a transition zone in the energy of the signal energy is observed that continues to a lower energy level. The moment of the change in energy level happens at around 5.7 hr. after shut-in. This is about 1.3 hr. after the closure point that is chosen by the G-function analysis. Also, there is about 100 psi difference between the closure chosen from this approach and G-function analysis.

Region 2 indicated by the yellow circle in Figure 5.15(b) is an indication of sudden pressure increases at two distinct times. While the medium-frequency bands (d6-d9) can capture these two events (Figure 5.15(b)), lower-frequency range bands (d10-d14) do not represent them in energy distribution plots (Figure 5.15(c)). That means, there is not any energy contribution from these events at lower frequency bands. Therefore, it can be said that the frequency range of these region 2 events are limited to [0.011094 Hz. -0.001387 Hz.]. On the other hand, fracture closure event can also be observed in low-frequency energy distribution plots, which is represented by an arrow in Figure 5.15(c). Since we can see the closure event at both medium and low-frequency range energy distributions, we can conclude that the pseudo-frequency of the closure event is [0.022188 Hz. - 0.0000433 Hz.] and can be captured by levels from (d6-d14). On the other hand, region 2 events cannot be observed at medium frequency levels, so we can differentiate those events from fracture related events such as closure. We believe that the two pressure spikes that we observe in region 2 are not related to fracture closure.

5.2.2 Discussions and Conclusions

A new methodology for analyzing and identifying the events that occur during the injection period of hydraulic fracturing and shut-in periods of DFIT is presented in this chapter. The methodology is based on wavelet decomposition technique, which represents signals as a group of frequencies. In addition to wavelet multiresolution analysis, energy density plots are used in our proposed methodology. Time localization properties of wavelet transformation make it possible to provide timely information with frequency bands simultaneously. Because wavelet transformation is sensitive to changes in the system, the discontinuities can be more visible in the wavelet domain than the time domain. We analyzed three cases in this study; two hydraulic fracturing treating cases in Marcellus and a horizontal DFIT case in Niobrara shale formations. The results of the proposed method are compared to moving reference point (MRP) method and G-function analysis. The following conclusions may be drawn from the observed results.

Hydraulic Fracturing Treatment - The pressure and rate data during the injection period of the hydraulic fracturing treatment were analyzed and there was no any observation of rock-related changes in the energy density plots at decomposition level 7 and beyond. However, it was observed that whenever there is a deviation in the EDP values of pressure from the rate at medium frequency levels, there is a rock-related event. The events can be localized in time by plotting the energy of the pressure and rate coefficients for a specific level that the deviation in EDPs is maximum. Two types of events in the energy density plots were shown. In the first type of events, which matched with peaks of MRP, we observed that there is no change in the energy distribution plot of the rate signal. However, in the second type of events that matched the bottoms in MRP, there were some fluctuations in the rate. This can be further investigated to distinguish between different events in the rock that is not possible with the conventional techniques. Finally, all of the rock-related events happened between the wavelet decomposition levels from 3 to 7 that is equivalent to [0.08875 Hz. -0.005547Hz.] pseudo-frequency band.

Diagnostics Fracture Injection Test (DFIT) - To estimate the time and frequency range of the closure event during pressure fall-off period, EDP slope was used to distinguish energy trends. Three different energy trends in the EDP were observed and each representing a frequency range. High-frequency range [0.355 Hz. -0.044375 Hz.] energy distributions did not capture any significant event. These levels (d1-d5) masked the effect of events occurring during the pressure fall-off period. Medium frequency range levels (*d6-d9*) captured significant, noticeable trends in their energy distributions. Based on these trends, it is concluded that the energy trends before and after the fully fracture closure are different, and there is a transition zone between before and after closure regions. This transition period can be a result of intermittent closure of the complex fracture network. In addition, the energy of the medium range decomposition levels before fracture closure was higher than after closure. End of the energy transition period was chosen as the closure of the fracture network, as the energy trend after that point is relatively constant and consistent. This constant energy trend is an indication that there is no energy contribution from the fracture network from this point forward. The analysis showed that the time of the fracture closure in the provided example is estimated at 5.7 hr. and the frequency range of the decomposition levels that capture this event is estimated as [0.022188 Hz. - 0.0000433 Hz.] using the pseudo-frequency table.

Finally, it can be said that the frequency band of the fracture behavior during propagation is different from the frequency band of the fracture closure. While the pseudo-frequency of fracture height growth is estimated as between [0.08875 Hz. -0.005547Hz.], fracture closure event demonstrated lower frequency band as [0.022188 Hz. - 0.0000433 Hz.].

5.3 Ambient Temperature Effect on Analysis of Horizontal Wells

This section presents a DFIT case which is affected by the ambient temperature variations, investigate the possible fracture closure pressure and time, and explains the limitations of proposed wavelet transformation methodology on this specific case.

5.3.1 Case 4 – Upper Wolfcamp Shale

This DFIT case was executed in Upper Wolfcamp formation with a pressure monitoring time of 12.5 days. The fall-off data was recorded by a surface pressure gauge with 1 second sampling rate. Results of the G-function plot estimate the fracture closure occurring at 15 hours and 1,381 psi (Figure 5.16). However, this conventional tangential methodology may result in under or overestimated closure pressure and time. One of the potential limitations of this methodology is the impact caused by the known and visible temperature effects, as it can be seen in the later G-function time (Figure 5.16).

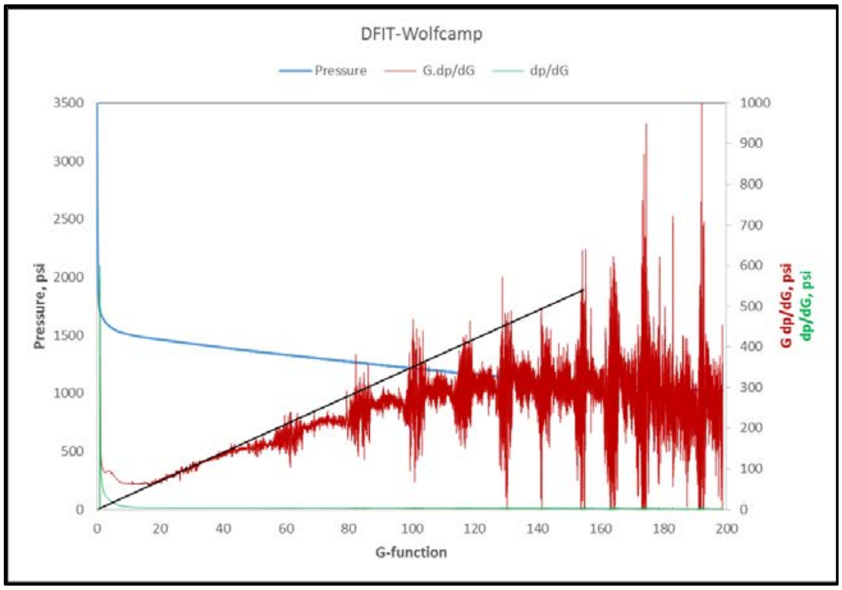

Figure 5.16 G-function analysis of DFIT Wolfcamp case.

Wavelet Analysis

In addition, wavelet analysis of this fall-off data demonstrates significant cyclic response in all multiresolution levels. The cyclic event occurs repeatedly every 24 hours which is caused by the ambient temperature effect on measured pressure (Figure 5.17). Tompkins *at el.* (2014) explained possible sources for this cyclic pressure response. According to their study, thermal compensation of the pressure recorder, thermal expansion/contraction of the fluid in the wellhead and the use of capillary tubing to connect the pressure recorder to the wellhead might be one of the reasons for this significant pattern. This cyclic pattern in both pressure and wavelet coefficients is a challenge for fracture diagnostic tools to properly analyze the DFIT fall-off data.

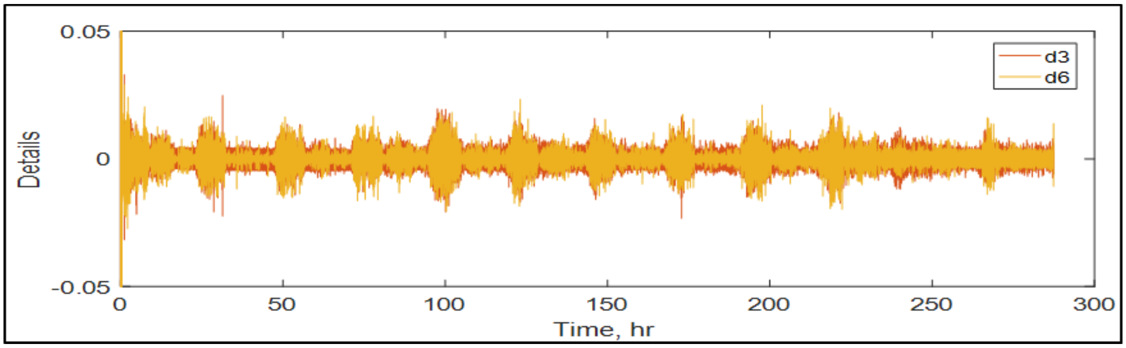

Figure 5.17 Multiresolution analysis of DFIT fall-off data and temperature effect.

Energy Density Plot (EDP)

The signal energy of the detail coefficients from a multiresolution analysis of the DFIT demonstrates a different trend compared to hydraulic fracturing injection cases. In DFIT cases, fraction of the total energy of each level increases constantly after a certain level, as it can be seen from Figure 5.18. According to Energy Density Plot, there are two different regions separating at level 9. Energy of each decomposition level increases constantly after level 9, while the higher frequency band intervals (levels 1 to 8) show alternating energy trend. The fracture closure is not a sudden event, but it is progressive and intermittent, in which fracture width and length decreases by time. Therefore, fracture closure consists of different events occurring at different frequency bands. In this particular case, the pressure fall-off data can be categorized by two main frequency bands (Figure 5.18). High frequency levels from 1 to 8 (0.355 Hz.-0.0027 Hz.) represents the events occurring 0.02 minutes to 6.01 minute time periods, while low-frequency levels from 9 to 19 (0.0014 Hz. and lower frequencies) represents the events occurring at a minimum of 12 minute period intervals.

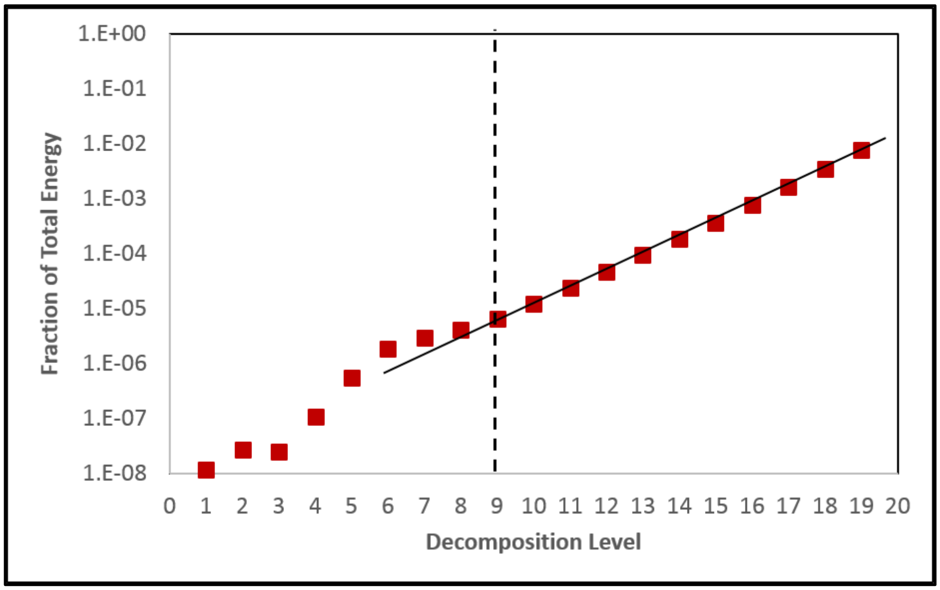

Figure 5.18 Energy Density Plot for fall-off data.

The energy distributions at level 9 and one level from each frequency range; level 5 and level 15 are plotted (Figure 5.19) and investigated further. The effects of ambient temperature variations can be seen in both Figure 5.19(a) and (b). However, it is important to point out that level 15 energy distribution demonstrates a different behavior than the higher frequency levels. The effect of ambient temperature on the recorded pressure readings are not as strong as in other frequency bands.

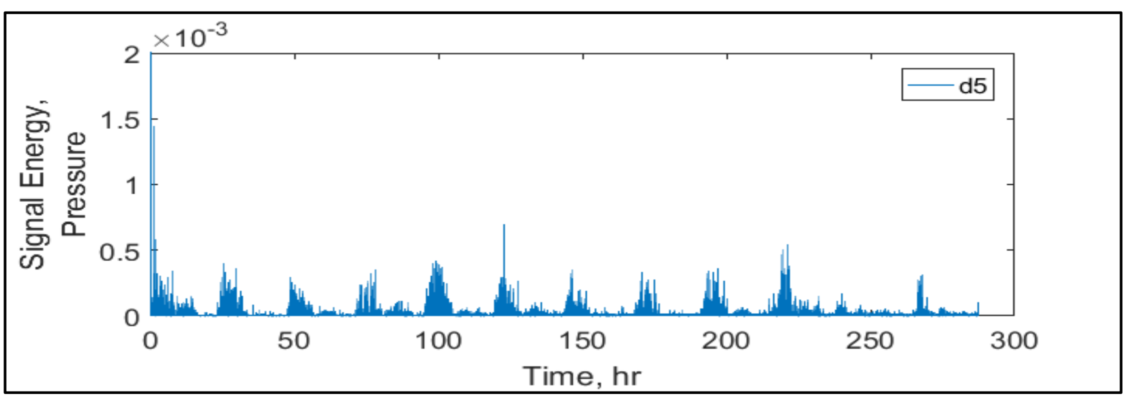

(a)

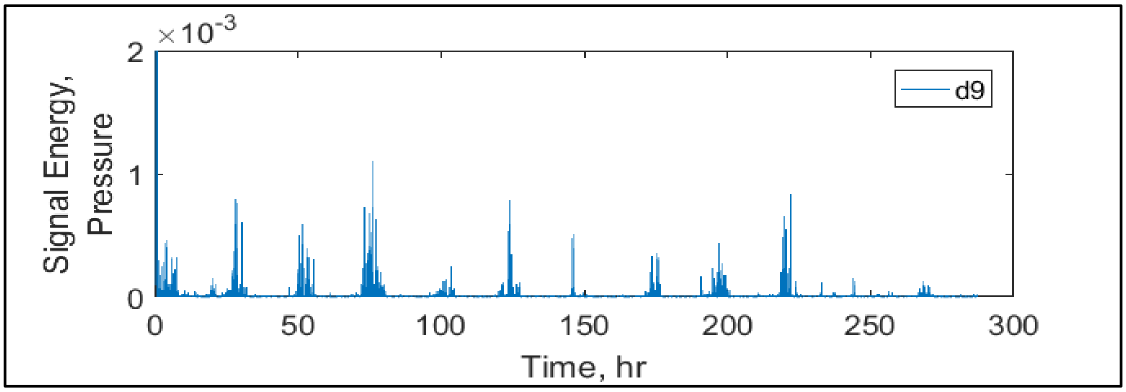

(b)

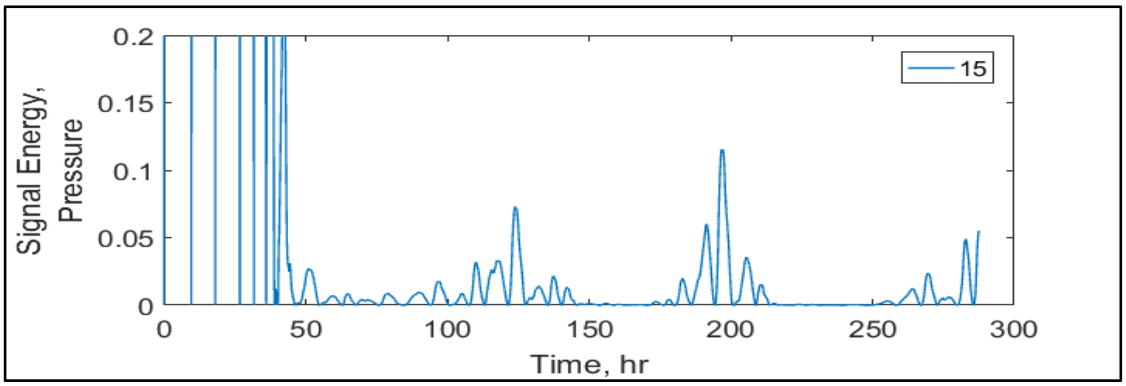

(c)

Figure 5.19 Distribution of Energy at (a) Level 5, (b) Level 9, and (c) Level 15.

Ambient temperature oscillations occur every 12 hours, and this effect can be seen easily by the noise component of the pressure signal. This temperature effect is the major noise component of the recorded pressure data, and it dissembles the closure events. According to the pseudo-frequency table created by *db4* wavelet, the equivalent decomposition level for capturing the events with 24 hr. time period is Level 15 (32 hr. time period). Therefore, the ambient temperature effect can be eliminated by wavelet decomposition at level 15, and the detail coefficients, or energy of the signal should only represent the pressure signal without this ambient temperature effect.

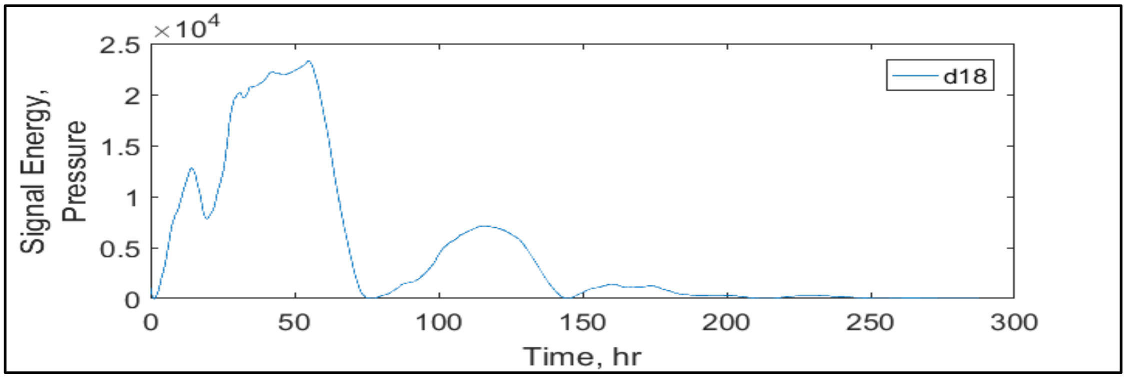

Figure 5.20 Distribution of Energy at Level 18.

Figure 5.20 demonstrates the distribution of signal energy at level 18 and the ambient temperature effect is not seen in the pressure signal. Even though, there is a major energy change at level 9, temperature effect limits the recorded pressure data to be investigated by wavelet transformation and the methodologies applied in previous horizontal DFIT cases. The energy distributions of the pressure at lower frequency bands, such as *d17,d18* demonstrates a very similar pattern which is effected by scaling of the wavelet used. In this research db4 was used in all the methodologies, and it decomposes the ambient temperature effect at level 15. Different wavelets with different frequency bands might eliminate these effects at lower decomposition levels, and might capture the noises causing by the fracture closure event. Therefore, it is recommended to have further analysis by either constructing a new wavelet or different filters to decompose pressure signal at different frequency bands.

CHAPTER VI

INFERRING INTERWELL CONNECTIVITY IN WATERFLOODING OPERATIONS

In this chapter, a new method for estimating IWC using signal processing techniques on the wavelet transform of the injection and production rate data is presented. In this approach, wavelet transform was used to perform a multiresolution analysis to obtain the details at different levels of noisy injection and production rates. Unlike the conventional use of the wavelet method, which denoises the data and smooth it, the analysis performed on the total system response involving noise. Then, cross-correlation between the variance of the details of noises was performed. The rest of this chapter is organized as follows. In the next section, the proposed methodology is explained. Discrete Wavelet Transform (DWT) that is used for the analysis is explained first. Then, a brief review of the conventional signal processing methods follows. Thereafter, five case studies are presented. The first three cases are synthetic cases to verify the proposed approach. Two field examples validated the proposed approach. Finally, the conclusions are discussed.

6.1 Problem Statement

Inter-well connectivity (IWC) is one of the most significant properties when evaluating the success of a waterflood project. IWC between injectors and producers is crucial to identify flow barriers, high permeability channels, or near wellbore issues to optimize operations and maximize oil production. Knowledge of IWC can improve an inadequate production by changing the waterflood pattern (i.e., location of the injection and producing wells) or optimizing the infill drilling well locations. Usually, recorded production and injection from the injectors and producers, and the reservoir geological data is used to determine IWC. However, due to the non-linear and non-stationary nature of this problem, it is difficult to identify the connectivity between a group of wells.

This chapter aims to reveal the connectivity map between several injectors and producers using signal processing techniques on the variance of the detail coefficients obtained from the wavelet transform of the injection and production rate data.

6.2 Introduction

Inter-well connectivity (IWC) is one of the most significant properties when evaluating the success of a waterflood. This connectivity has been obtained from various physics-based methods such as simulations, tracers and using heuristics and semi-analytical tools like capacitance-resistance model (CRM). Production and injection data are a key piece of information required to compute the IWC. In this chapter, a new method for estimating IWC using signal processing techniques on the wavelet transform of the injection and production rate data is presented.

First, the injection and production rates are subjected to multiresolution analysis using the wavelet transform to determine the detail coefficients. The variance of the detail coefficients is then computed and is ready to be processed using various signal processing techniques. Signal processing techniques such as cross-correlation, Spearman correlation, and Kendal correlation are used to identify the level of relationship between the processed injection and production data in wavelet scale space. Based on the correlation coefficients, a new IWC link parameter is proposed for characterizing the IWC between well pairs. The IWC link parameters between well pairs are then plotted for visual representation.

Several simulation models for multi-well systems, established water-flood patterns, and for randomly placed wells were created to establish a new IWC link parameter. The resulting injection and production rates were analyzed using the methodology and the new IWC link parameter is established in terms of cross-correlation coefficient. In addition, several simulations for a heterogeneous reservoir were performed to compute and compare the accuracy of the new IWC link parameter. Finally, the methodology is subjected to real field waterflooding, and compared against the CRM results, which shows a good agreement. The visual representation gives new insight into whether the connectivity is being affected by the reservoir or from near wellbore events (such as changes in skin).

This chapter integrates signal processing techniques and waterflood IWCs. Novel use of wavelet transforms coupled with variance for processing the injection and production rate data is proposed. It must be emphasized that wavelet is used in this context for processing and not for smoothing or data compression. Ultimately, this method can be implemented as a real-time automated monitoring system. Moreover, the new IWC link parameter provides insights by identifying problematic IWC, well-completion issues, and high perm channels for taking timely operational decisions.

6.3 Methodology

Dynamic pressure and rate information are related to reservoir properties, and correlation of either one for injector-producer pairs provide essential information about the connectivity of the wells. There have been statistical methodologies applied for connectivity analysis to resolve uncertainty between wells and determine the degree of communication between them, so injection and production rate correlations can be treated as a good indication of communication in the reservoir. In this section, we present a review on the wavelet method and several signal processing methods such as Spearman, Pearson, Kendal, and cross-correlation methods that are used as a combination of wavelet. Then, we explain the procedure of our proposed approach in analyzing the rate data from injector and producers.

Details are the noise component of the rate data, and crucial information related to reservoir and well can be obtained from these wavelet coefficients at different resolution levels. Therefore, the multiresolution analysis for both injection and production data are conducted to understand the relationship between the wavelet detail coefficients. Figure 6.1 shows the detail coefficients at level-5 (*d5*) for an injector and a producer. The amplitude variations of each detail coefficients are investigated and analyzed in this study.

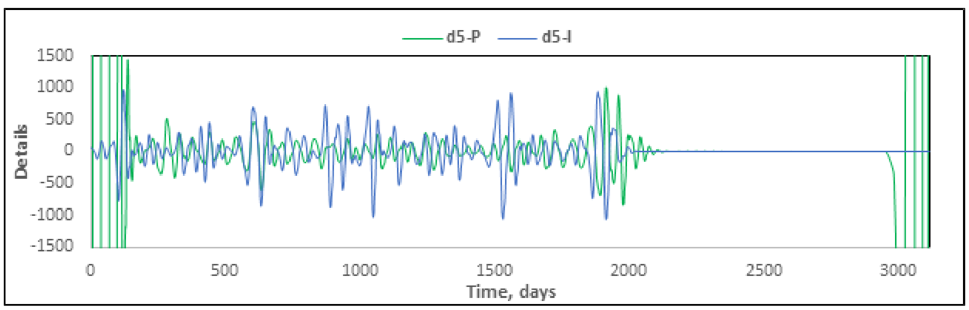

Figure 6.1 An example showing the detail coefficients of level 5 (d5) for a producer and an injector.

6.3.1 Signal Processing Techniques

Correlation is a term in statistics referring to any association between variables, though is commonly used to reveal the linear relationship between two continuous variables. There are two main types of widely used correlations, namely, Pearson's product moment correlation and Spearman's rank correlation coefficient (Mukaka, 2012). Pearson's method is used when both sample data are normally distributed, while the

Spearman method is used when one or both variables are skewed or ordinal and is robust when extreme values are present. The following equation can calculate Pearson's linear correlation coefficient

$$r_{xy} = \frac{\sum_{i=0}^{n}(x_i - \bar{x})(y_i - \bar{y})}{\left\{\sum_{i=0}^{n}(x_i - \bar{x})^2 \sum_{i=0}^{n}(y_i - \bar{y})^2\right\}^{1/2}}. \tag{6.1}$$

In Equation (6.1), r refers to the Pearson's correlation coefficient, n is the sample size, x_i and y_i are the individual sample points, and $\bar{x}$ and $\bar{y}$ are samples means.

6.3.2 Spearman's Rho

Spearman correlation between two variables is equal to Pearson's correlation between the rank values of these two variables. Though the Pearson's correlation captures the linear relationship, Spearman correlation calculates the monotonic relationship between the variables. The Spearman rank correlation can be calculated by

$$r_s = 1 - \frac{6\sum d_i^2}{n(n^2-1)}, \tag{6.2}$$

where, d_i the difference between the two ranks of each observation and n is the sample size. For studies that applied Spearman's rank correlation for the IWC one may refer to Heffer, 1997; Soeriawinata and Kelkar, 1999; Refunjol and Lake, 1997.

6.3.3 Kendall's Tau Coefficient

Kendall rank correlation (Kendall, 1955) is another correlation coefficient to evaluate the degree of similarity between two sets of ranks given to a same set of objects. Kendall coefficient is defined as

$$\tau = \frac{2K}{n(n-1)}, \tag{6.3}$$

where,

$$K = \sum_{i=0}^{n-1} \sum_{j=i+1}^{n} \xi^*(x_i, x_j, y_i, y_j) \tag{6.4}$$

and

$$\xi^*(x_i, x_j, y_i, y_j) = \begin{cases} 1 & \text{if} \quad (x_i - x_j)(y_i - y_j) > 0 \\ 0 & \text{if} \quad (x_i - x_j)(y_i - y_j) = 0 \\ -1 & \text{if} \quad (x_i - x_j)(y_i - y_j) < 0. \end{cases} \tag{6.5}$$

Values of Kendall's coefficient varies between -1 and 1, where -1 means that the two columns are inversely correlated and 1 means that the two columns are directly and strongly correlated. The value of 0 indicates that there is no relationship between the two ranks.

6.3.4 Cross-correlation

Cross correlation measures the similarity between two signals, where one signal is shifted (lagged). The technique is commonly used in signal processing for finding a known short feature in a long signal. Therefore, it is suited for pattern recognition applications. In this study, we used the cross-correlation method for determining the maximum likelihood of similarity between signals that are lagging in time. Because the receiver signal will have a smaller scale, and the source signals may not be of the same scale, normalized cross-correlation was used in this study. Cross-correlation will show superior performance against other methods because it considers the shifting of the signals as well as the correlation between them. Following two examples will highlight this further.

6.3.4.1 Example 1

Consider the source and receiver signals in that are shifted in time. Both source and receiver signals are generated using mathematical functions in this example. Please note that the units of the time and signal magnitude are not necessary on the figure and depending on signal type may vary. For example, in terms of pressure and rates that are subject of this study, time lag can be observed in minute or hours and magnitude of the signal will be in psi or bbl. Figure 6.2 (a) shows that the receiver signal lagged by 150 time units. Multiple correlation measures were chosen and applied to the signals in. The results are shown in Table 6.1. Application of cross-correlation on this example is shown in Figure 6.2(b), which determines the lag as the maximum correlation (peak). The peak value also quantifies the correlation between the signals. The negative sign on the lag means that the lagged signal must be shifted left. It is evident that cross-correlation outperforms other statistical measures because of consideration of time lag. Therefore, cross-correlation was chosen as the measure to determine the degree of correlation in this study.

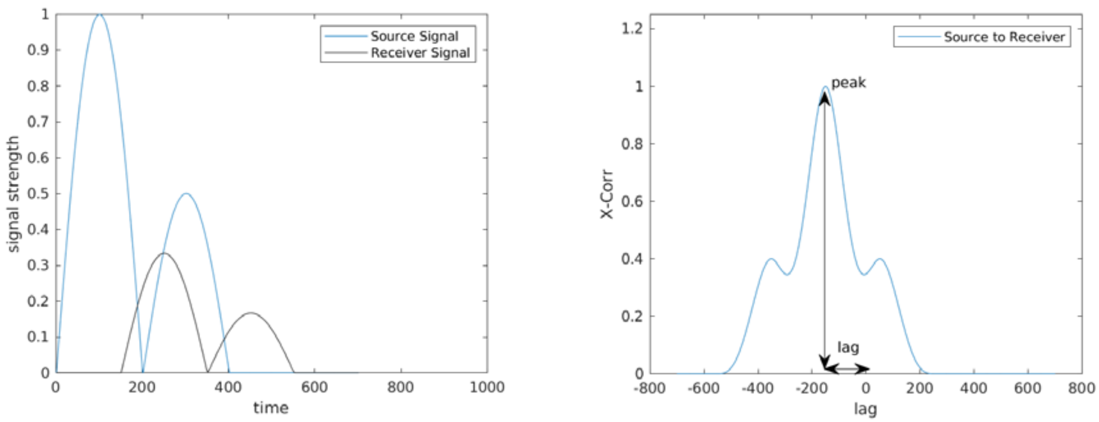

(a) **(b)**

Figure 6.2 (a) Source signal and receiver signal lagged by 150 time units, (b) After application of cross-correlation, lag is determined as 150 time units.

Table 6.1 Comparison of signal processing techniques for Example 1.

Correlation	**X-Corr**	**Pearson**	**Spearman**	**Kendal**
Degree of similarity	1	-0.11736	-0.02812	-0.0171

6.3.4.2 Example 2

Another example with two sources and one receiver is demonstrated in Figure 6.3(a). It should be noted that the receiver signal was contrived as a linear superposition of the two source signals. Source 1 contributed 1/3 and Source 2 contributed 1/6. Source 2 is sent with a lag of 150 time units from Source 1, and receiver is lagged with 300 time units from Source 1. Cross correlation also determined the lags almost exactly as 174 and 301 time units. The results should show a stronger correlation between the pair Source 1 and Receiver than the pair Source 2 and Receiver, which is what is observed in Table 6.2 and Figure 6.3 (b).

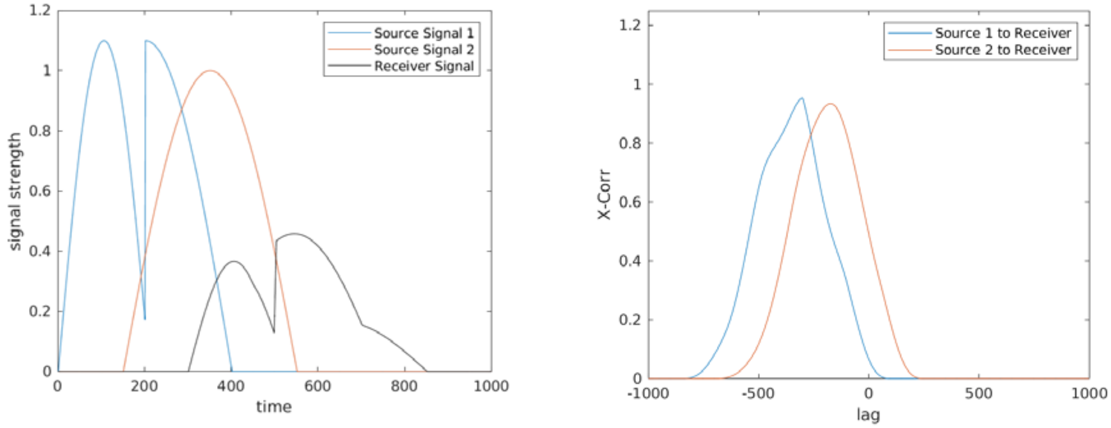

(a) (b)

Figure 6.3 (a) Source 1, Source 2 and receiver signals with lags of 0, 150 and 300 respectively, (b) After application of cross-correlation, the lag is determined as 174 and 301.

This example is chosen to study the performance of different correlations when the receiver signal is composed of multiple sources. It relates to the multiple injectors influencing the rates on a producer well. Also, it was tested whether the cross-correlation method is valid for multiple sources on a single receiver. Table 6.2 shows the results for all correlations for the signal pairs. Again, it is observed that cross-correlation yields superior performance even if the receiver signal is convoluted with multiple source signals. It should be noted that the shortcomings of other techniques become evident with these examples. Therefore, cross-correlation was selected for the analysis that proceeds from this point forward.

Table 6.2 Comparison of signal processing techniques for Example 2.

Correlation	Pair	X-Corr	Pearson	Spearman	Kendal
Degree of similarity	**Source 1 And Receiver**	0.95	-0.49	-0.53	-0.43
Degree of similarity	**Source 2 And Receiver**	0.93	0.20	0.22	0.17

6.3.5 Method of Analysis

The proposed method consists of selecting an injector and producer pair and applying discrete wavelet transform (DWT) on them. The variance between the details level is then used for determining the correlation between the well pairs. The whole methodology can be summarized as follows:

Step 1. Load injector and producer rate data and preprocess.

Step 2. Apply DWT on producer and injector rates and get the details for specified levels.

Step 3. Calculate the variance between the detail levels (variance vs time).

Step 4. Select an injector and producer pair and compute the correlation coefficient peak between the respective variances and save them as linkages. Do for all possible pairs.

Step 5. Save the linkages as table (e.g. Table 6.3) and plot them on figure (e.g. Figure 6.4).

6.3.6 Results and Discussions

Injectors and producers can be treated as a complete system in waterflooding applications. While injectors are considered as the stimulus of the system, producers are the response of that stimulus and are affected by the porous media. It is essential to know the relationship between the injector's stimulus and the producer's response to understand the reservoir characteristics and inter-well connectivity. Porous media cause a time lag and attenuation during propagation of the injection rate signals that results in a response signal in the rates from production wells (Hou *et al.*, 2011). This delay and attenuation of the injection signal mainly depend on the well locations, the distance between injector-producer pairs, low permeability barriers, or seals, and reservoir fluid characteristics. In order to investigate the effects of well distance, impermeable layers on signal lag and attenuation, injector-producer pairs are studied by a reservoir simulator for different cases. In this section, five case studies were presented to evaluate the performance of the proposed methodology for IWC. Three of the cases are synthetic, and two cases are actual recorded field data. The reason for presenting the synthetic cases are: firstly, to verify the proposed approach against the cases in which inter-well connectivity's are known (as model inputs); secondly to compare our proposed methodology against other existing approaches. Finally, two real field cases were analyzed and discussed the insights from the result of the proposed IWC approach.

6.3.6.1 Synthetic Case 1

A simulation case of two producers and one injector was constructed to study the effect of distance on interwell connectivity. P1 was located 1000 ft. from the injector and P2 is located at 500 ft. Figure 6.4 represents the interwell connectivities visually. It was observed that the proposed method can infer the relative distances of the wells correctly. Table 6.3 shows the result of running this methodology and comparison with Spearman method.

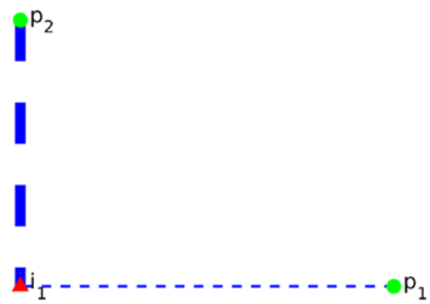

(a)

(b)

Figure 6.4 Synthetic Case 1 Interwell connectivity map on the variance of d3 -d5 based on (a) cross correlation peak (b) Spearman correlation coefficient.

Table 6.3 Synthetic Case 1 Interwell connectivity color coded table, showing results for cross correlation peak on variance of d3-d5.

	X-Corr I1	**Spearman I1**
P1	0.56	0.88
P2	1.0	1.0

6.3.6.2 Synthetic Case 2

The simulation case above was modified to add another producer and an injector to study the effect of interference of multiple injectors on the producers. The schematic in Figure 6.5 shows three producers and two injectors along with their respective interwell connectivity. It can be observed that the proposed method is able to infer the relative distances of the wells correctly, and again verifies the proposed method.

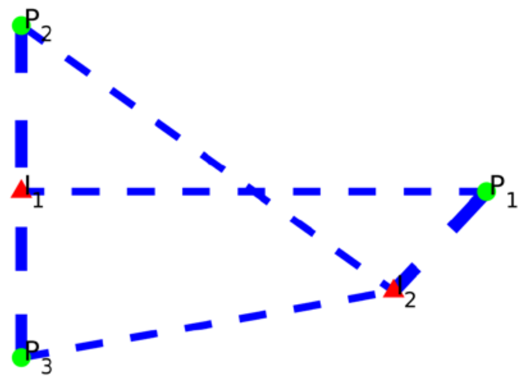

(a)

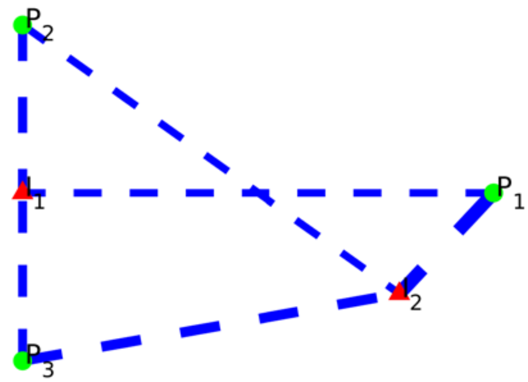

(b)

Figure 6.5 Synthetic Case 2 Interwell connectivity map on the variance of d3-d5 based on (a) cross correlation peak, (b) Spearman correlation coefficient.

Table 6.4 shows the well interconnectivities after running this methodology. The interconnectivity between the pairs I1, P2 and I1, P3 should be equal because of symmetry. Moreover, I2 should be best connected to P1 than any other producer. The proposed method confirms both observations. However, cross-correlation link numbers do not exactly represent the distances. This is due to development of a slightly complex flow pattern because of well to well interference.

Table 6.4 Synthetic Case 2 Interwell connectivity color coded table, showing results for cross correlation peak on variance of d3-d5.

X-Corr	I1	I2
P1	0.35	0.44
P2	0.43	0.35
P3	0.42	0.35

6.3.6.3 Synthetic Case 3

Yousef, et al. (2006) and Lake et al., (2007) presented several synthetic cases for evaluating the performance of their proposed capacitance-resistance method (CRM). The rates that were used and the spreadsheet of their analyses are publicly available and may be found in Sayarpour (2015). In one of the cases, the model was a square reservoir composed of 5 injectors and 4 producers. Letter I to represents the injectors and letter P represents producers. In the model, the permeability of the reservoir is 5 md, except on two streaks between I1 and P1, and I3 and P4. The geometry of the reservoir that was used for the study is shown in Figure 6.6. This model was used by Yousef et al (2006) as an example for verification of the CRM method.

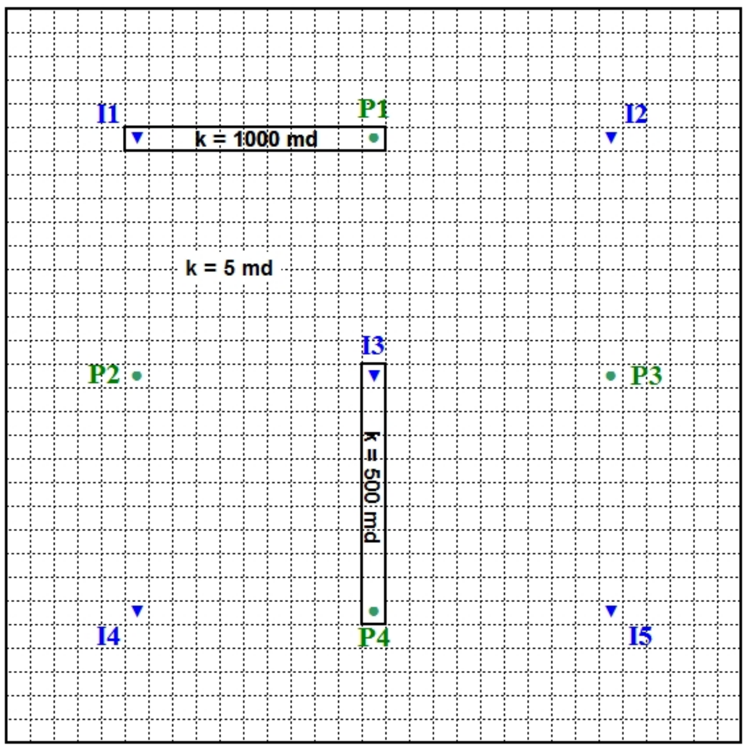

Figure 6.6 Permeability map with well locations used in the simulation of the synthetic case 3 (Sayarpour, 2015).

A comparison between different methods for analyzing the data for the synthetic case 3 is presented in Table 6.5. The relationships between injection-production pairs were summarized to compare the performance of the models with respect to each other. Since the input model is designed in a way to have an idea about IWC even before the simulation, it is relatively easy to evaluate the performance of different well pairs. From the model, it is obvious that the connection between the wells with higher permeability paths (i.e., I1-

P1 and I3-P4) should be stronger than other pairs. All models can capture these relationships correctly. Other than these two strong relationships, in most of other pairs a good agreement between these models was observed. However some differences between methods at a few injection-production pairs are also observed.

Table 6.5 Comparison between CRM, the proposed approach, and other signal processing techniques.

Pairs	CRM	The proposed Methodology	Spearman	Pearson	Kendal
I1-P1	0.96	1	1	1	1
I3-P4	0.86	0.66	1	1	1
I1-P2	0.01	0.08	0	0.24	0
I1-P3	0	0.06	0.29	0.06	0.26
I1-P4	0.03	0.06	0.17	0.18	0.14
P1-I2	0.47	0.44	0.81	0.99	0.77
I2-P4	0.54	0.30	0.54	0.61	0.51
I3-P1	0.1	0	0.31	0.04	0.31
I4-P4	0.67	0.5	0.5	0.61	045
I5-P2	0.02	0.1	0.33	0.22	0.28
I5-P4	0.63	0.52	0.68	0.82	0.65

6.3.6.4 Field Example 1

Having verified the technique by simulation data, the methodology is applied to real field recorded data from 6 producers and 4 injectors. The results are displayed in Table 6.6 and Figure 6.7. A remark must be made on the mismatch between Spearman and cross correlation results. Because the cross-correlation method considers the lag in the signals, as discussed in earlier section, it represents the inter-well connectivities more accurately compared to Spearman’s correlation which ignores the lag time.

Another interesting observation is the connectivity of P5 with all injectors. This could allude to the development of high permeable flow path between them, or a sign of early water breakthrough. It can also be observed that I2 and I4 are not well connected to P3 and

P4. This warrants further investigation on the operator’s part to remedy and take steps to optimize the waterflood.

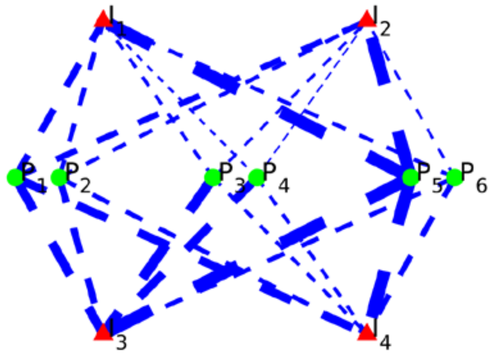

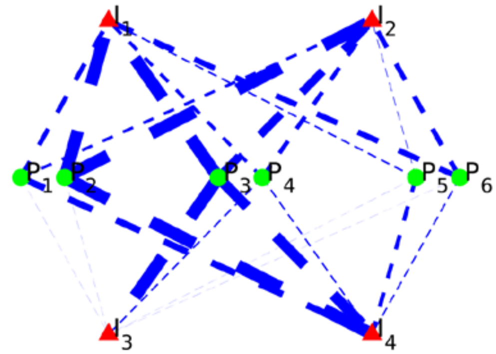

Figure 6.7 Case 4 Inter-well connectivity map on the variance of d3-d5 based on (a) cross correlation peak, (b) Spearman correlation coefficient.

Table 6.6 Case 4 Inter-well connectivity color coded table, showing results for cross correlation peak on variance of first five levels.

X-Corr	I1	I2	I3	I4
P1	0.80	0.76	0.89	0.86
P2	0.68	0.63	0.80	0.68
P3	0.59	0.55	0.93	0.61
P4	0.51	0.41	0.87	0.60
P5	1.00	1.00	1.00	1.00
P6	0.63	0.53	0.68	0.74

6.3.6.5 Field Example 2

Data from six producers and three injectors were analyzed using the proposed methodology. Table 6.7 and Figure 6.8 summarize the analysis results. Again, the mismatch between cross-correlation and Spearman’s method is because the cross-correlation method considers the time lag in the signals, and therefore better represents the inter-well connectivity's. It may be observed that P3 is very well connected to all three injectors. Possible reasons could be well damage, existence of a flow barrier, or P3 being in a different pay zone. Because of the lack of information related to full data, definite conclusions are not easy to make. However, the power of this method becomes evident in the early identification of problematic wells.

Table 6.7 Case 5 Inter-well connectivity color coded table, showing results for cross correlation peak on variance of d3-d5.

X-Corr	I1	I2	I3
P1	0.82	0.89	0.78
P2	0.65	1.00	0.87
P3	0.66	0.54	0.61
P4	0.63	0.39	0.65
P5	0.43	0.57	0.86
P6	1.00	0.72	1.00

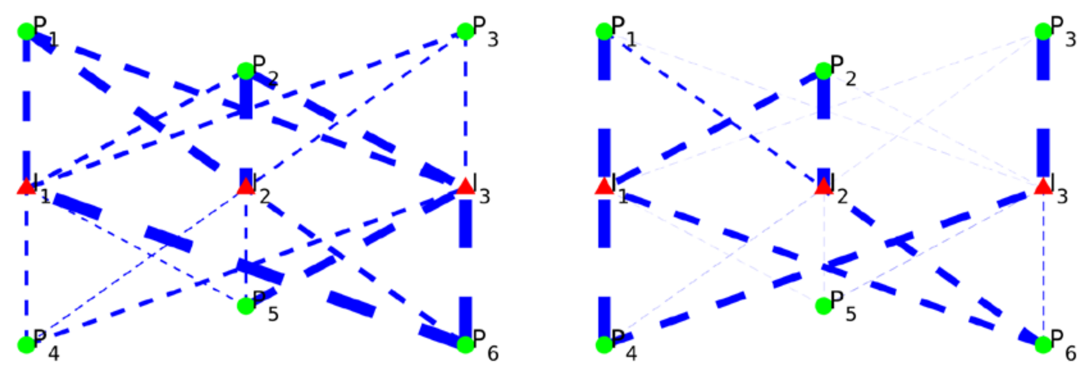

(a) **(b)**

Figure 6.8 Case 5 Inter-well connectivity map on the variance of d3-d5 based on (a) cross correlation peak, (b) Spearman correlation coefficient.

6.4 Discussions and Conclusions

In this chapter, a new method for estimating inter-well connectivity using signal processing techniques specifically the wavelet transforms of the injection and production rate data was presented. The variance of the detail coefficients of the analyzed data is used in combination with the cross-correlation technique.

The advantages of using cross-correlation method on the variance of the detail coefficients of the injection and production signals using two mathematical examples were demonstrated. Also, it was shown that the accuracy of the proposed method to the changes in the injection or production rates. The proposed technique was verified and showed a close agreement with simulated input data and CRM in several cases.

Overall, five cases were analyzed in this study out of which three were synthetic cases and two field examples. Because the proposed method depends only on rate data, and it delivers IWC based on signal processing techniques, it is recommended to use it alongside other methods to enhance certainty of the analysis.

Finally, it should be noted that although the presented method is generally in good agreement with other existing methods, a comparison between these methods applied to the real field data would be beneficial.

Overall, the study in this chapter synergizes the signal processing techniques and waterflood IWCs by involving the wavelet transforms coupled with variance analysis for processing the injection and production rates. Specifically, discrete wavelet transform was used for processing the nonstationary rate data and analyzing the noise component, instead of smoothing or data compression. Moreover, the new IWC link parameter provides insights by identifying problematic IWC, well-completion issues, high-permeability channels, among others for on-time operational decisions. Ultimately, this method offers the potential for implementation in a real-time automated monitoring system as a part of ‘big data’ analysis. The novelty of the proposed approach ensures that reliable injector/producer connectivity can be discerned rapidly for management of secondary recovery processes.

CHAPTER VII

CONCLUSIONS

A new diagnostic tool for the identification of fracture behavior during hydraulic fracturing operations and Diagnostic Fracture Injection Tests was developed. This new methodology consists of the following components;

1) Multiresolution analysis which decomposes the pressure signals into various resolution levels by discrete wavelet transformation,
2) Pseudo-frequency bands of each resolution level,
3) Partitioned energy of the wavelet decomposition levels, that is represented by Energy Density Plots (EDP), and
4) Automatic detection of various patterns within the wavelet coefficients by Change Point Detection algorithm.

Unlike the current fracture diagnostic tools, this new methodology is also applicable to infer interwell connectivities of injector-producer pairs during waterflooding operations, thus leading to better diagnostics beyond the wellbore.

Besides, unlike other fracture diagnostic tools, the developed diagnostic tool does not require any assumptions related to fracture geometry. For example, G-function methodology was developed based on simplistic assumptions of the fracture dimensions, but the developed tool is mainly based on the concept of intermittent fracture propagation and closure. Also, the new methodology does not require any prior information, for instance, closure pressure is required in Nolte-smith method to understand fracture behavior, but the developed tool is mainly based on real field data without any assumptions or prior information. Also, unlike other diagnostic tools for fracture closure diagnosis such as log-log plot, the developed methodology does not require data smoothing which may result in losing critical information about the reservoir and the fracture.

Moreover, the developed diagnostic tool can identify various fracture events by decomposing recorded pressure and rate signals into different pseudo-frequency bands. Therefore, these frequency bands can be used for classification of fracture events by the developed tool and they can be used to distinguish between fracture propagation and closure events.

The developed methodology is sensitive to physical changes in the system, therefore it is capable of identifying introduction of the proppant to the fracture and formation. These changes in the fracture dimensions can also be represented by the energy of the signal. In addition, change point detection algorithm is designed to detect changes in variance of the pressure signal automatically which is less subjective compared to conventional tangential fracture diagnostic tools. This change point detection algorithm divides the wavelet coefficients into segments with different patterns, and it detects the times of pattern changes automatically. This change point detection tool can be used to identify multiple closure events automatically to determine fracture closure time and pressure in DFITs.

The developed diagnostic tool can be used for early detection of potential problems such as screen-out, to identify fracture behavior anomalies such as fracturing fluid loss, dilation, and height growth in conjunction with the MRP method. In addition, it can be used to distinguish the rock-related and rate-related events and to localize fracture behavior in time with their occurring frequency bands. Also, it can be used to estimate and infer interwell connectivities in waterflooding operations. The conclusions from each application of developed tool to hydraulic fracturing, DFIT, and waterflooding operations are explained in more details in a separate chapter as below.

7.1 Hydraulic Fracturing Injection Field Cases

Based on the results of the completed analysis in hydraulic fracturing injection cases in vertical wells in different formations, it is evident that the new developed methodology may be used as an effective fracture treatment diagnostic tool that aids the identification of potential hydraulic fracturing problems and fracture behavior anomalies. Furthermore, it provides an independent means of analyzing pressure data.

1) One of the advantages of developed tool is the early detection of screen-out and tip-screen-out anomalies. As the Cotton Valley example in Chapter 4.1.3, wavelets captures early signs of a screen-out from pressure data prior to real-time diagnostics based on pressure increase monitoring. This is definitely advantageous to initiate risk mitigations and troubleshooting techniques to minimize and potentially prevent the negative impact of screen-outs.
2) Because the developed diagnostic tool by wavelets is sensitive to any physical changes in pressure signals, once the proppant is introduced to the fracturing treatment system, the analysis shows a significant change in details amplitude as demonstrated in Travis Peak formation field example discussed in Chapter 4.1.4.
3) Developed methodology may be used to identify severe fracturing fluid loss and dilation in conjunction with the MRP method.

7.2 Diagnostic Fracture Injection Test (DFIT) Field Cases

The results from both conventional tangent-based diagnostic methods and wavelet analysis demonstrate very similar results capturing the closure events. However, unlike other techniques, the developed diagnostic tool reveals more information and captures more events during progressive intermittent fracture closure. Some of the main conclusions of this chapter are:

1) Discrete Wavelet Transformation (DWT) captures discontinuities within pressure signal by representing the signal in wavelet-domain which cannot be revealed in time-domain while the outcome is less prone to interpretation errors.
2) Unlike conventional diagnostic methodologies, developed tool does not require data smoothing which could result in potential misinterpretations.
3) Change point detection algorithm is designed to detect changes in variance automatically which is less subjective and less impacted by the interpretation of the analyst, so this methodology reduces the uncertainty in DFIT analysis to estimate closure time and pressure.
4) Wavelet analysis is very sensitive to physical changes in the system, in case of DFIT, these physical changes are related to the intermittent decrease in fracture width and length. Therefore, fracture closure can be well identified from wavelet coefficients. Once the fracture network has completely closed, physical changes are minimized, as a result, the detail coefficients show a smooth pattern after closure event. This change in variance is easily detected by change-point technique.

7.3 Hydraulic Fracturing Injection in Horizontal Wells Field Cases

The pressure and rate data from multistage fracturing in horizontal wells were analyzed by wavelet analysis and signal energy concepts. The following observations are concluded based on the analysis:

1) It was observed that whenever there is a deviation in the EDP values of pressure from the rate at medium frequency levels, there is a rock-related event. The events can be localized in time by plotting the energy of the pressure and rate coefficients for a specific level that the deviation in EDPs is maximum.
2) Two types of events in the energy density plots were observed. In the first type of events, which matched with peaks of MRP, there is no change in the energy distribution plot of the rate signal. However, in the second type of events that matched the bottoms in MRP, there were some fluctuations in the rate. This can be further investigated to distinguish between different events in the rock that is not possible with the conventional techniques.
3) Finally, all of the rock-related events happened between the wavelet decomposition levels from 3 to 7 that is equivalent to [0.08875 Hz. -0.005547Hz.] pseudo-frequency band.

7.4 Diagnostic Fracture Injection Testing (DFIT) in Horizontal Wells Field Cases

To estimate the time and frequency range of the closure event during pressure fall-off period, EDP slope was used to distinguish energy trends. The following conclusions were interpreted:

1) Three different energy trends in the EDP were observed and each representing a frequency range. High-frequency range [0.355 Hz. -0.044375 Hz.] energy distributions did not capture any significant event. These levels (d1-d5) masked the effect of events occurring during the pressure fall-off period. Medium frequency range levels (*d6*-*d9*) captured significant, noticeable trends in their energy distributions.
2) Based on these trends, it can be concluded that the energy trends before and after the fully fracture closure are different, and there is a transition zone between before and after closure regions. This transition period can be a result of intermittent closure of the complex fracture network.
3) The energy of the medium range decomposition levels before fracture closure was higher than after closure. End of the energy transition period was chosen as the closure of the fracture network, as the energy trend after that point is relatively constant and consistent. This constant energy trend is an indication that there is no energy contribution from the fracture network from this point forward.
4) The analysis showed that the time of the fracture closure in the provided example is estimated at 5.7 hr. and the frequency range of the decomposition levels that capture this event is estimated as [0.022188 Hz. - 0.0000433 Hz.] using the pseudo-frequency table.
5) Finally, it can be said that the frequency band of the fracture behavior during propagation is different from the frequency band of the fracture closure. While the pseudo-frequency of fracture height growth is estimated as between [0.08875 Hz. -

0.005547Hz.], fracture closure event demonstrated lower frequency band as [0.022188 Hz. - 0.0000433 Hz.].

7.5 Interwell Connectivity

1) The advantages of using cross-correlation method on the variance of the detail coefficients of the injection and production signals using two mathematical examples were demonstrated. Also, it was shown that the accuracy of the proposed method to the changes in the injection or production rates. The proposed technique was verified and showed a close agreement with simulated input data and CRM in several cases.
2) Overall, five cases were analyzed in Chapter 6 out of which three were synthetic cases and two field examples. Because the proposed method depends only on rate data, and it delivers IWC based on signal processing techniques, it is recommended to use it alongside other methods to enhance certainty of the analysis.
3) Finally, it should be noted that although the presented method is generally in good agreement with other existing methods, a comparison between these methods applied to the real field data would be beneficial.

REFERENCES

Aballe, A., Bethencourt, M., Botana, F. J., and Marcos, M. 1999. "Using Wavelets Transform in the Analysis of Electrochemical Noise Data." *Electrochimica Acta* **44**(26): 4805-4816. https://doi.org/10.1016/S0013-4686(99)00222-4.

Abry, P. 1997. Ondelettes Et Turbulences: Multirésolutions, Algorithmes De Décomposition, Invariance D'échelle Et Signaux De Pression. Diderot éd. Paris.

Adeli, H., Zhou, Z., Dadmehr, N. 2002. "Analysis of EEG records in an epileptic patient using wavelet transform." *Journal of Neuroscience Methods*.

Albertoni, A. and Lake, L.W. 2003. "Inferring Interwell Connectivity Only From Well-Rate Fluctuations in Waterfloods." *SPE Reservoir Evaluation & Engineering* **6**(1):6-16. SPE-83381-PA. https://doi.org/10.2118/83381-PA.

Al-Husain, H. M., Soliman, M. Y., Stegent, N. A. 2017. "Application of Moving Reference Point MRP Method to Cotton Valley and Travis Peak Sand Fracturing Treatments." Presented at the SPE HFC, Woodlands, Texas, 24-26 January. SPE-184855-MS. https://doi.org/10.2118/184855-MS.

Allen, R. L. and Mills, D. W. 2004. Signal Analysis: Time, Frequency, Scale, and Structure, first edition. Piscataway, New Jersey: Wiley-IEEE Press.

Athichanagorn, S., Horne, R.N., Kikani, J. 1999. "Processing and Interpretation of Long-term Data from Permanent Downhole Pressure Gauges." Presented at the SPE Annual Technical Conference and Exhibition, Houston, TX, 3-6 October. SPE-56419-MS. https://doi.org/10.2118/56419-MS.

Bachman, B., Hawkes, R. V. 2007. Gas Well Testing and Evaluation. In Modern Fracturing Enhancing Natural Gas Production, M. J. Economides, T. Martin, Chapter 3, 41-90. Houston, Texas: Energy Tribune Publishing Inc.

Bai, J. 2006. "Estimation of a Change Point in Multiple Regression Models". *The Review of Economics and Statistics* **79**(4). https://doi.org/10.1162/003465397557132.

Barree, R.D. and Mukherjee, H.1996. "Determination of Pressure Dependent Leakoff and Its Effect on Fracture Geometry." Presented at the SPE Annual Technical Conference and Exhibition, Denver, Colorado, 6-9 October. SPE-36424-MS.https://doi.org/10.2118/36424-MS.

Barree, R.D., Barree, V.L., and Craig, D. 2009. "Holistic Fracture Diagnostics: Consistent Interpretation of Prefrac Injection Tests Using Multiple Analysis Methods." *SPE Production & Operations* **24**(03): 396-406. SPE-107877-PA. https://doi.org/10.2118/107877-PA.

Bernasconi, G., Rampa, V., Abramo, F. 1999. "Compression of Downhole Data." Presented at the SPE/IADC Drilling Conference, 9-11 March, Amsterdam, Netherlands. SPE-52806-MS. https://doi.org/10.2523/52806-MS.

Boggess, A., Narcowich, F.J. 2009. A First Course in Wavelets with Fourier Analysis. Wiley, second edition. John Wiley & Sons.

Burnett, M. D., Castagna, J., Ziga, G., Figon, L., Martinez, T., Tellez, M., Vila, R., Mendez, E. 2003. "Application of Spectral Decomposition to Gas Basins in Mexico." Presented at the SEG Annual Meeting, Dallas, Texas, 26-31 October, SEG-2003-2332. https://doi.org/10.1190/1.1817827.

Burrus, C.S., Gopinath, R.A., Guo, H. 1998. Introduction to Wavelets and Wavelet Transforms: A Primer, first edition. Prentice Hall.

Chandrasekhar, E. and Rao, V.E. 2012. "Wavelet Analysis of Geophysical Well-log Data of Bombay Offshore Basin, India." *Mathematical Geosciences* **44**(8): 901-928. https://doi.org/10.1007/s11004-012-9423-4.

Chen, J., Gupta, A. K. 1997. “Testing and Locating Variance Changepoints with Application to Stock Prices.” *Journal of the American Statistical Association*, **92**(438), 739-747. doi:https://doi.org/10.1080/01621459.1997.10474026.

Chen, J., Gupta, A. K. 2011. Parametric Statistical Change Point Analysis with Applications to Genetics, Medicine, and Finance. Birkhäuser Basel. doi:http://dx.doi.org/10.1007/978-0-8176-4801-5.

Craig, D., Blasingame, T. A. 2006. “Application of a New Fracture-Injection/Falloff Model Accounting for Propagating, Dilated, and Closing Hydraulic Fractures.” Presented at the SPE Gas Technology Symposium, Calgary, Canada, 15-17 May. SPE-100578-MS. doi:https://doi.org/10.2118/100578-MS.

Craig, D. and Blasingame, T. A. 2006. Application of a New Fracture-Injection/Falloff Model Accounting for Propagating, Dilated, and Closing Hydraulic Fractures. Presented at the SPE Gas Technology Symposium, Calgary, Alberta, 15-17 May. SPE-100578-MS. https://doi.org/10.2118/100578-MS.

Daubechies, I. 1995. Ten Lectures on Wavelets, first edition. SIAM: Society for Industrial and Applied Mathematics.

Dinh, A. V. and Tiab, D. 2008. “Interpretation of Interwell Connectivity Tests in a Waterflood System.” Presented at the SPE Annual Technical Conference and Exhibition, Denver, Colorado, 21-24 September. SPE-116144-MS. https://doi.org/10.2118/116144-MS.

Tiab, D. and Dinh, A. 2007. “Inferring Interwell Connectivity from Well Bottomhole Pressure Fluctuations in Waterfloods.” Presented at the Production and Operations Symposium, Oklahoma City, Oklahoma, 31 March-3 April. SPE-106881-MS. https://doi.org/10.2118/106881-MS.

Engelder, T., Lash, G.G., Uzcategui, R.S. 2009. "Joint sets that enhance production from Middle and Upper Devonian gas shales of the Appalachian Basin." *AAPG Bulletin* **93**: (7) 857-889. https://doi.org/10.1306/03230908032.

Faust, O., Acharya,U.R., Adeli, H., Adeli, A. 2015. "Wavelet-based EEG processing for computer-aided seizure detection and epilepsy diagnosis." *Seizure* **26**:56-64. British Epilepsy Association.

Fourier, J. 1822. Theorie analytique de la chaleur, par M. Fourier. Chez Firmin Didot, père et fils.

Guan, L., Du, Y., and Li, L. 2004. "Wavelets in Petroleum Industry: Past, Present and Future." Presented at the SPE Annual Technical Conference and Exhibition, Houston, Texas, 26-29 September. SPE-89952-MS. https://doi.org/10.2118/89952-MS.

Haar, A. 1910. "Zur Theorie Der Orthogonalen Funktionensysteme." *Mathematische Annalen* **69**(3): 331-371. https://doi.org/10.1007/BF01456326.

Heffer, K.J., Fox, R.J., McGill, C.A., and Koutsabeloulis, N.C. 1997. "Novel Techniques Show Links between Reservoir Flow Directionality, Earth Stress, Fault Structure and Geomechanical Changes in Mature Waterfloods." *SPE Journal* **2**(02): 91-98. SPE-30711-PA. https://doi.org/10.2118/30711-PA.

Hou, J., Li, Z., Liu, Y., Zang, Y., Wang, C., Luo, F. 2011. "Inferring Reservoir Interwell Dynamic Connectivity Based on Signal Processing Method." Presented at the International Petroleum Technology Conference, Bangkok, Thailand, 7-9 February. IPTC-14328-MS. https://doi.org/10.2523/IPTC-14328-MS.

Jansen, F.E. and Kelkar, M.G. 1996. "Exploratory Data Analysis of Production Data." Presented at the Permian Basin Oil and Gas Recovery Conference, Midland, Texas, 27-29 March. SPE-35184-MS. https://doi.org/10.2118/35184-MS.

Jansen, F.E. and Kelkar, M.G. 1997. “Application of Wavelets to Production Data In Describing Inter-Well Relationships.” Presented at the SPE Annual Technical Conference and Exhibition, San Antonio, Texas, 5-8 October. SPE-38876-MS. https://doi.org/10.2118/38876-MS.

Junsheng, C., Dejie, Y., and Yu, Y. 2005. “Time–energy density analysis based on wavelet transform.” *NDT & E International* **38** (7): 569-572. https://doi:10.1016/j.ndteint.2005.02.002.

Kang, Y.M. 2008. “Acoustic Emission Signal Processing Based on Wavelet Analysis.” Presented at the ISRM International Symposium-5th Asian Rock Mechanics Symposium (ARMS5), 24-26 November.Tehran, Iran.

Kaviani, D. 2009. “Interwell Connectivity Evaluation from Wellrate Fluctuations: A Waterflooding Management Tool.” Doctoral dissertation, Texas A&M University, College Station, Texas.

Kaviani, D. and Valkó, P.P. 2010. “Inferring Interwell Connectivity Using Multiwell Productivity Index (MPI).” *Journal of Petroleum Science and Engineering* **73**(1-2): 48-58. https://doi.org/10.1016/j.petrol.2010.05.006.

Kendall, M.G., 1948. Rank correlation methods. Oxford, England: Griffin.

Ladd, M.D. and Wilson, G.R. 1993. “Frequency Resolution Properties of the Wavelet Transform for Detecting Harmonically Related Narrowband Signals.” *IEEE International Conference on Acoustics, Speech, and Signal Processing* **4**: 420-423. doi:10.1109/ICASSP.1993.319684.

Lake, L.W., Liang, X., Edgar, T.F., Al-Yousef, A. 2007. “Optimization of Oil Production Based on A Capacitance Model of Production and Injection Rates.” Presented at the SPE Hydrocarbon Economics and Evaluation Symposium, Dallas, Texas, 1-3 April. SPE-107713-MS. https://doi.org/10.2118/107713-MS.

Lei, L., Wang, C. and Liu, X. 2013. “Discrete Wavelet Transform Decomposition Level Determination Exploiting Sparseness Measurement.” *International Journal of Electrical,* *Computer, Energetic, Electronic and Communication Engineering* **7**(9):691-694. https://doi.org/10.5281/zenodo.1087700.

Liu, F., Mendel, J.M. and Nejad, A.M. 2009. "Forecasting Injector/Producer Relationships from Production and Injection Rates Using an Extended Kalman Filter." *SPE Journal* **14**(04): 653-664. SPE-110520-PA. https://doi.org/10.2118/110520-PA.

Liu. C.L. 2010. A Tutorial of the Wavelet Transform.

Mallat, S. G. 1989. "A Theory for Multiresolution Signal Decomposition: The Wavelet Representation." *IEEE Transactions and Pattern Analysis and Machine Intelligence* **11**(7). https://doi.org/10.1515/9781400827268.494.

Marongiu-Porcu, M., Ehlig-Economides, C. A., Economides, M. J. (2011). "Global Model for Fracture Falloff Analysis." Presented at the SPE North American Unconventional Gas Conference and Exhibition. Woodlands, Texas, 14-16 June. SPE-144028-MS. https://doi.org/10.2118/144028-MS.

McClure, M. W., Blyton, C. J., Jung, H., Sharma, M. S. 2014. "The Effect of Changing Fracture Compliance on Pressure Transient Behavior during Diagnostic Fracture Injection Tests." Presented at the SPE Annual Technical Conference and Exhibition, Amsterdam, Netherlands, 27-29 October. SPE-170956-MS. https://doi.org/10.2118/170956-MS.

Morlet, J., Arens, G., Fourgeau, E., Giard, D. 1982. "Wave Propagation and Sampling Theory-Part I: Complex Signal and Scattering in Multilayered Media." *Geophysics* **47**(2): 222-236. https://doi.org/10.1190/1.1441328.

Mukaka, M.M. 2012. "A Guide to Appropriate Use of Correlation Coefficient in Medical Research." *Malawi Medical Journal* **24**(3):69-71.

Nolte, K. G., Maniere, J. L., Owens, K.A. 1997. “After-Closure Analysis of Fracture Calibration Tests.” Presented at the SPE Annual Technical Conference and Exhibition, San Antonio, Texas, 5-8 October. SPE-38676-MS. https://doi.org/10.2118/38676-MS.

Nolte, K.G. and Smith, M.B. 1979. “Interpretation of Fracturing Pressures.” Presented at the SPE Annual Technical Conference and Exhibition, Las Vegas, Nevada, 23-26 September. SPE-8297-MS. https://doi.org/10.2118/8297-MS.

Nolte, K.G. 1986. “A General Analysis of Fracturing Pressure Decline with Application to Three Models.” *SPE Formation Evaluation* **1** (06): 571-583. SPE-12941-PA. https://doi.org/10.2118/12941-PA.

Nwaonu,S., Gebril, A.M.M., Cottis, R.A. 2007. “Wavelet Analysis of EN Data.” In Corrosion 2007. NACE International Corrosion Conference and Expo.

Page, E. S. 1954. “Continuous Inspection Schemes.” *Biometrika* **41**(1-2): 100-115. https://doi.org/10.1093/biomet/41.1-2.100.

Panda, M.N. and Chopra, A.K. 1998. “An Integrated Approach to Estimate Well Interactions.” Presented at the SPE India Oil and Gas Conference and Exhibition, New Delhi, India, 17-19 February. SPE-39563-MS. https://doi.org/10.2118/39563-MS.

Pirayesh, E., Soliman, M.Y., Rafiee, M. 2013. “Make Decision On The Fly: A New Method To Interpret Pressure-Time Data During Fracturing-Application To Frac Pack.” Presented at the SPE Annual Technical Conference and Exhibition, New Orleans, Louisiana, 30 September-02 October. SPE-166132-MS. https://doi.org/10.2118/166132-MS.

Popov, D., Gapochkin,A., Nekrasov, A. 2018. “An Algorithm of Daubechies Wavelet Transform in the Final Field When Processing Speech Signals.” *Electronics* **7**(7):120. https://doi.org/10.3390/electronics7070120.

Press, W.H., Teukolsky S.A., Vetterling W.T., Flannery B.P. 1992. Numerical Recipes in C-The Art of Scientific Computing. Second Edition.

Prokoph, A., Agterberg, F.P. 2000. "Wavelet analysis of well-logging data from oil source rock, Egret Member, offshore eastern Canada." *AAPG Bulletin* **84**(10):1617-1632. https://doi.org/10.1306/8626bf15-173b-11d7-8645000102c1865d.

Reeves, J., Chen, J. 2007. "A Review and Comparison of Changepoint Detection Techniques for Climate Data." *Journal of Applied Meteorology and Climatology* **46**:900-915. https://doi.org/10.1175/JAM2493.1.

Refunjol, B.T. and Lake, L.W. 1999. Reservoir Characterization Based on Tracer Response and Rank Analysis of Production and Injection Rates. In Reservoir Characterization: Recent Advances AAPG Memoir 71, Schatzinger, R.A., Jordan, J.F., Chapter 15, 209-218.

Sayarpour, M., Zuluaga, E., Kabir, C.S. and Lake, L.W. 2009. "The use of capacitance–resistance models for rapid estimation of waterflood performance and optimization." *Journal of Petroleum Science and Engineering* **69** (3-4): 227-238. https://doi.org/10.1016/j.petrol.2009.09.006.

Sayarpour, M. 2015. CRM Generator. https://www.researchgate.net/publication/280579204_CRM_Generator (accessed 2019).

Saritha, C., Sukanya, V., Murthy, Y.N. 2008. "ECG Signal Analysis Using Wavelet Transforms." Bulg. J. Phys. **35**(1): 68-77.

Sifuzzaman, M., Islam, M.R. and Ali, M.Z. 2009. "Application of wavelet transform, and its advantages compared to Fourier transform." *Journal of Physical Sciences* **13**: 121-134.

Smith, M.T., Macdonald, D.D., 2009. "Wavelet Analysis of Electrochemical Noise Data." *Corrosion* **65** (7): 438-448. Paper No 05355. https://doi.org/10.5006/1.3319148.

Soeriawinata, T. and Kelkar, M. 1999. “Reservoir Management Using Production Data.” Presented at the SPE Mid-Continent Operations Symposium, Oklahoma City, Oklahoma, 28-31 March. SPE-52224-MS. https://doi.org/10.2118/52224-MS.

Soliman, M.Y., Daneshy,A.A. 1991. “Determination of Fracture Volume and Closure Pressure from Pump-In/Flowback Tests.” Presented at the Middle East Oil Show, Bahrain, 16-19 November. SPE-21400-MS. https://doi.org/10.2118/21400-MS.

Soliman, M. Y., Ansah, J., Stephenson, S. et al. 2001. “Application of Wavelet Transform to Analysis of Pressure Transient Data.” Presented at the ATCE, New Orleans, Louisiana, 30 September- 3 October. SPE-71571-MS. https://doi.org/10.2523/71571-MS.

Soliman, M.Y., Ansah, J., Stephenson, S. and Mandal, B. 2003. “Application of Wavelet Transform To Analysis of Pressure Transient Data.” *SPE Reservoir Evaluation & Engineering* **6**(02): 89-99. SPE-83670-PA. https://doi.org/10.2118/83670-PA.

Soliman, M. Y., Wigwe, M., Alzahabi, A., Pirayesh, E., Stegen, N. 2014. “Analysis of Fracturing Pressure Data in Heterogeneous Shale Formations.” *Hydraulic Fracturing Journal* **1**(2): 8-12.

Strang, G., Nguyen, T. 1996. Wavelets and Filter Banks. Wellesley-Cambridge Press.

Surjaatmadja, J.B., Stephenson, S., Bhaumik, C., Thompson, S. and Cheng, A. 2002. “Analysis of Generated And Reflected Pressure Waves During Fracturing Reveals Fracture Behavior.” Presented at the SPE Annual Technical Conference and Exhibition, San Antonio, Texas, 29 September- 2 October. SPE-77598-MS. https://doi.org/10.2118/77598-MS.

Tian, C. and Horne, R.N. 2016. “Inferring Interwell Connectivity Using Production Data.” Presented at the SPE Annual Technical Conference and Exhibition, Dubai, UAE, 26-28 September. SPE-181556-MS. https://doi.org/10.2118/181556-MS.

Tompkins, D., Waldman, N., Redman, M. 2014. "Effect of Ambient Temperature Change on Diagnostic Fracture Injection Tests." *Journal of Petroleum Technology* **66** (9): 33-36.

Truong, C., Oudre, L., & Vayatis, N. 2018. "Selective review of offline change point detection methods."arXiv preprint. doi:http://arxiv.org/abs/1801.00718.

Unal, E., Siddiqui, F., and Soliman, M.Y. 2018. "Wavelet Analysis of Fracturing Pressure Data." Presented at the SPE Hydraulic Fracturing Technology Conference and Exhibition, Houston, Texas, 23-25 January. SPE-189885-MS. https://doi.org/10.2118/189885-MS.

Unal, E., Siddiqui, F., Soliman, M.Y., and Dindoruk, B. 2019. "Wavelet Analysis of DFIT Data to Identify Fracture Closure Parameters." Presented at the SPE Hydraulic Fracturing Technology Conference and Exhibition, Woodlands, Texas, 5-7 February. SPE-194326-MS. https://doi.org/10.2118/194326-MS.

Unal, E., Rezaei,A., Siddiqui,F., Likrama,F., Soliman, M.Y., Dindoruk, B. 2019. "Improved Understanding of Dynamic Fracture Behavior in Unconventional Horizontal Wells Using Wavelet Transformation." Presented at the SPE Annual Technical Conference and Exhibition, Calgary, Canada, 20 September-02 October. SPE-195889-MS.

Unal, E., Siddiqui, F., Rezaei, A., Eltaleb, I., Kabir, S., Soliman, M.Y., Dindoruk, B. 2019. "Use of Wavelet Transform and Signal Processing Techniques for Inferring Interwell Connectivity in Waterflooding Operations." Presented at the SPE Annual Technical Conference and Exhibition, Calgary, Canada, 20 September-02 October. SPE- 196063-MS.

Valens, C. 1999. A Really Friendly Guide to Wavelets. Citeseerx. http://citeseerx.ist.psu.edu/viewdoc/summary?doi=10.1.1.34.29 (accessed 2017).

Viberti,D., Verga,F., Delbosco, P. 2005. “Application of the Wavelet Analysis to Treat PDG Pressure Data.” Presented at the Offshore Mediterranean Conference and Exhibition, Ravenna, Italy, March 16-18. OMC-2005-118.

Xie, L., Yan, P., Lu, W., Chen, M., and Wang, G. 2018. “Comparison of seismic effects during deep tunnel excavation with different methods.” *Earthquake Engineering and Engineering Vibration* **17**(3): 659-675. https://doi.org/10.1007/s11803-018-0452-y.

Yousef, A.A., Lake, L.W. and Jensen, J.L. 2006. “Analysis and Interpretation of Interwell Connectivity from Production and Injection Rate Fluctuations Using a Capacitance Model.” Presented at the SPE/DOE Symposium on Improved Oil Recovery, Tulsa, Oklahoma, 22-26 April. SPE-99998-MS. https://doi.org/10.2118/99998-MS.

Zhai, D., Mendel, J.M. and Liu, F. 2009. “A New Method for Continual Forecasting Of Interwell Connectivity in Waterfloods Using an Extended Kalman Filter.” Presented at the SPE Western Regional Meeting. Society of Petroleum Engineers, San Jose, California. SPE-110520-PA. https://doi.org/10.2118/110520-PA.